



Detectors for γ -ray astronomy

Alberto Carramiñana

Instituto Nacional de Astrofísica, Óptica y Electrónica
Luis Enrique Erro 1, Tonantzintla, Puebla, México



Reunión de la División de Rayos Cósmicos SMF
Puebla, 27 de noviembre de 2019

Detectors (I)

- Gamma rays
- Gamma-ray observatories
- Gamma-ray space observatories
- Earth as a particle detector
- Atmospheric Cherenkov telescopes
- Air shower arrays
- HAWC

Gamma rays

- γ rays are the most energetic form of electromagnetic radiation, manifested as quanta.
- They are intrinsically related to high energy particles:
 - HE particles are needed to produce high energy γ rays
 - HE γ rays indicate the production sites of HE particles, i.e. cosmic rays
 - cosmic rays are a background for the study of γ rays
- Astrophysical γ rays point to cosmic accelerators and provide unique diagnostics about extreme processes in the Universe.

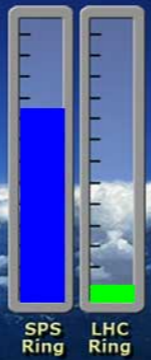
Man made gamma rays



JLong 2004

LHC: The Large Hadron Collider

The protons have not yet been accelerated to their full energy.
You need to supply more energy by raising the accelerator handle...



SPS now at 306.0 GeV (68)%...

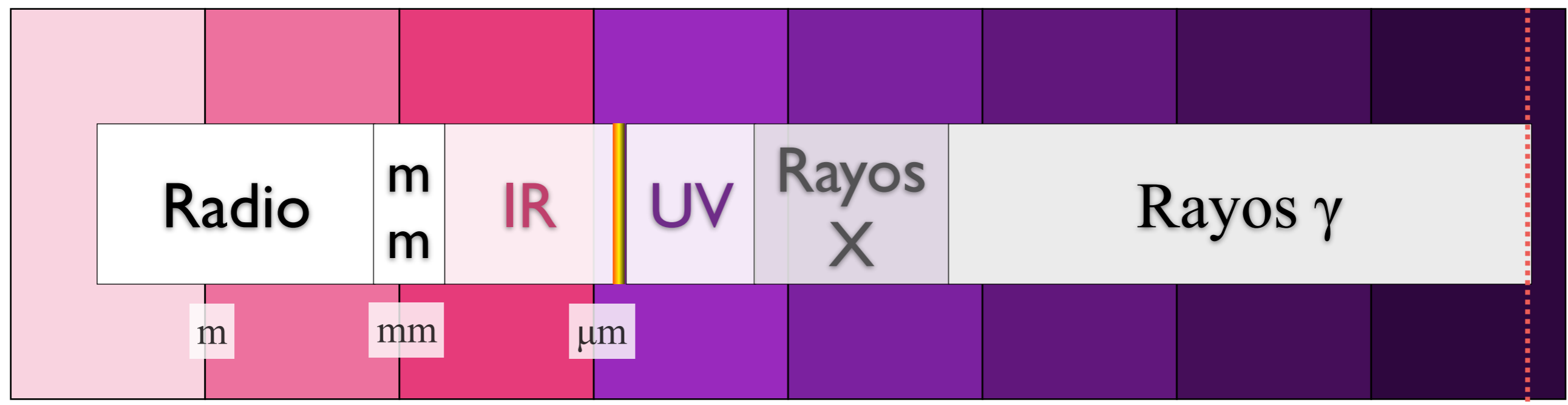
Lift handle to accelerate the stream



γ -ray detectors @ DRC-SMF - nov 2019



neV μeV meV eV keV MeV GeV TeV PeV



MHz GHz THz



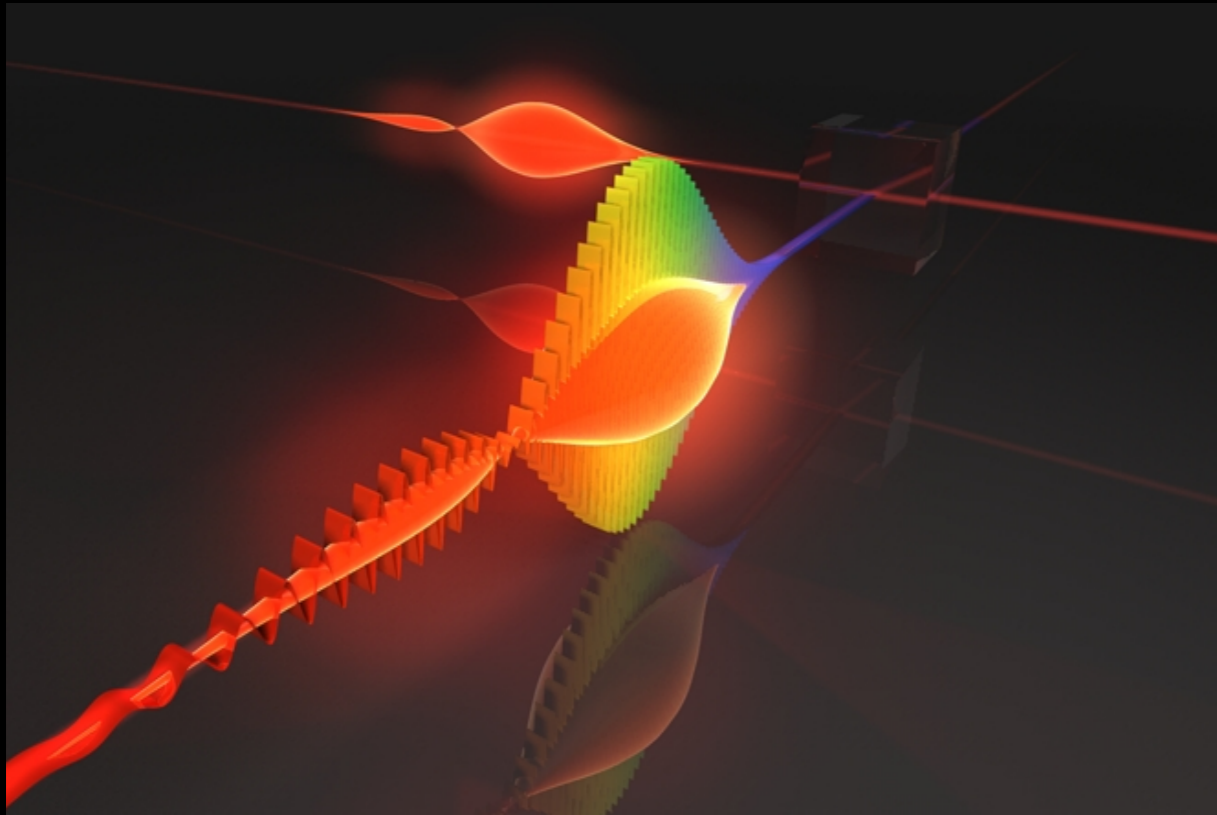
No térmico (e) → **Térmico** → No térmico (RCs)



γ -ray detectors @ DRC-SMF - nov 2019



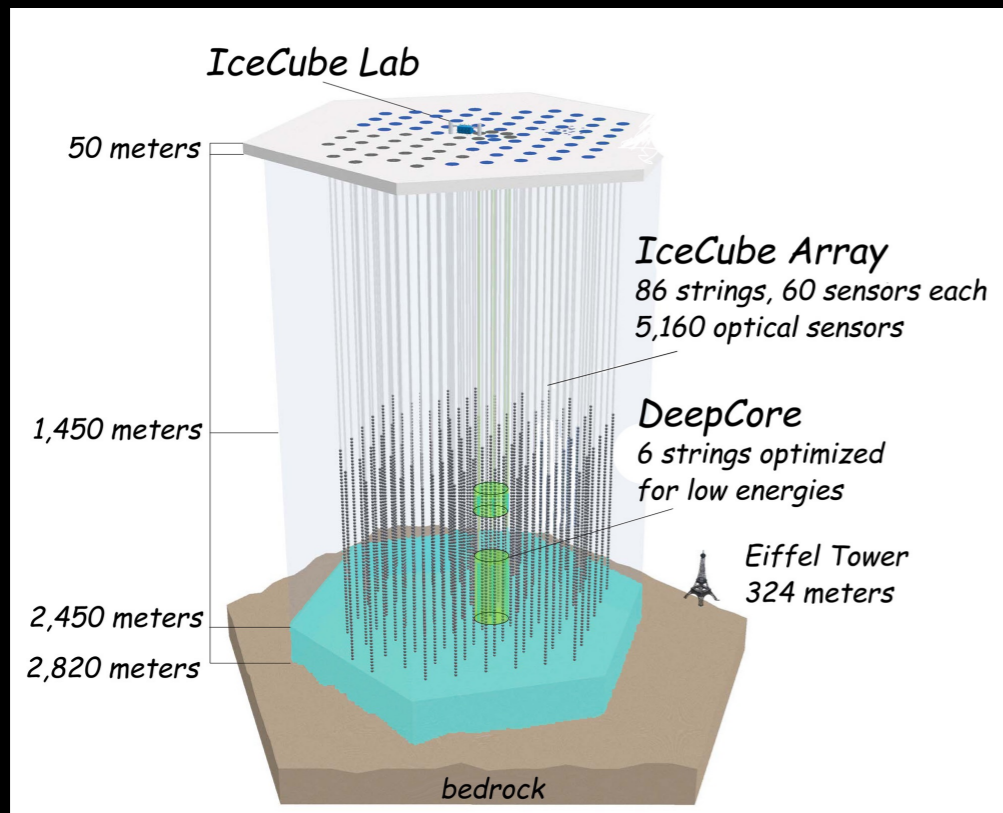
Electromagnetic radiation



Cosmic particles



Neutrinos



Gravitational waves



γ -ray production

Nuclear decay	Historical $\{\alpha, \beta, \gamma\}$ - low energy γ rays (100s keV).
Matter - antimatter annihilation	Electrons produce 511 keV photons.
Bremsstrahlung	Relativistic electrons interacting with matter.
Synchrotron	Relatively inefficient to produce HE photons. Efficient to produce seed photons.
Compton scattering	Efficient production of high-energy γ rays through the interaction of a radiation field.
Nuclear collisions	Efficient production of HE γ rays through interaction with matter, or radiation, and π^0 decay.

γ -ray absorption

Photo-electric effect

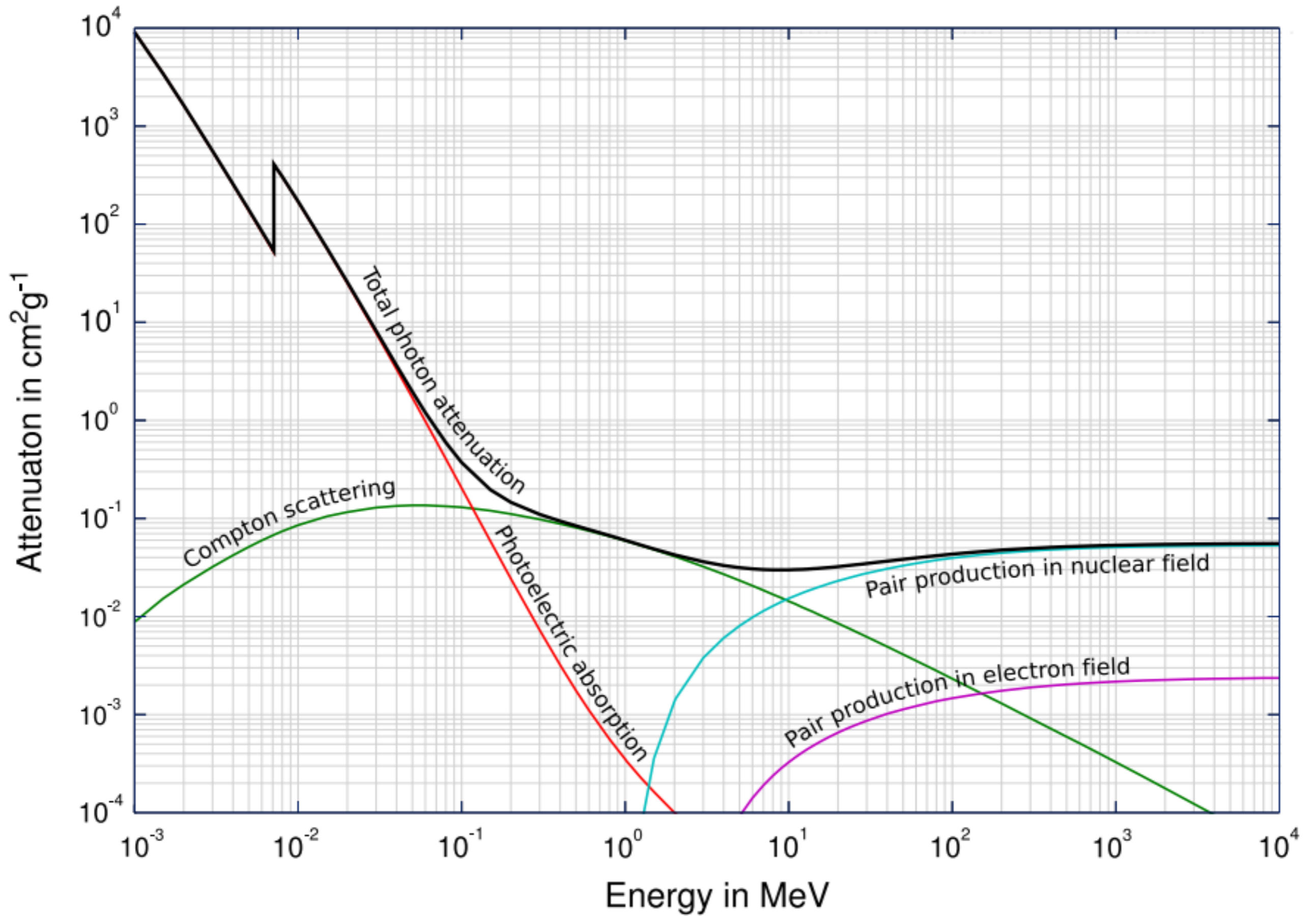
Absorption of a X ray or low-energy γ ray by matter, releasing an electron.

Compton scattering

Interaction with electrons at rest produce a photon of lower energy.

Pair production

Can occur with a radiation field ($\gamma\gamma \rightarrow e^-e^+$);
with matter ($\gamma Z \rightarrow e^-e^+ Z$);
with a magnetic field ($\gamma B \rightarrow e^-e^+B$).



γ -ray observatories

- Space telescopes relying on:
 - photo-electric effect: like BATSE, OSSE, Swift-BAT. Technology shared with hard X-ray telescopes.
 - Compton scattering: COMPTEL.
 - pair production: from OSO-3 to *Fermi-LAT*.
- Ground-based observatories:
 - detection of Cherenkov in the atmosphere: MAGIC, HESS, VERITAS, CTA.
 - detection of secondary particles: MILAGRO, Tibet AS- γ , HAWC, LHAASO, ... SWSO.

Energy ranges

10^9 eV

10^{12} eV

10^{15} eV

10^{18} eV

10^{20} eV

Cosmic rays

Satélites

Kaskade

HAWC

Pierre Auger

MeV

GeV

TeV

PeV

EeV

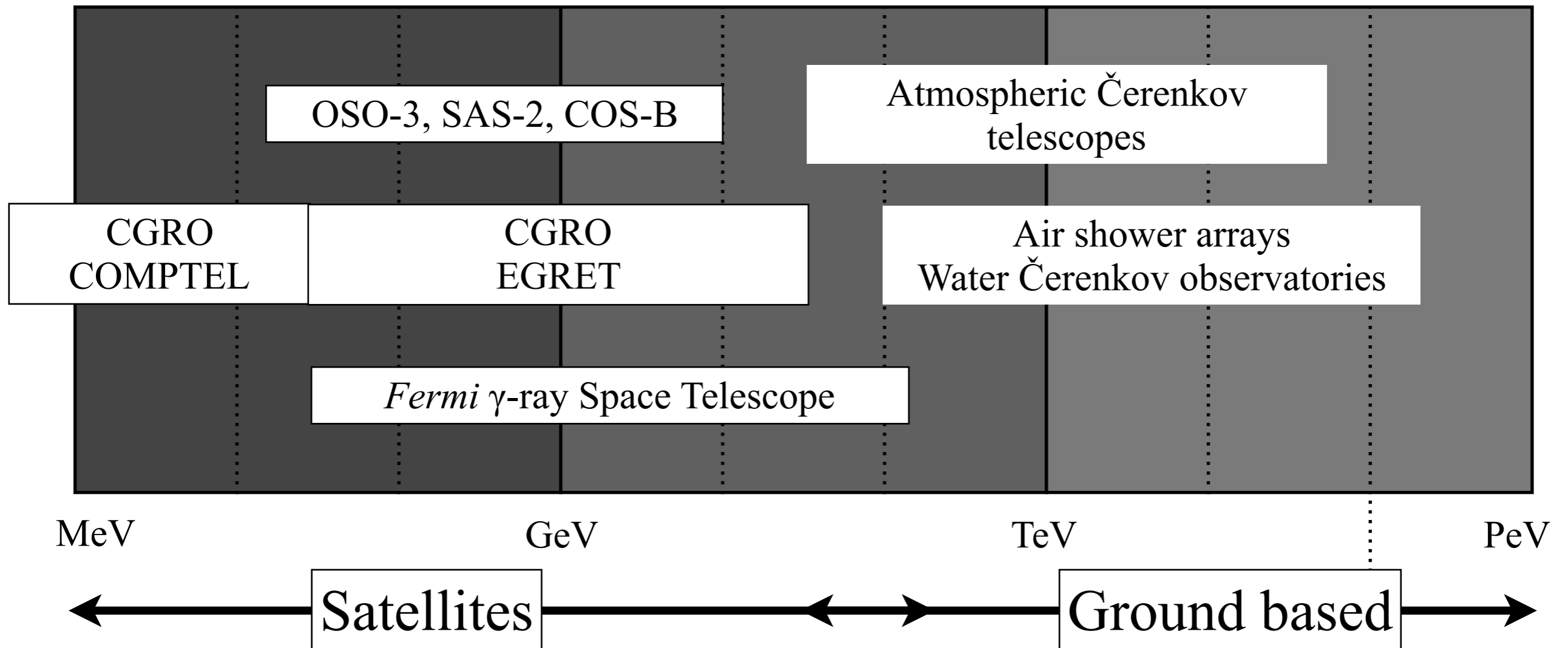
Gamma rays

AČT

Fermi-LAT

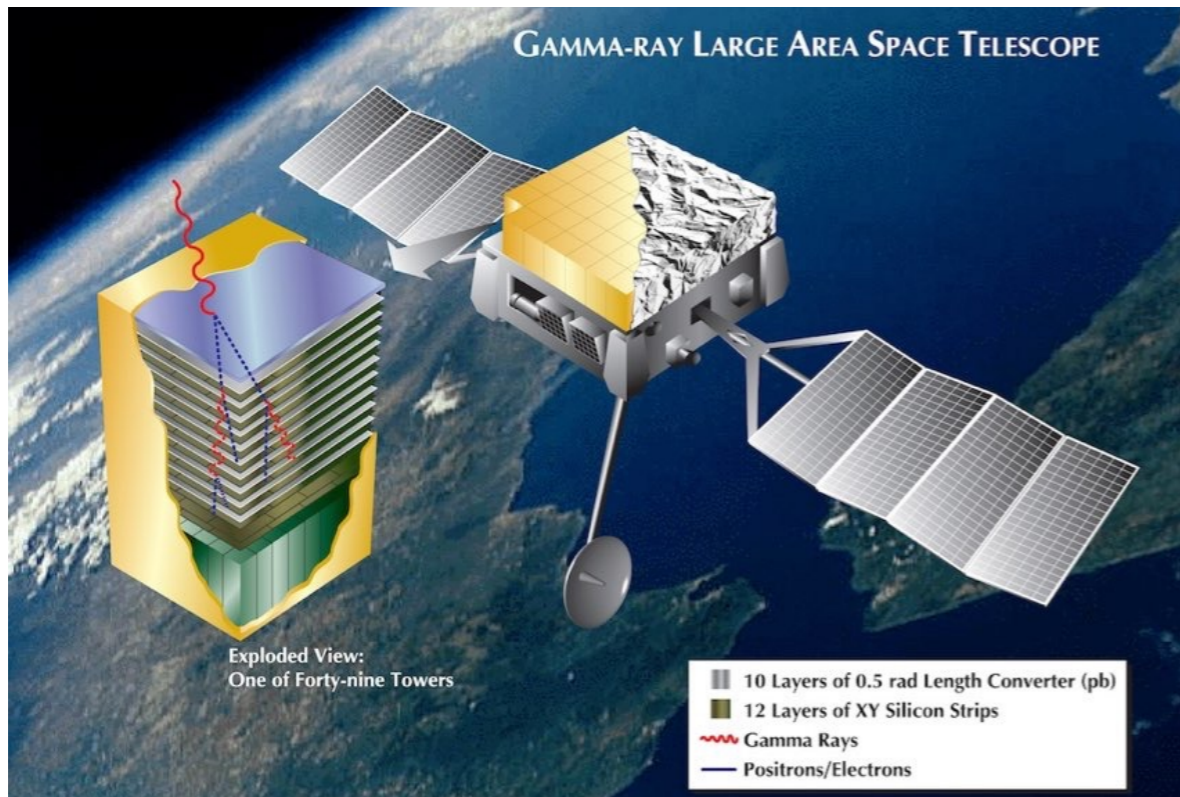
HAWC

The γ -ray band

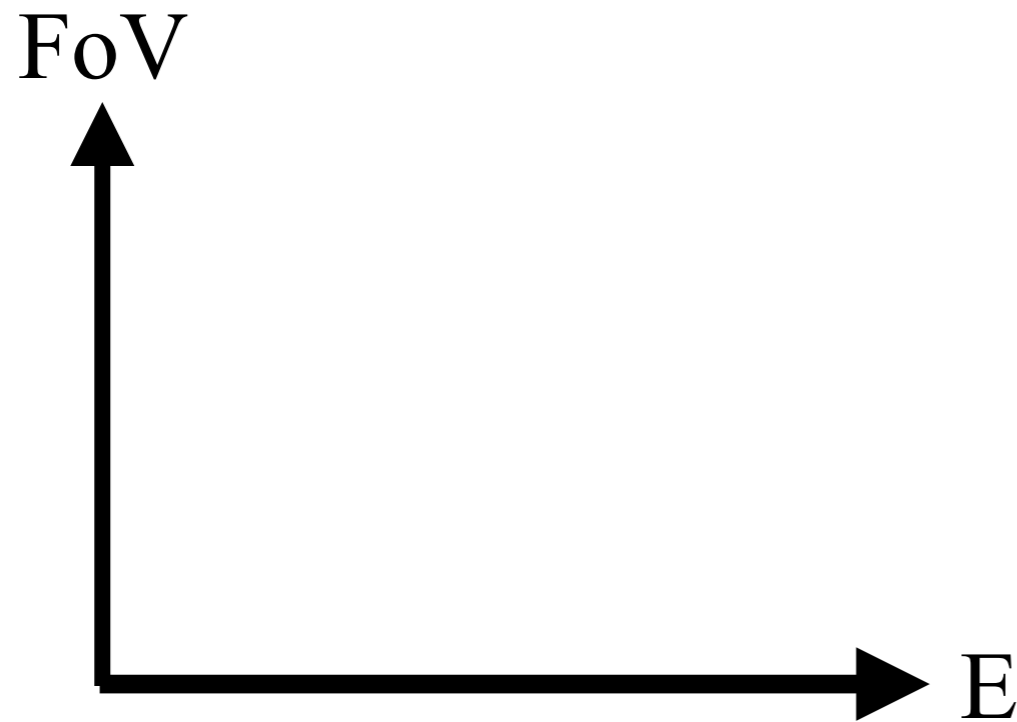


$$\gamma + \text{CMB} \rightarrow e^- + e^+$$

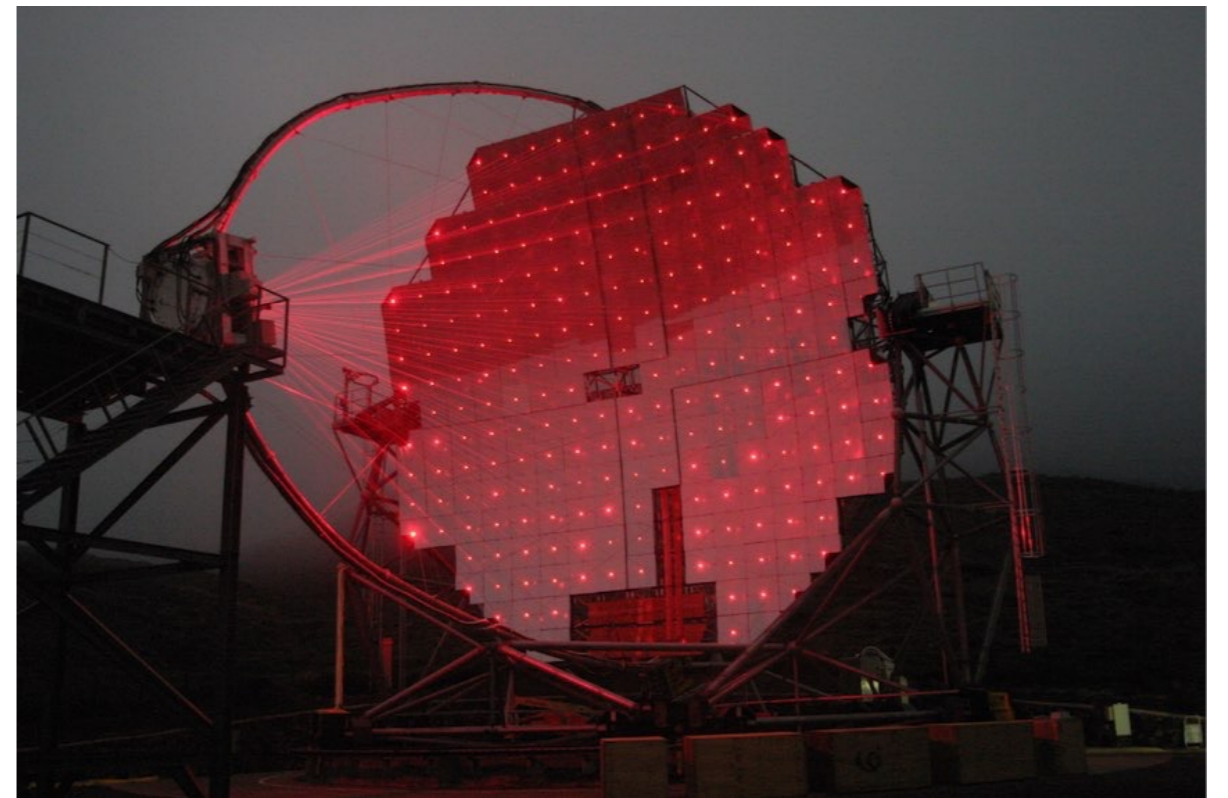
Sr



Deg



GeV



TeV

Sr

Pair production telescopes

30 MeV - 100 GeV
Small effective area
Background free
Large field of view and duty cycle

Sky surveys and monitoring
Transient events (AGN, GRB, GW)
Extended diffuse emission

Air shower arrays

100 GeV - 100 TeV
Large effective area
Good background suppression
Large field of view and duty cycle

Partial sky surveys and monitoring
Extended sources
Transient events (AGN, GRB, GW)
The highest energies

Deg

FoV



Atmospheric Cherenkov telescopes

30 GeV - 30 TeV
Large effective area
Excellent background suppression
Limited field of view and duty cycle

Detailed studies of known sources
Follow-up of reachable transients
High resolution spectra
Deep surveys of limited regions of the sky

GeV

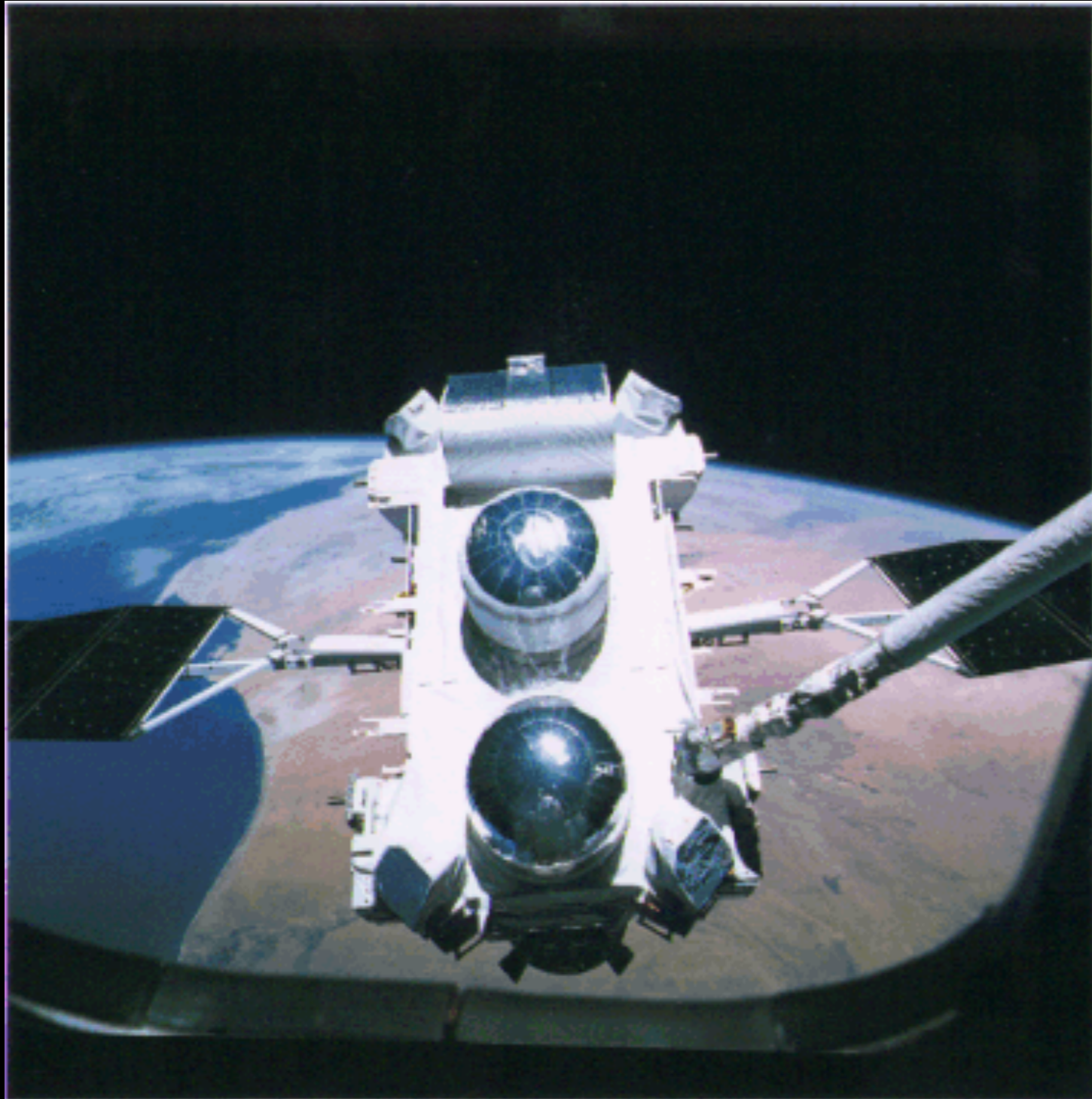
TeV



γ -ray space observatories

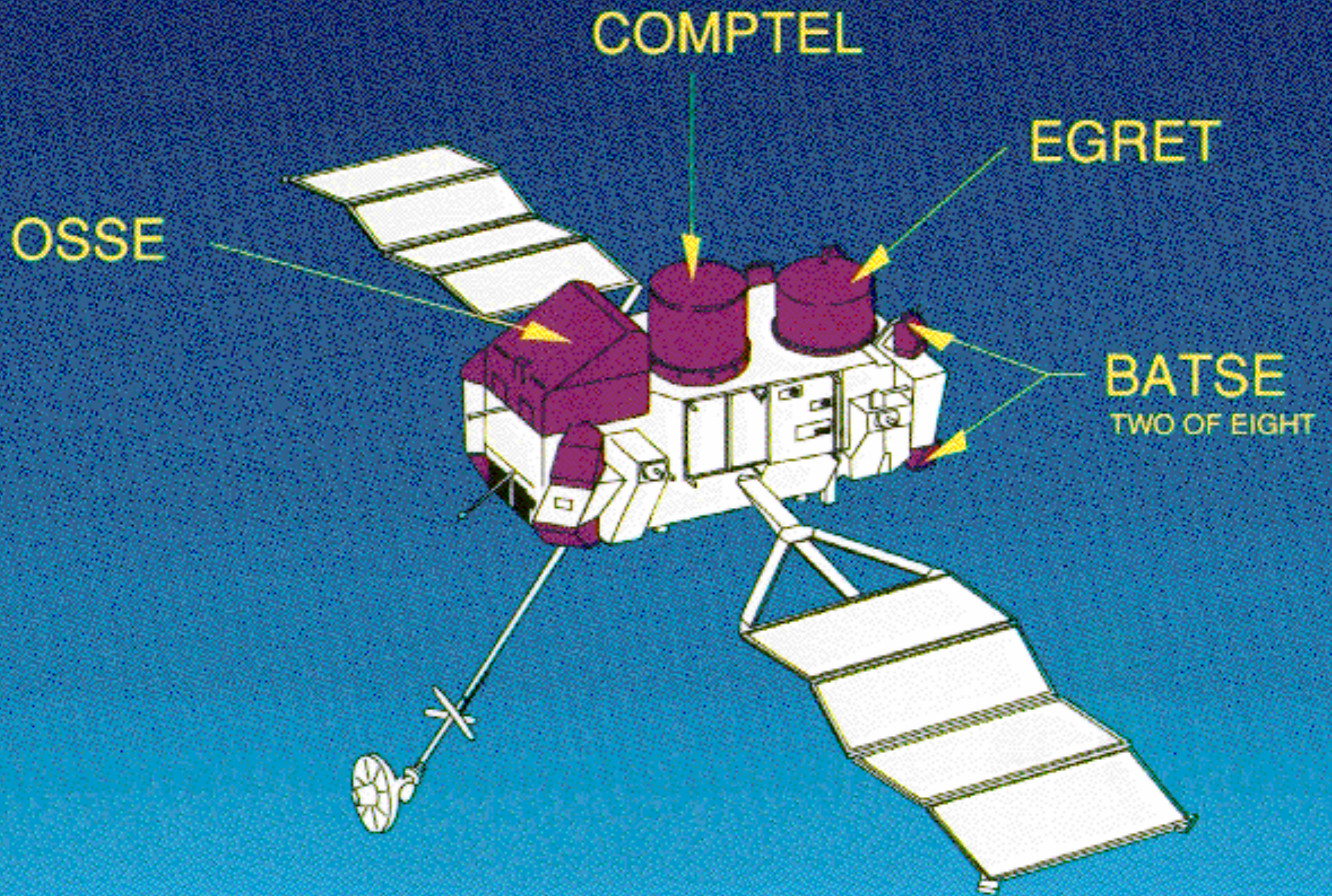
1967 - 1968	OSO 3	Pair prod.	Galactic Plane detection
1972 - 1973	SAS 2	Pair prod.	Pulsars: Crab, Vela, γ 195+5
1975 - 1982	Cos B	Pair prod.	Galactic diffuse emission, first catalogues, 3C 273.
1991 - 2000	CGRO	Multiple	BATSE, OSSE, COMPTEL, EGRET
2007 to now	AGILE	Pair prod.	Similar design to <i>Fermi</i> -LAT, 1/16 the size
2008 to now	Fermi	GBM & LAT	Current GeV ground-breaker

Compton Gamma-Ray Observatory



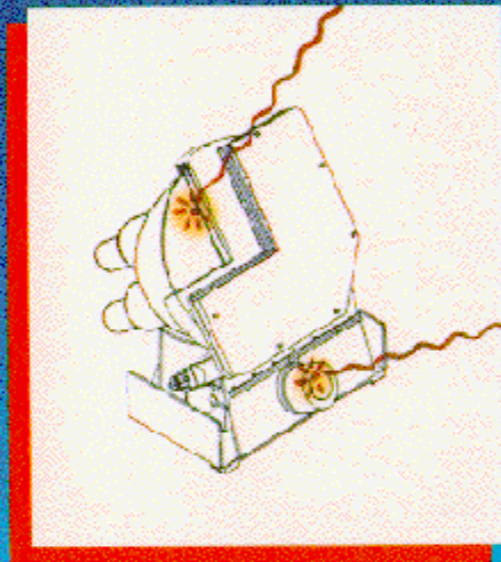
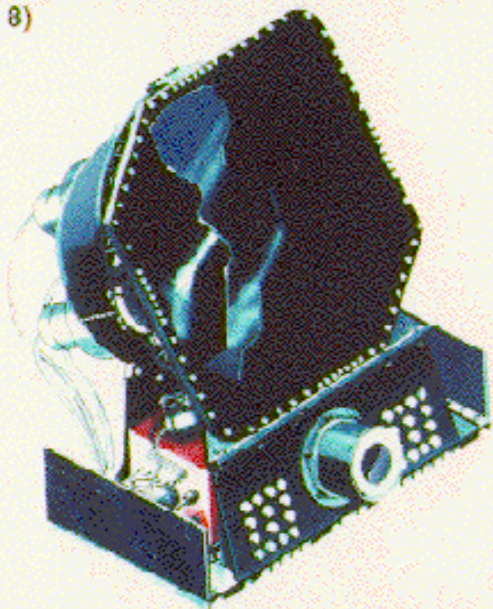
1991-2000

GRO Instruments

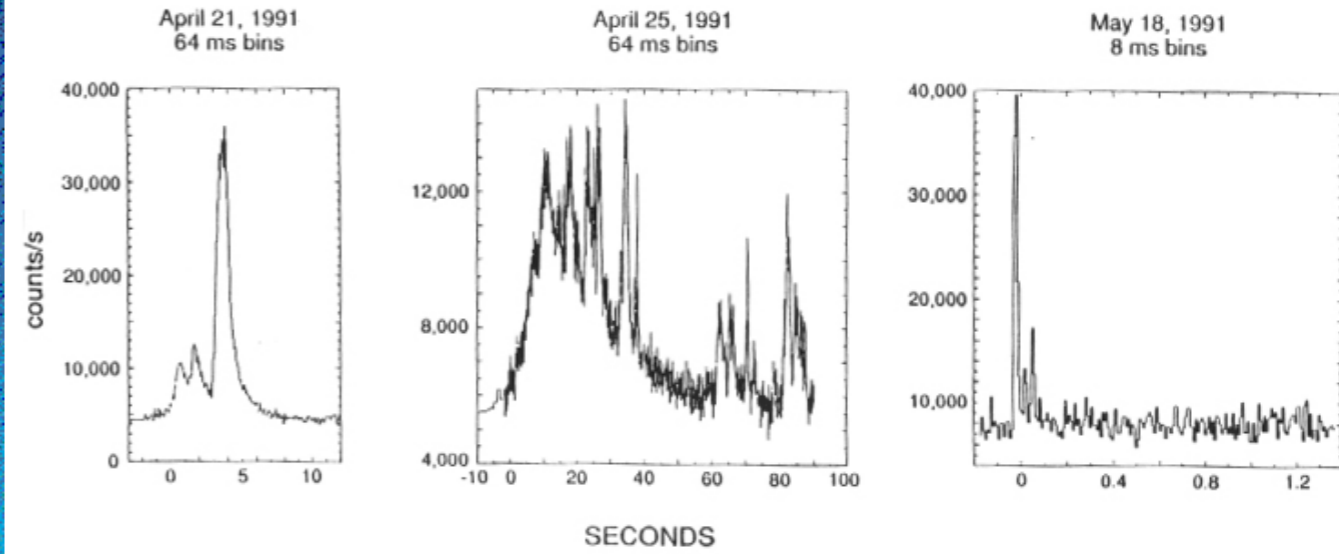


Burst and Transient Source Experiment (BATSE)

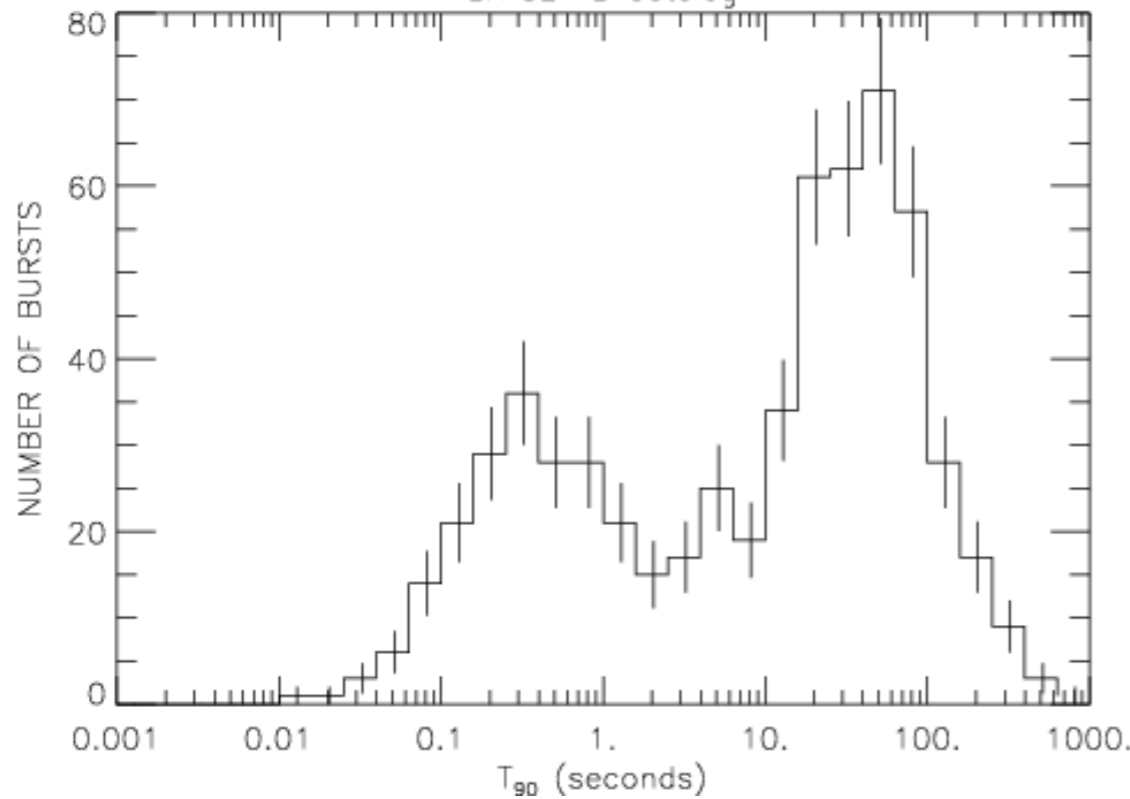
BATSE
DETECTOR MODULE
(1 OF 8)



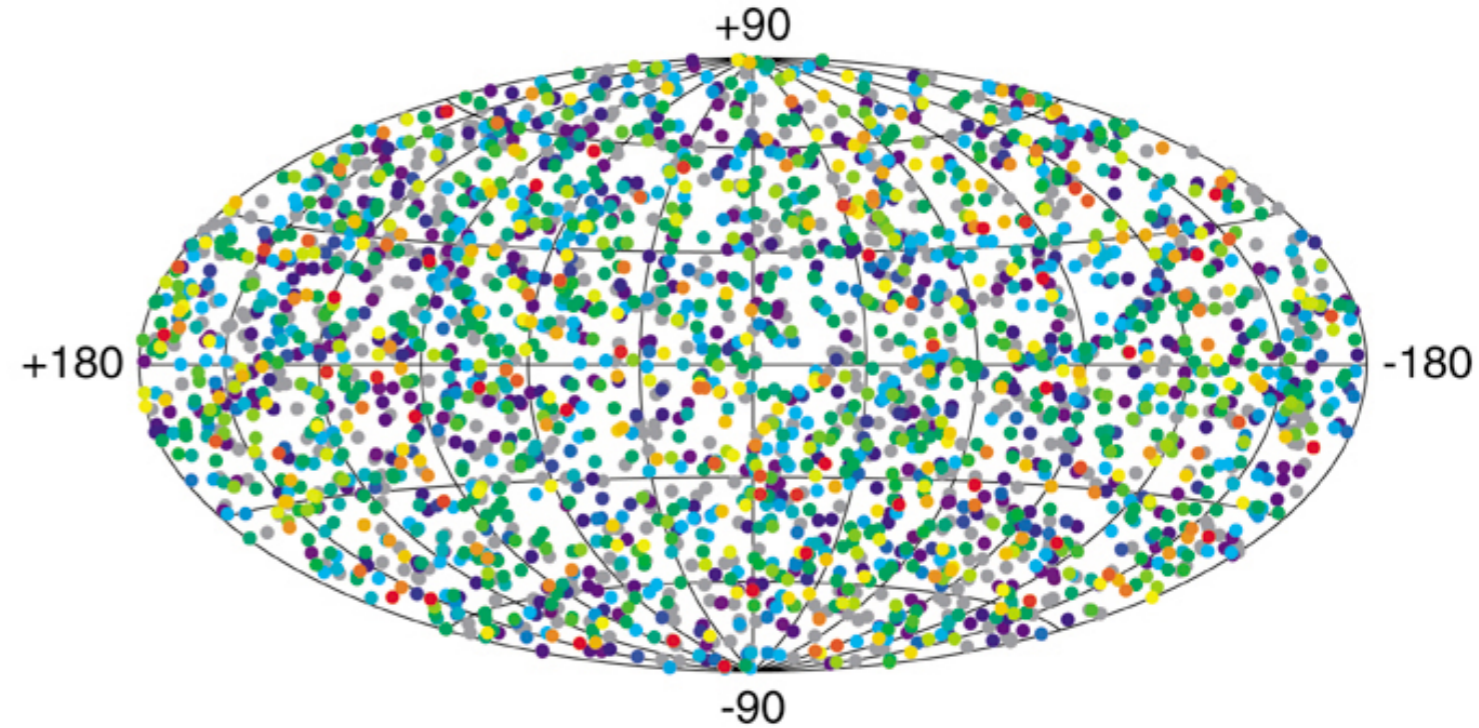
BATSE—GRO 3 Types of Gamma-Ray Bursts 50-300 keV



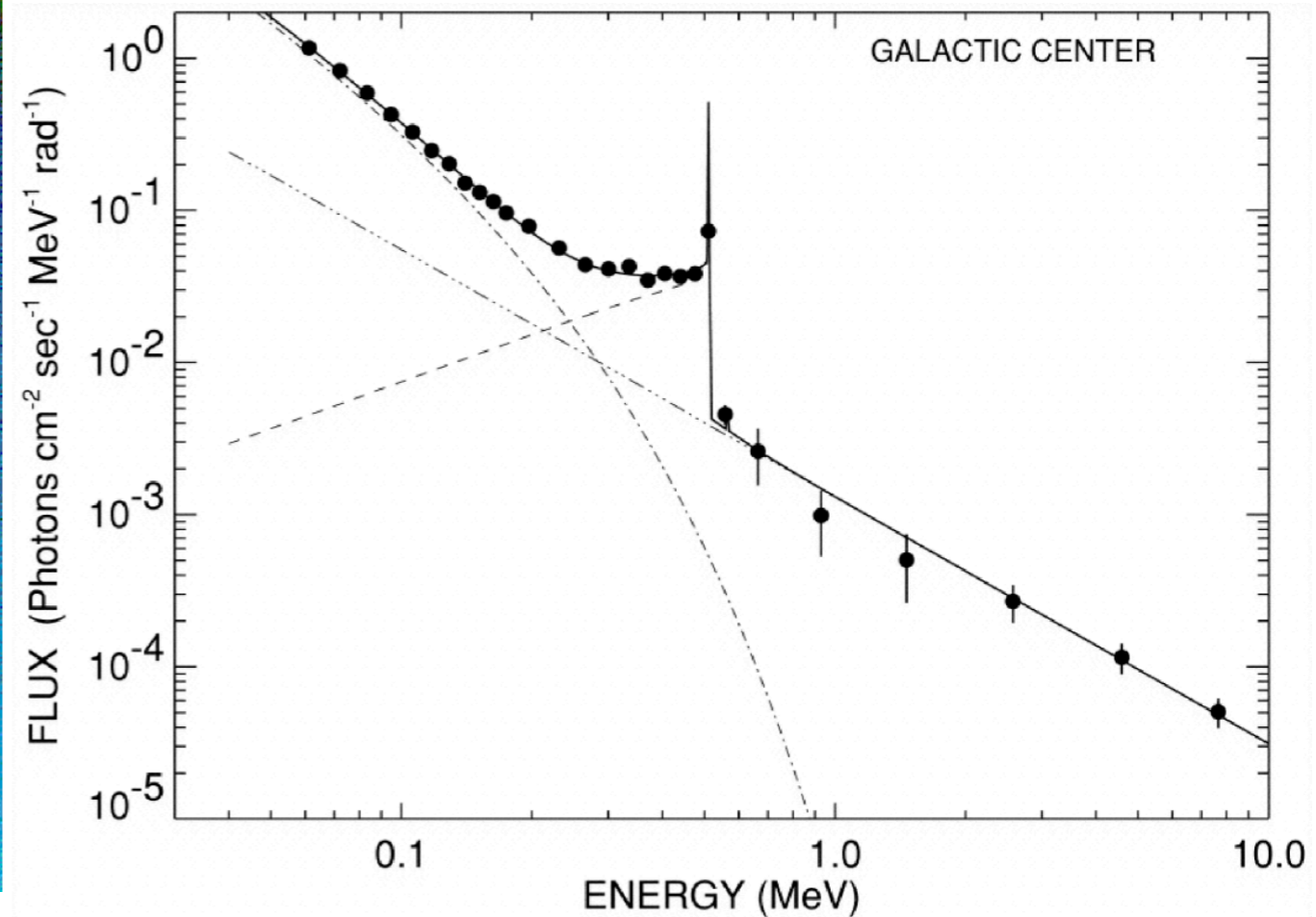
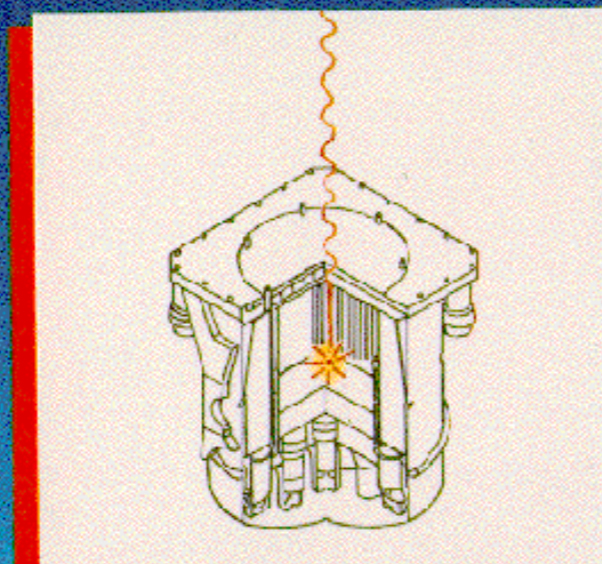
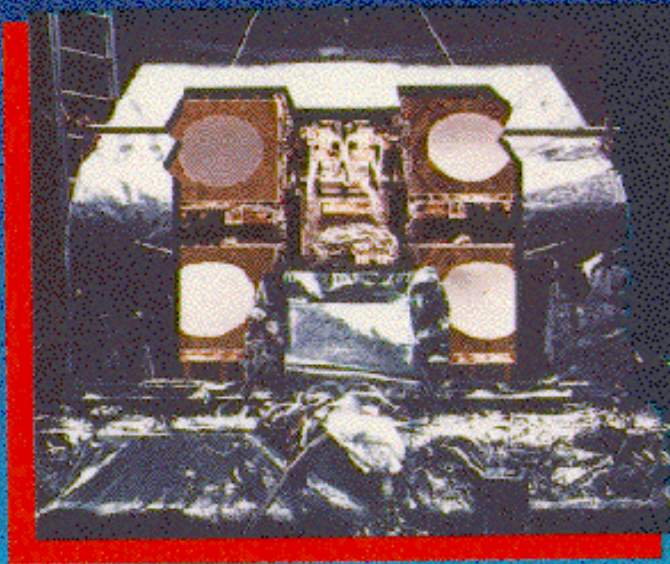
BATSE 4B Catalog



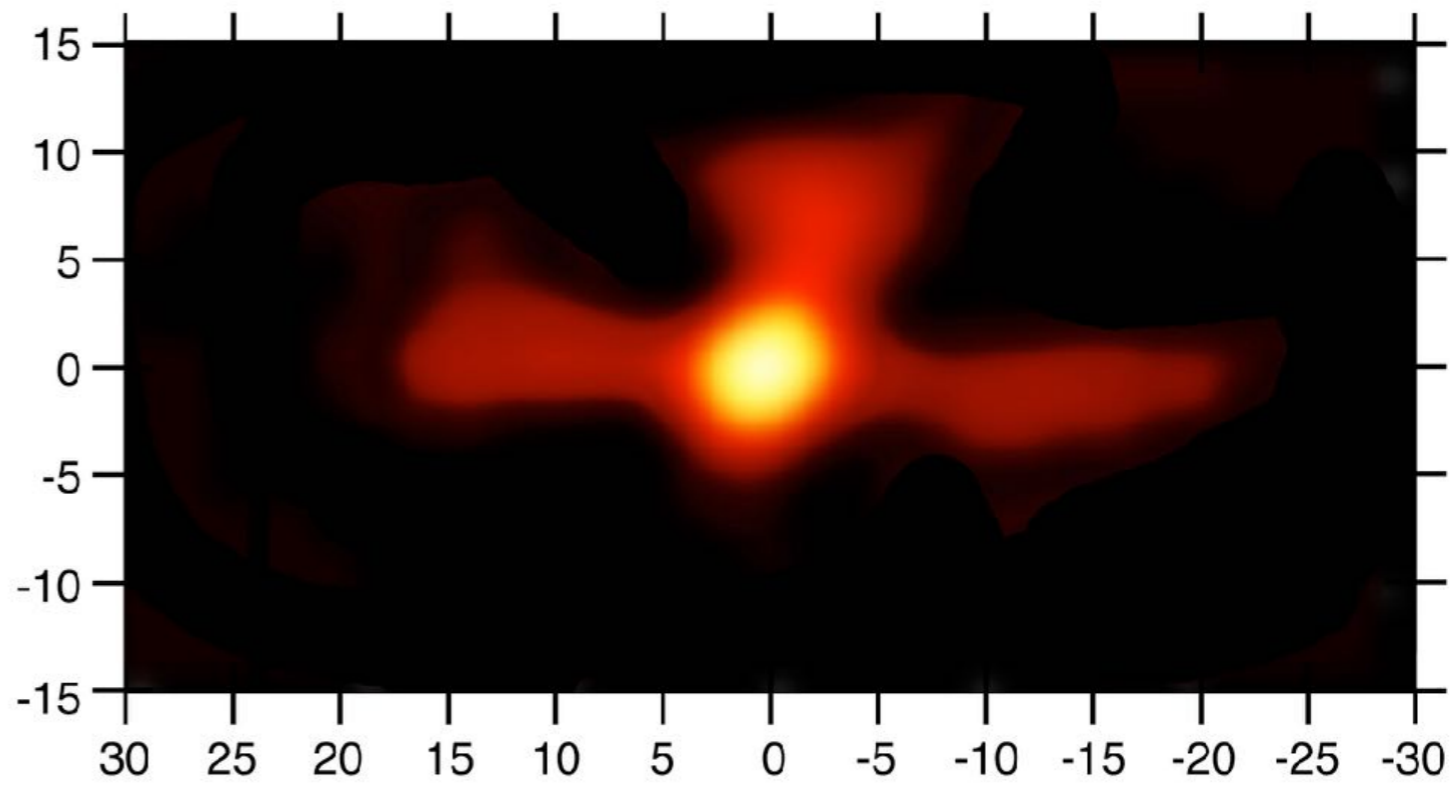
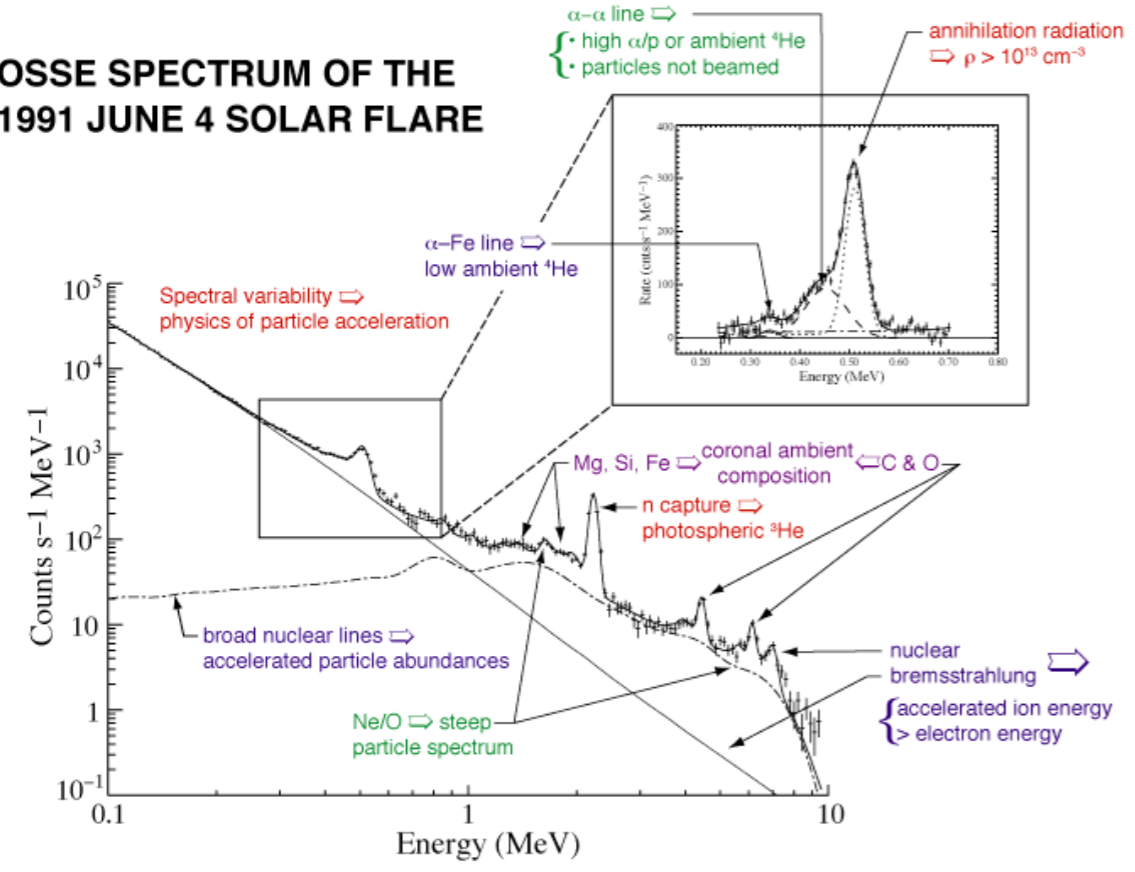
2704 BATSE Gamma-Ray Bursts



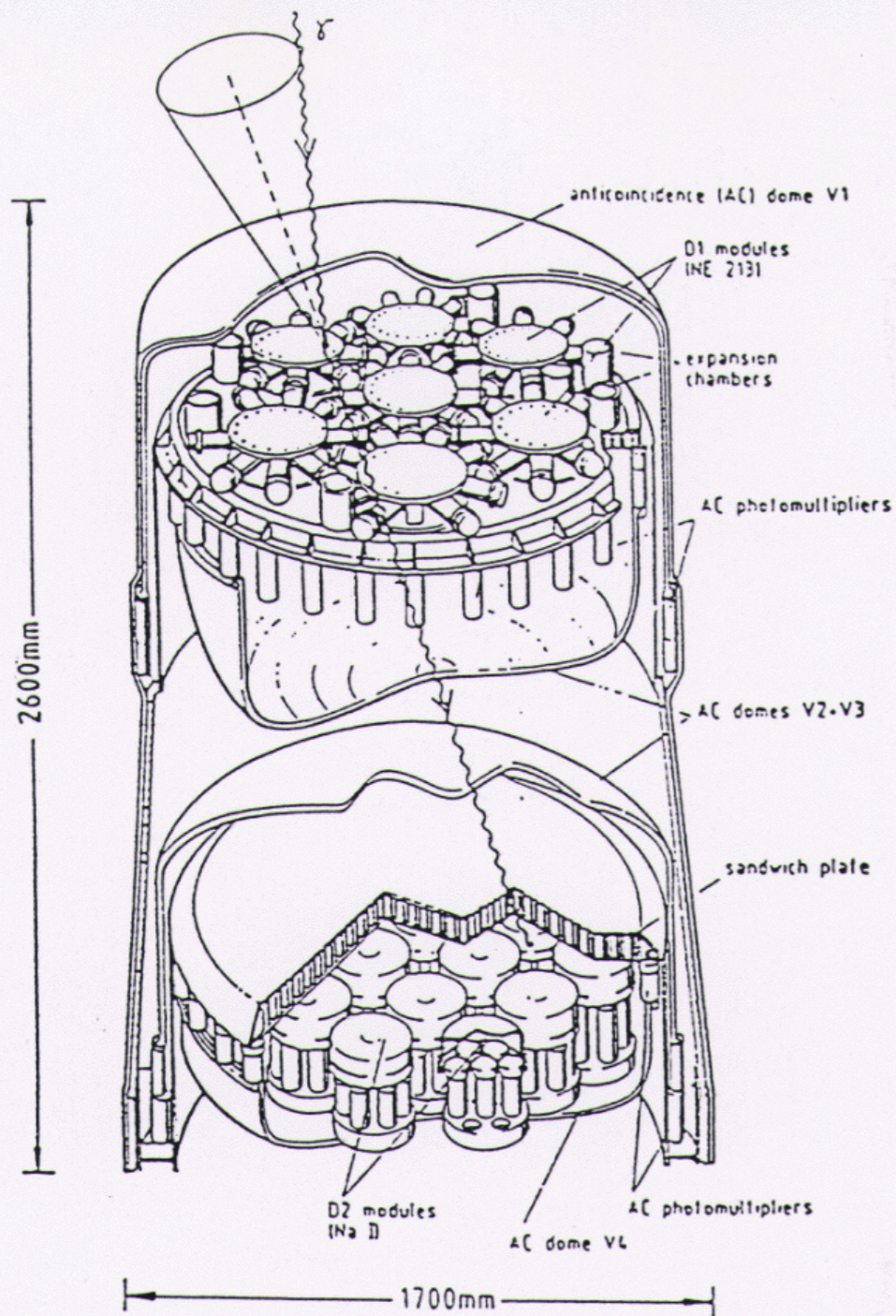
Oriented Scintillation Spectrometer Experiment (OSSE)



OSSE SPECTRUM OF THE 1991 JUNE 4 SOLAR FLARE



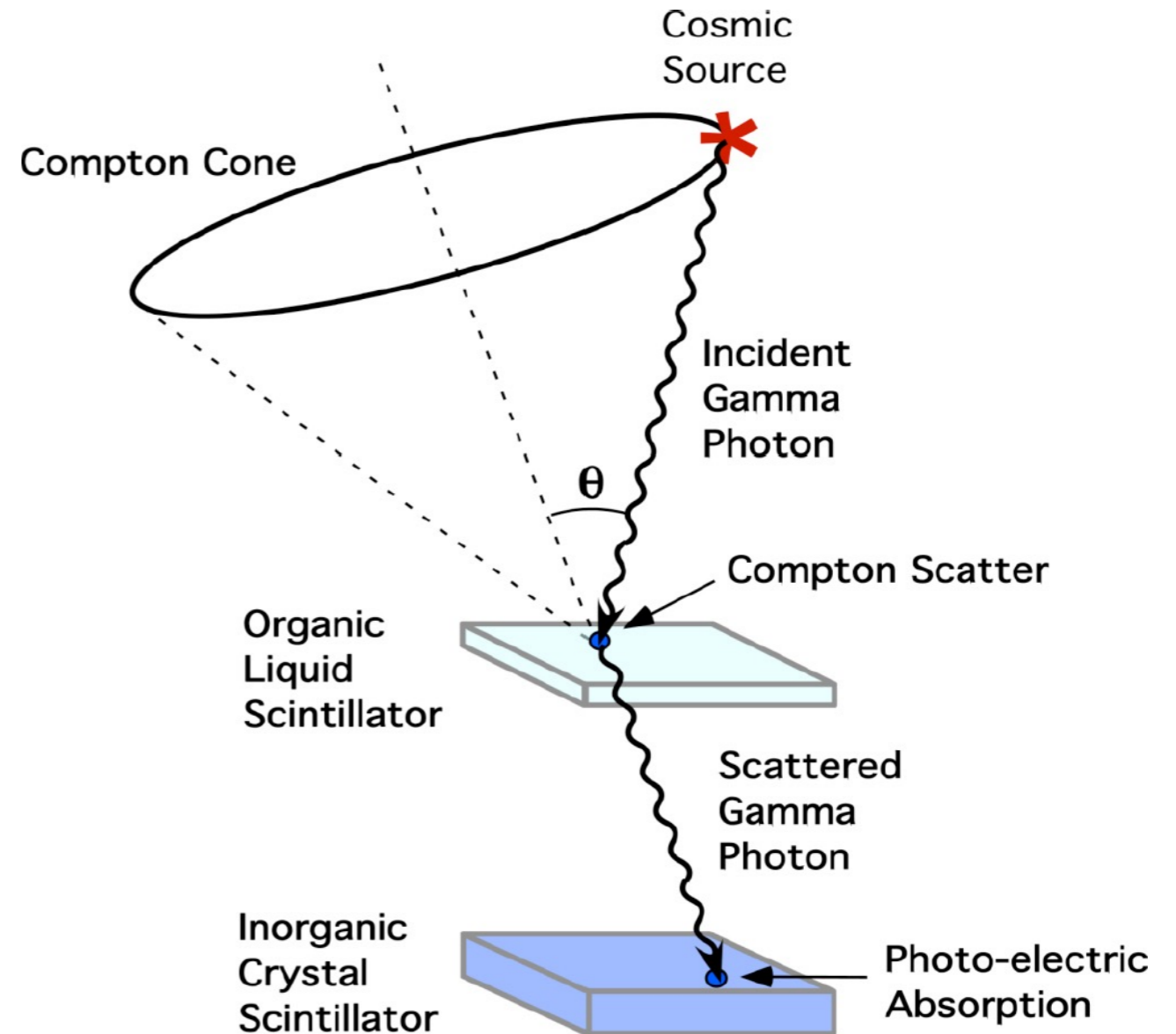
CGRO-COMPTEL



Schematics of COMPTEL

$$E_T = E_1 + E_2$$

$$\cos \bar{\nu} = 1 - \frac{m_0 c^2}{E_2} + \frac{m_0 c^2}{E_1 + E_2}$$



Only Compton telescope put in orbit so far.
Compton scattering has an azimuthal uncertainty.

COMPTEL

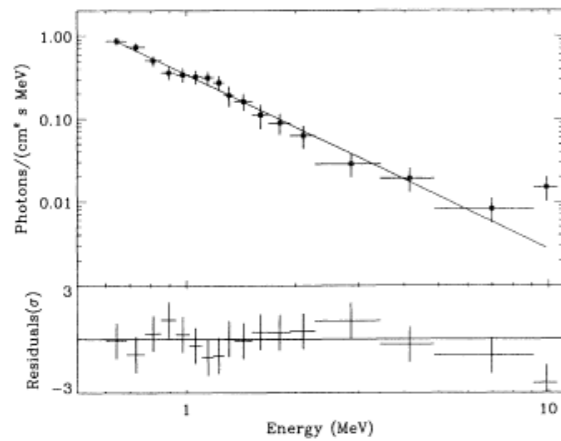
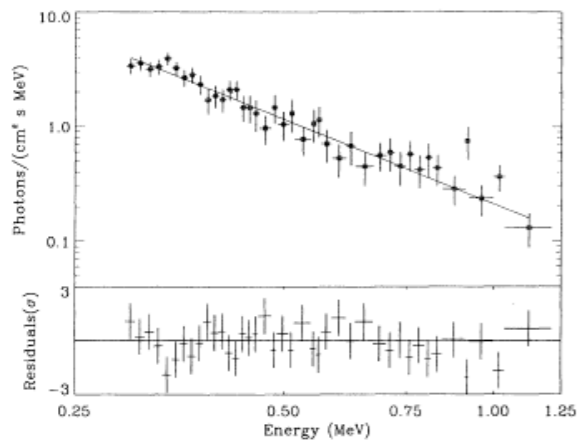


Fig. 5. GRB 910425: The upper panel shows the deconvolved spectrum for 39 s of data from D2-14 and the lower panel shows the equivalent spectrum obtained from the D2-7 detector

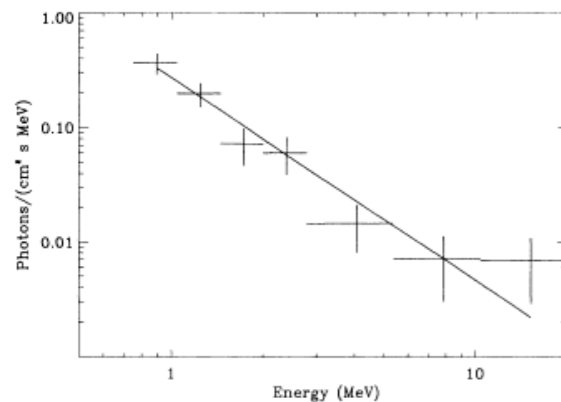


Fig. 7. The straight line represents the best high range model for the 4th tail spectrum of GRB 910425, extrapolated to low range energies. The circles are the low range data points and the asterisks are the high range data points. There is good agreement in the overlap energy region, but a soft excess between 300 and 450 keV is visible in the low range detector data

the low range spectrum of the 4th tail (time interval 4). This was confirmed by re-analysis of the D2-14 data in the energy interval 0.45–1.3 MeV, whereupon the α values for all time intervals in the D2-14 and D2-7 detectors were found to be in agreement to within 1σ . This feature may be interpreted as a potential 511 keV redshifted line candidate. Further study of the origin of the possible soft component (e.g. from background fluctuations) is being undertaken and will be discussed in a future publication.

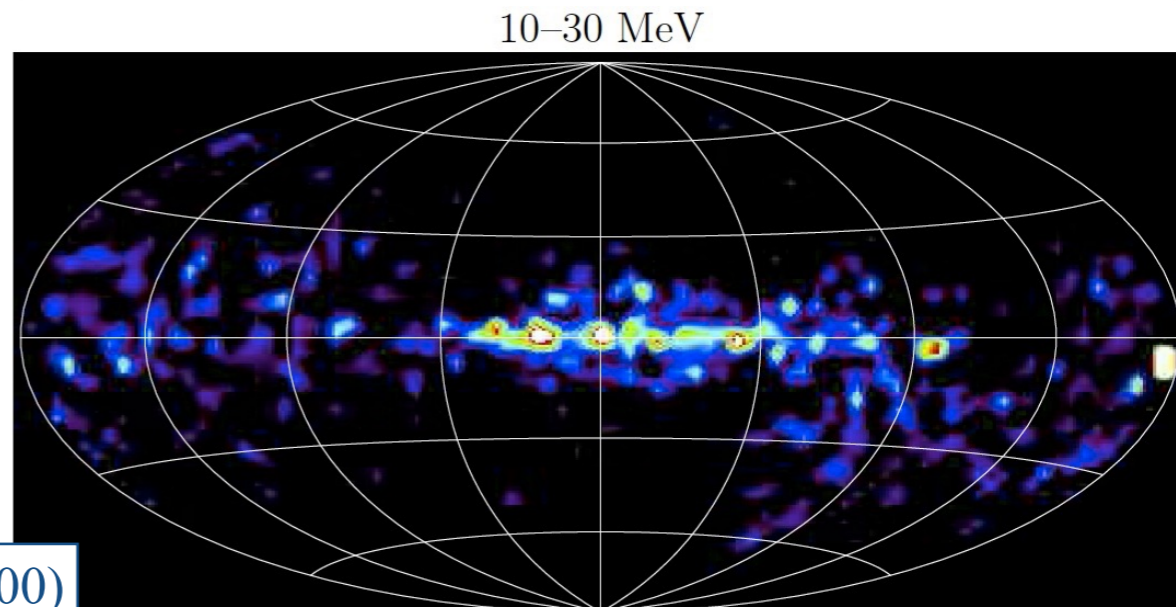
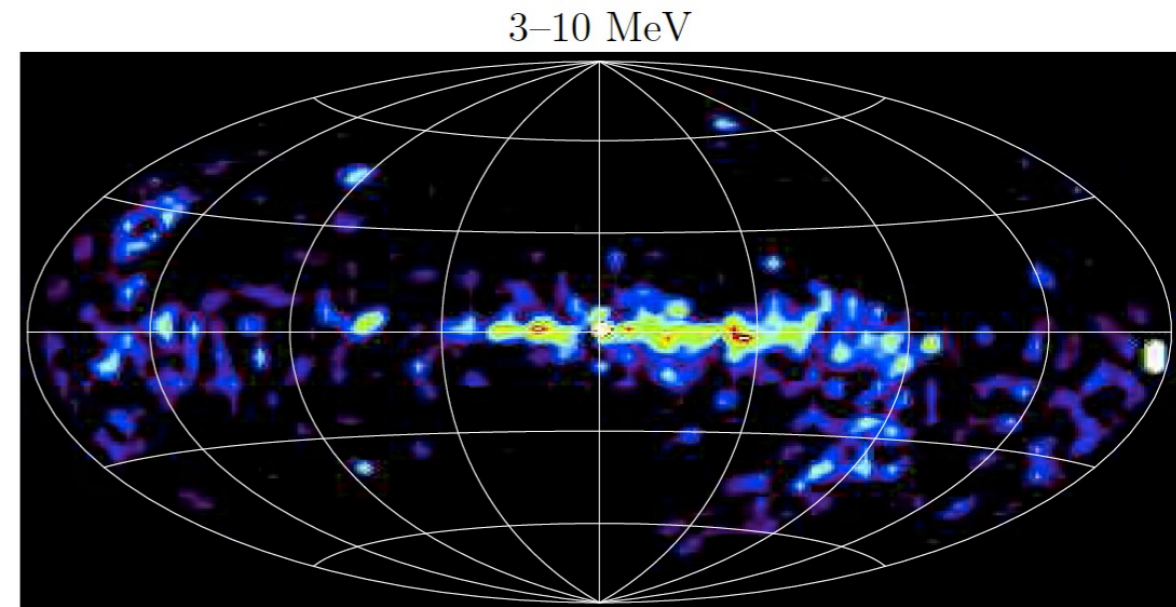
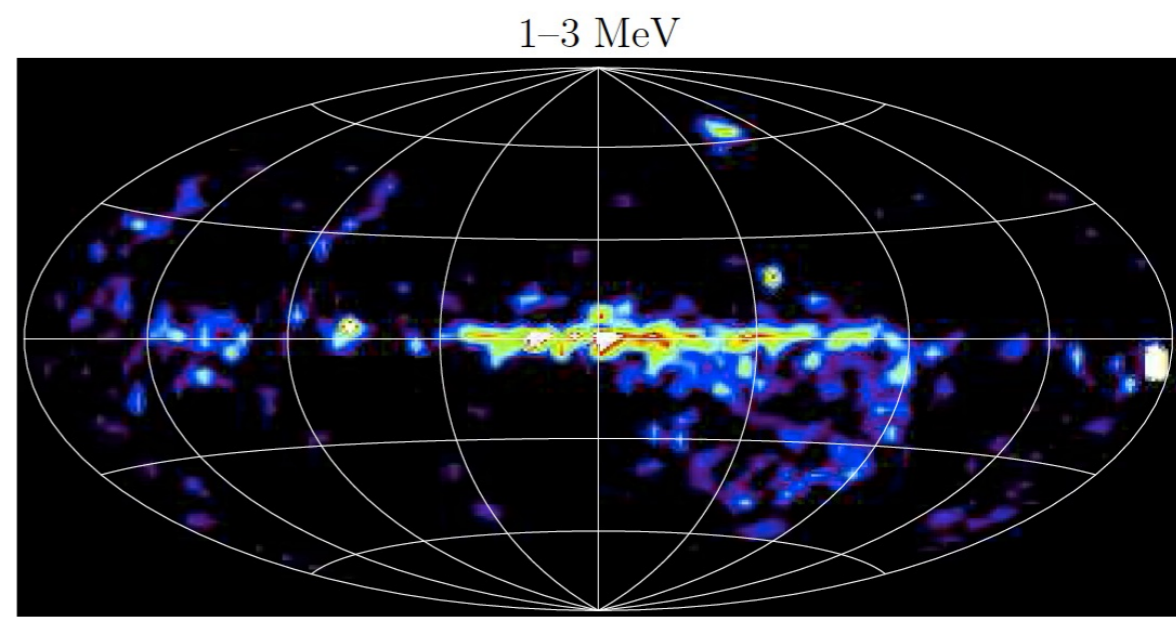
No evidence of significant spectral evolution on the 6 s time scale was detected in this burst.

Spectroscopic results from BATSE have been presented for GRB 910425 in Schaefer et al. (1992), hereafter referred to as S92. Integrating over 39 s, BATSE obtains a single power law model with $\alpha=1.55$ (minimum fit energy of 100 keV). The models with curvature do not significantly improve the fit results. This value for α is slightly harder than the COMPTEL values obtained from the independent low and high range burst modules but is in better agreement with the telescope data. The error on the BATSE slope is not known, so all the fit results may be compatible within the errors.

4.2. GRB 910503

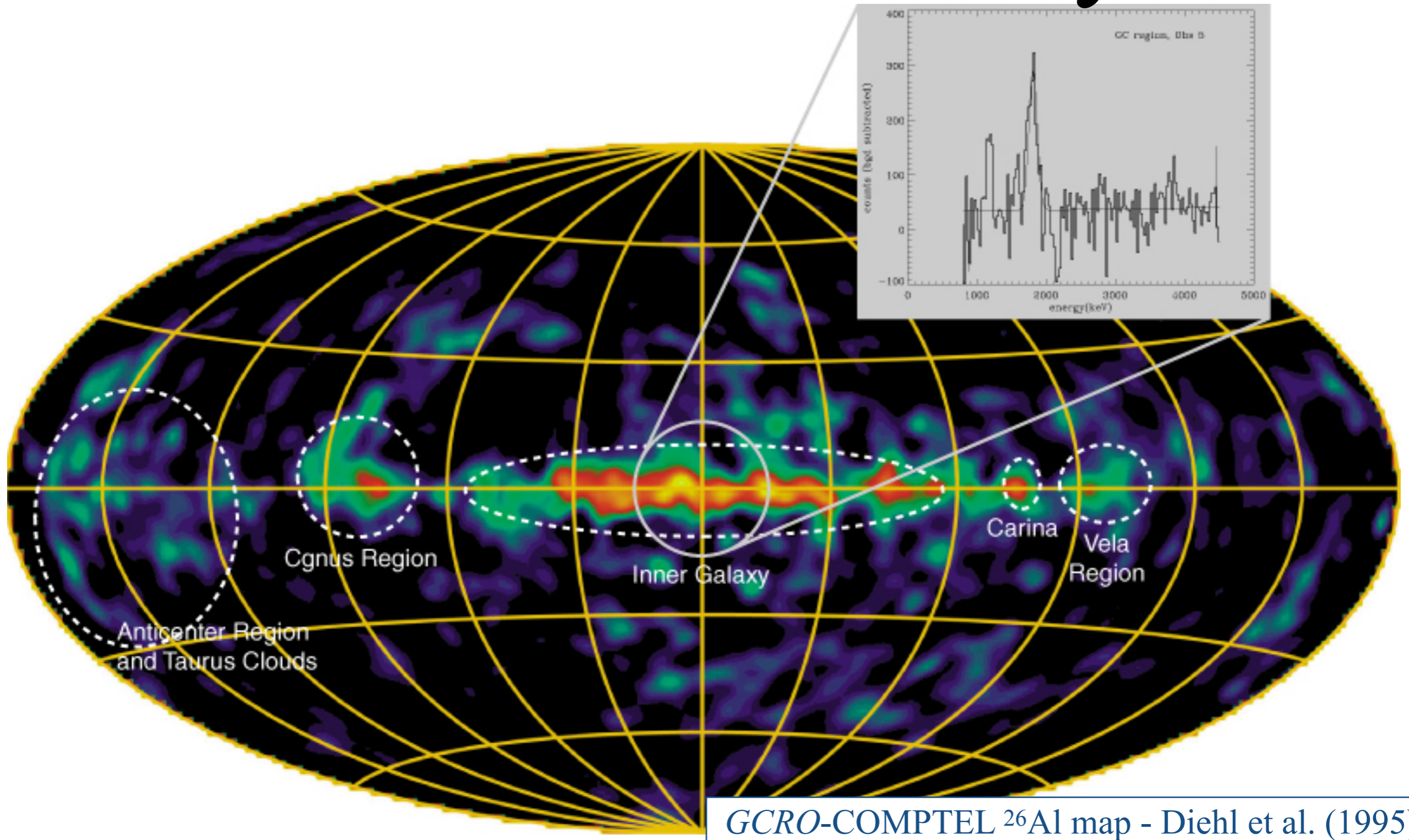
This was the strongest burst observed by COMPTEL ($S(\geq 0.6 \text{ MeV}) = 1.5^{+0.19}_{-0.17} \times 10^{-4} \text{ erg cm}^{-2}$) during the first year of operation (Fig. 8).

At that time, 3 detectors out of 21 (D1-7, D2-1 and D2-5) were not in operation, resulting in 73% operational efficiency in the telescope mode. The time history of the telescope data (Fig. 9) demonstrates the strength of the event, since the high count rate ($\geq 23 \text{ Hz}$, normal event rate $\sim 6 \text{ Hz}$) led to a saturation of the event data buffer prior to transmission. Rapid



GRBs - Hanlon et al. 1994 + Comptel Catalog - Schönfelder et al. (2000)

^{26}Al in the Galaxy



GCRO-COMPTEL ^{26}Al map - Diehl et al. (1995)

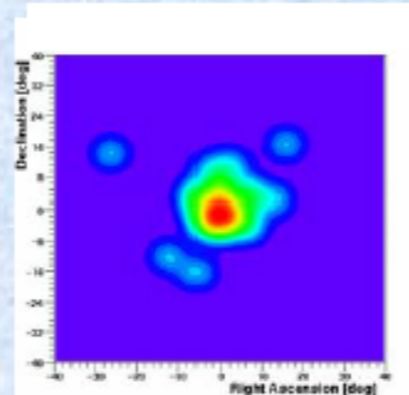
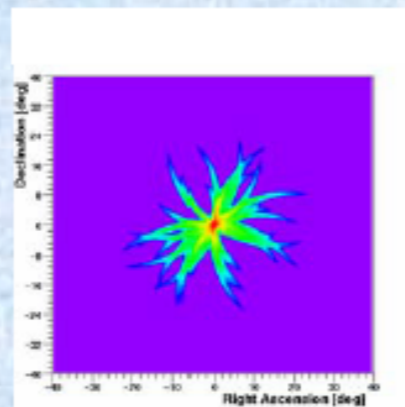
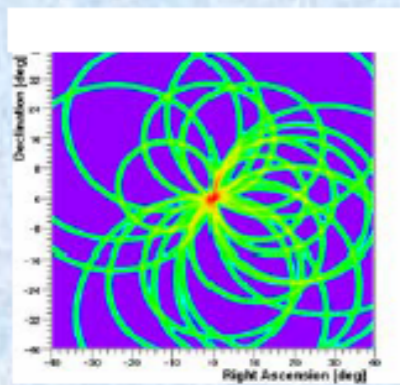
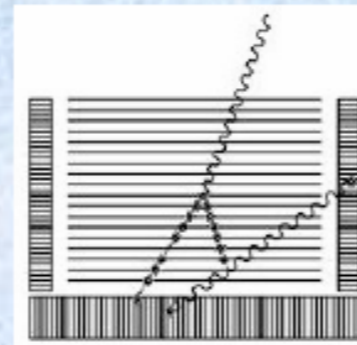
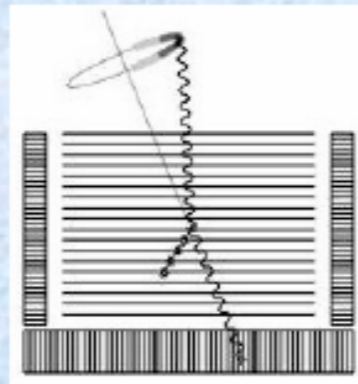
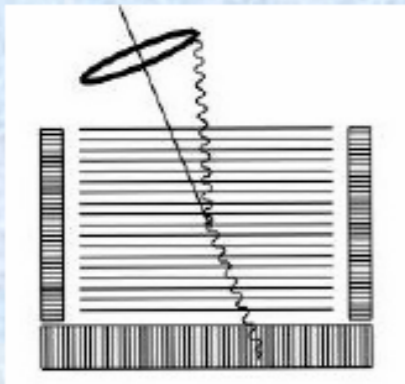
Telescope Schematics

Detectors using Compton Scattering and Pair Creation

Classical Compton
Event Circles
(no electron
tracking)

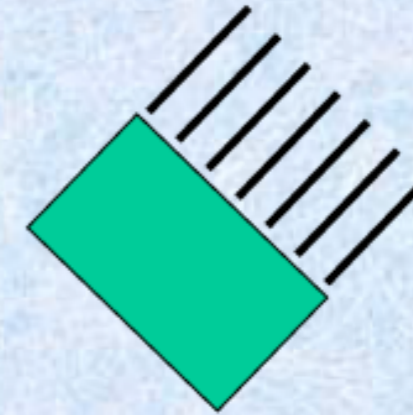
Compton arcs
for events with
electron track or
3rd interaction

Direct imaging of
pair-creation
events

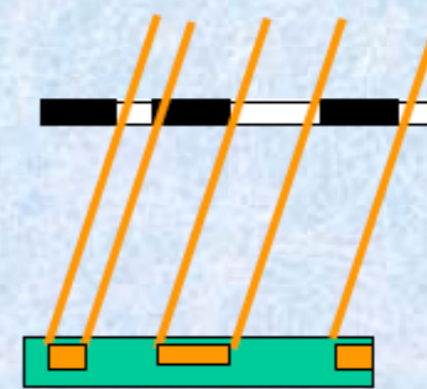


Cosmic Frontiers, Berlin, May 2004

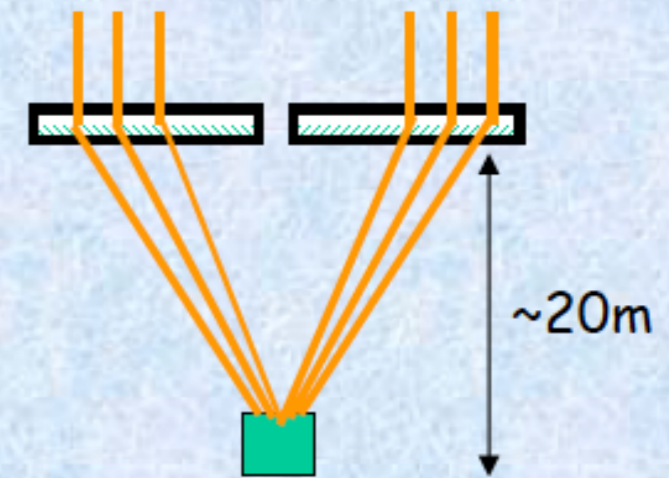
Collimated Detectors



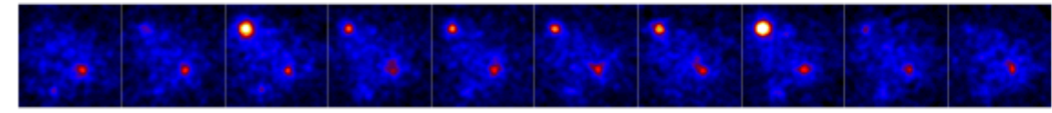
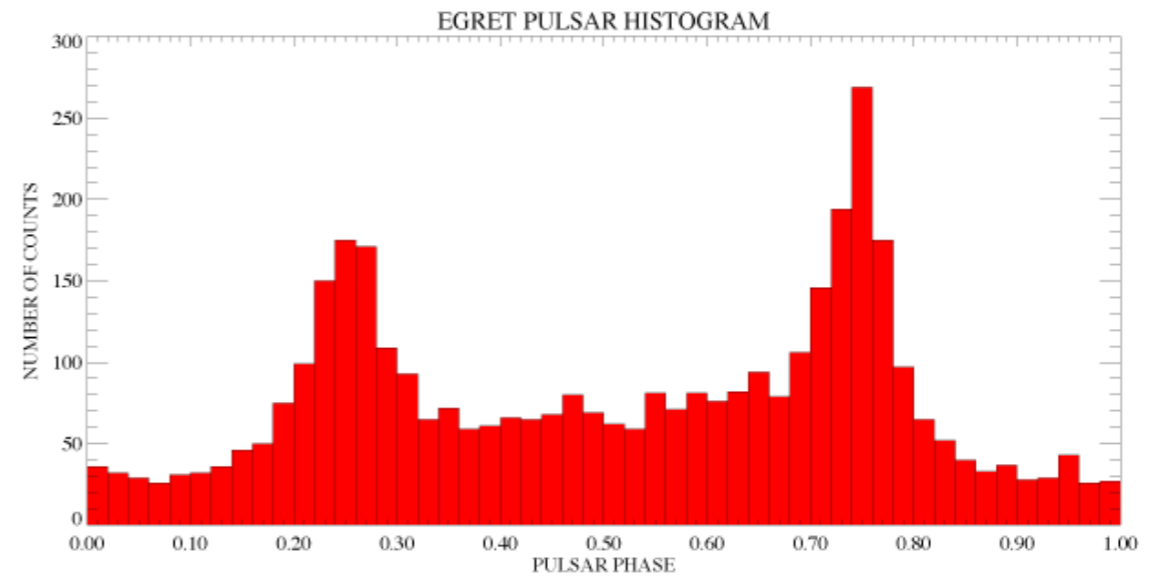
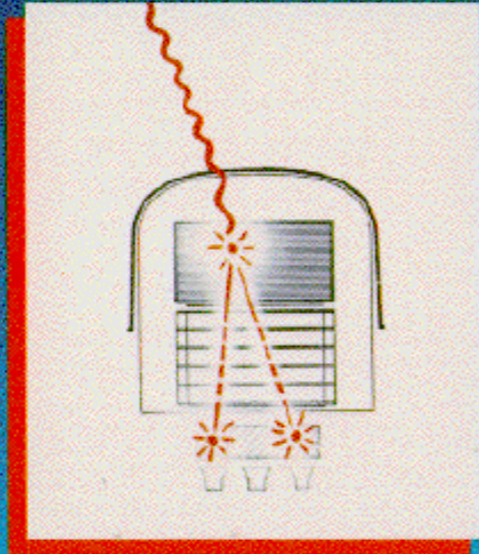
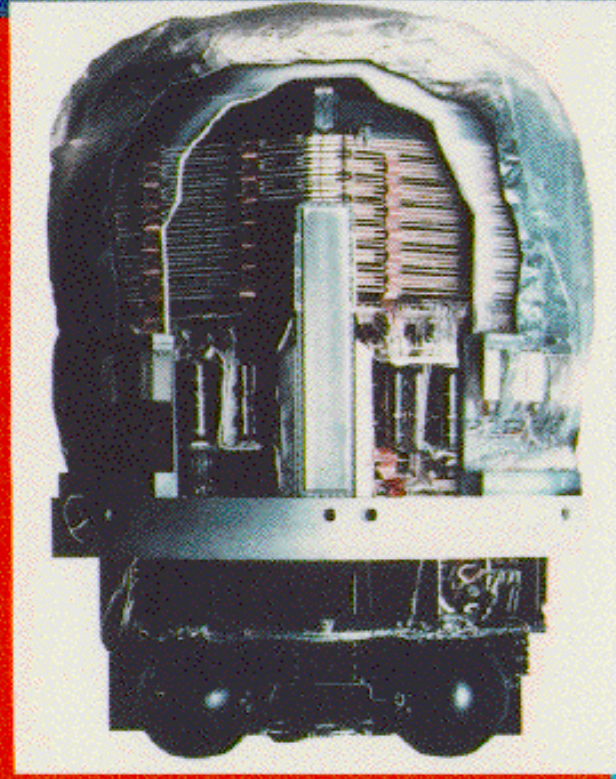
Coded Mask Systems



Laue Lens Telescope

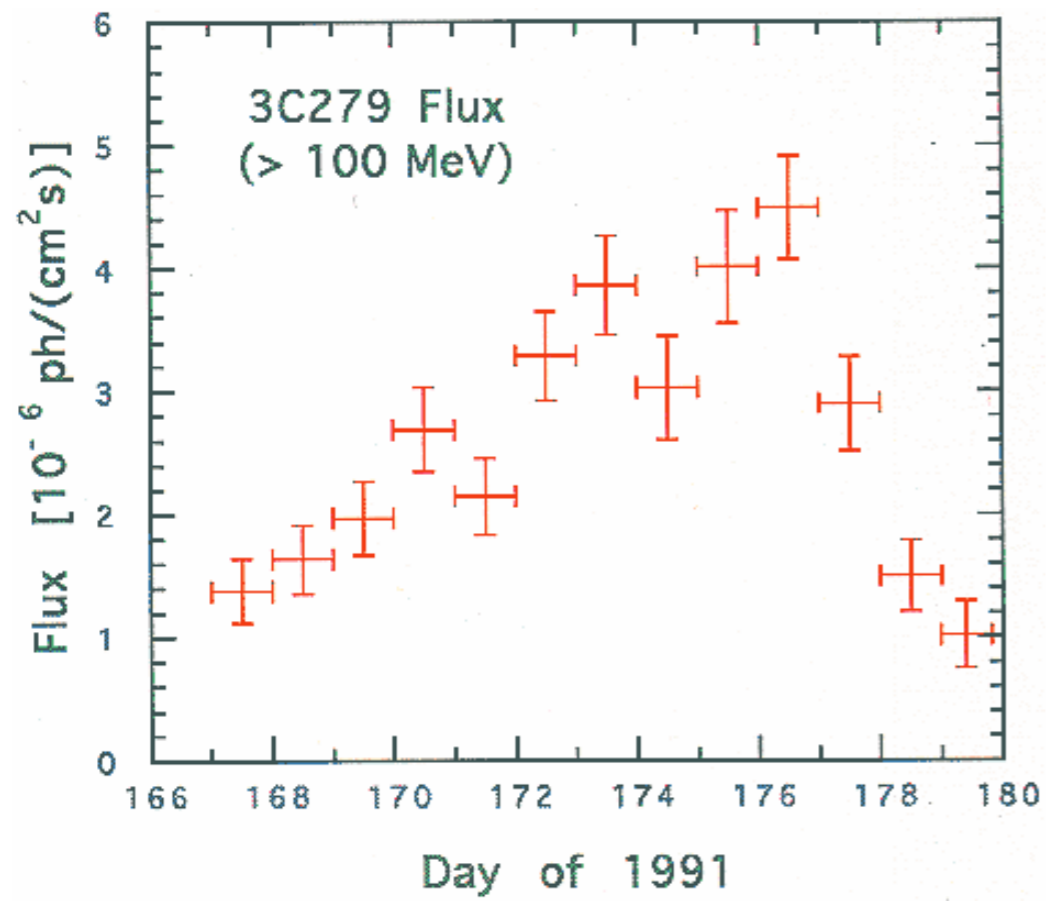
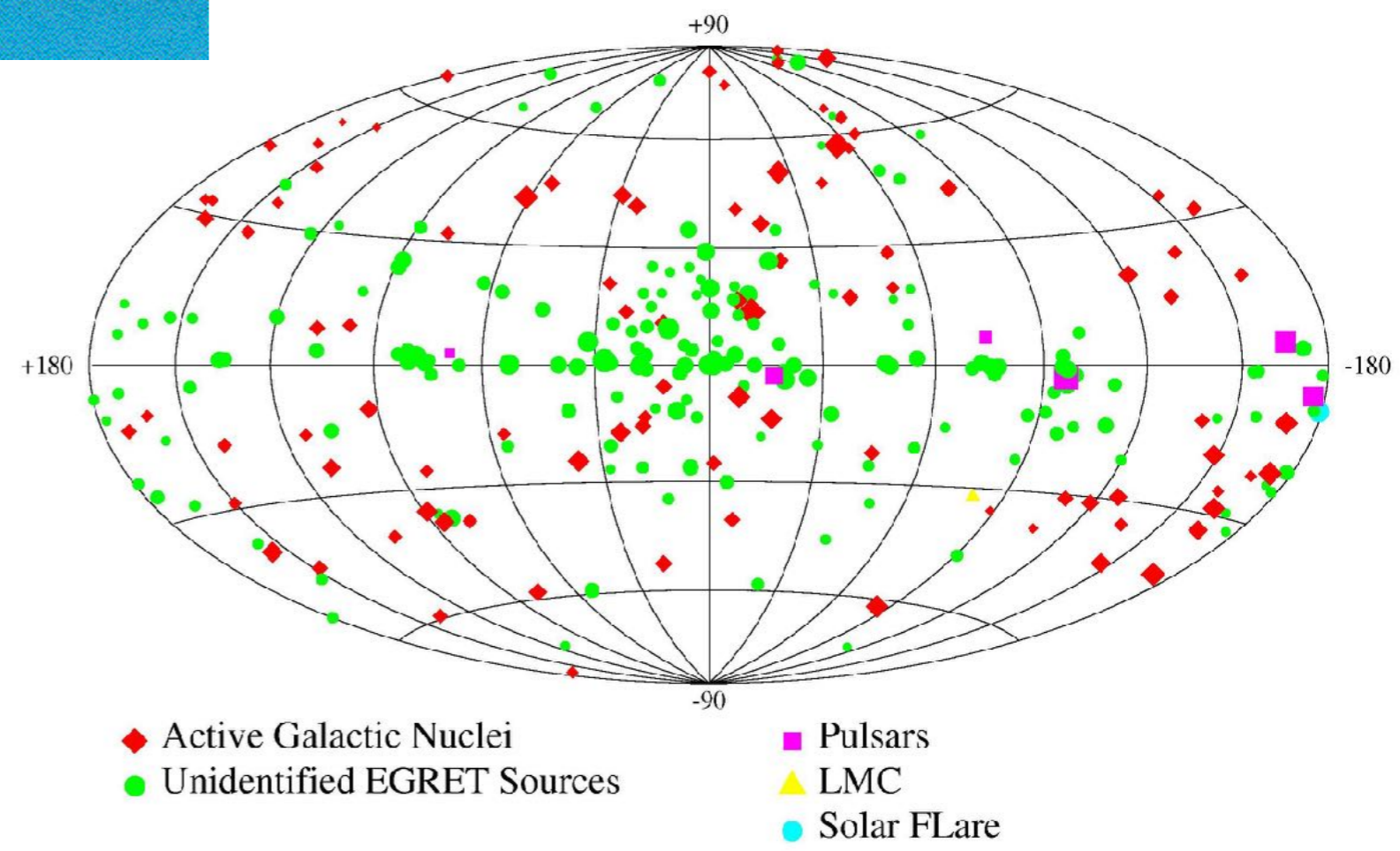


Energetic Gamma Ray Experiment Telescope (EGRET)



Third EGRET Catalog

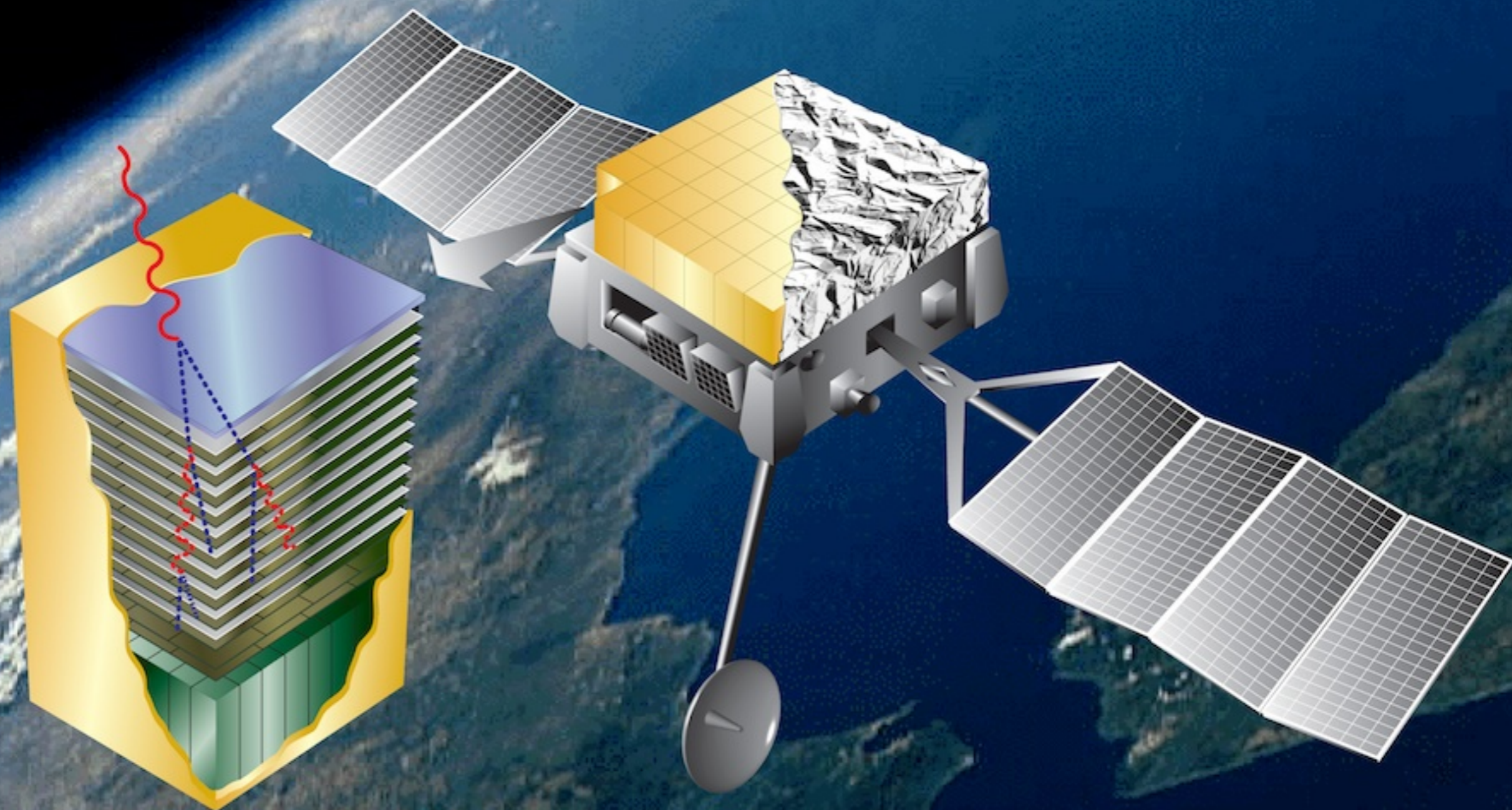
E > 100 MeV







γ-ray detectors @ DRC-SMF - nov 2019



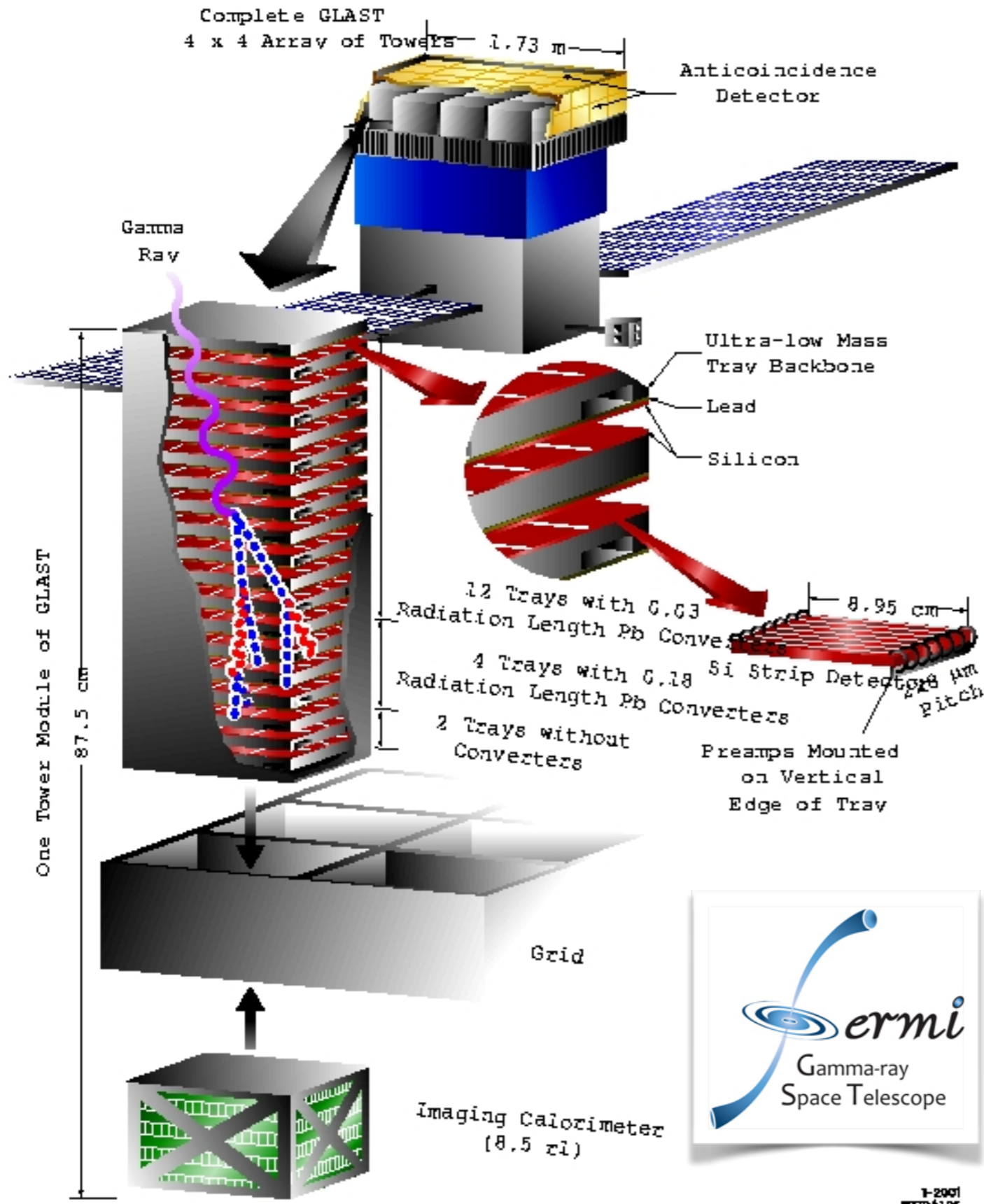
GAMMA-RAY LARGE AREA SPACE TELESCOPE



Exploded View:
One of Forty-nine Towers

-  10 Layers of 0.5 rad Length Converter (pb)
-  12 Layers of XY Silicon Strips
-  Gamma Rays
-  Positrons/Electrons

Some Dimensions are Distorted
for Clarity of Presentation



Fermi-LAT

- *Fermi γ -ray Space Telescope* in orbit since August 2008.
- LAT follows the standard design of a pair production telescope:
 - Converter
 - Tracker
 - Calorimeter
- Over one order of magnitude improvements from CGRO-EGRET

Fermi Gamma-ray Space Telescope (2008–)

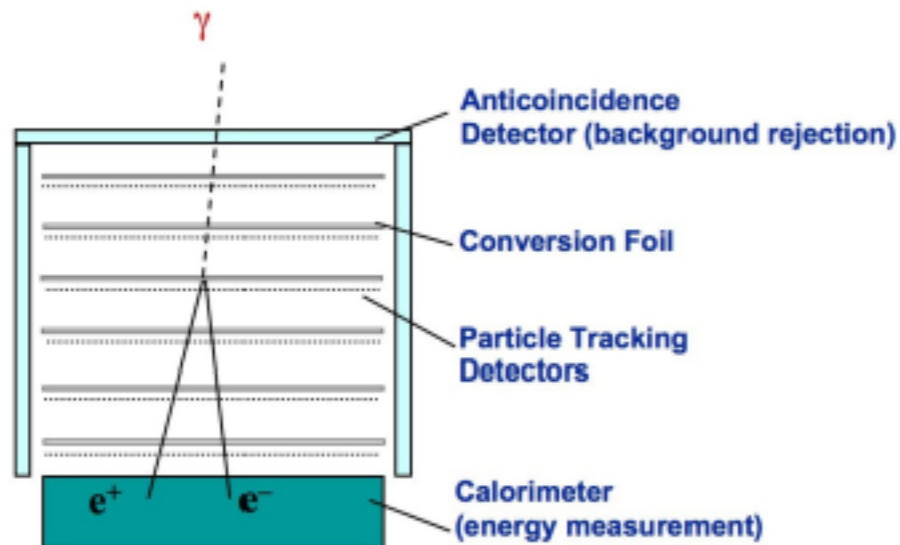
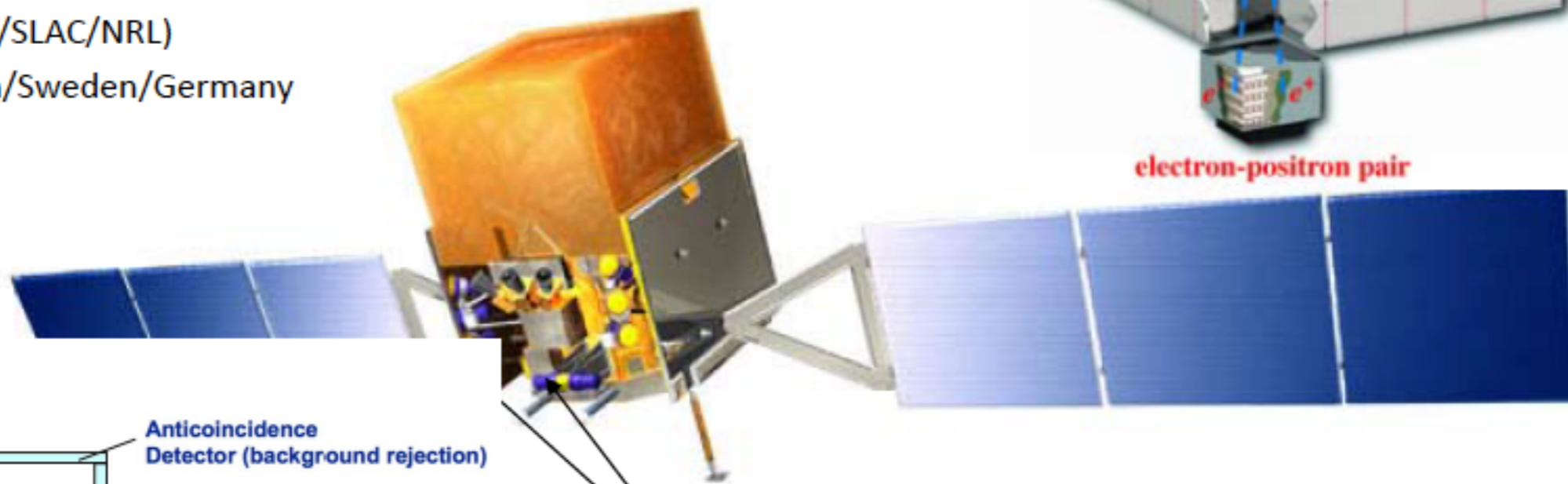
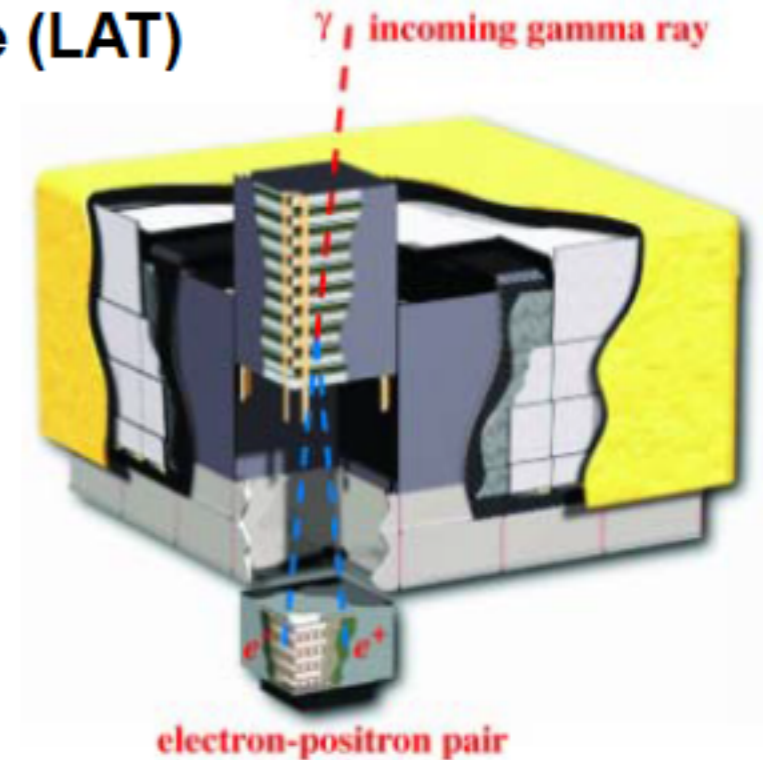
- ❑ NASA/DoE Project
- ❑ Launched June 11, 2008
- ❑ NRL Fermi Involvement
 - Calorimeter
 - Environmental testing
 - Interdisciplinary scientist

USA (GSFC/SLAC/NRL)

Italy/Japan/Sweden/Germany

Large Area Telescope (LAT)

20 MeV → 300 GeV
2.4 sr Field of View

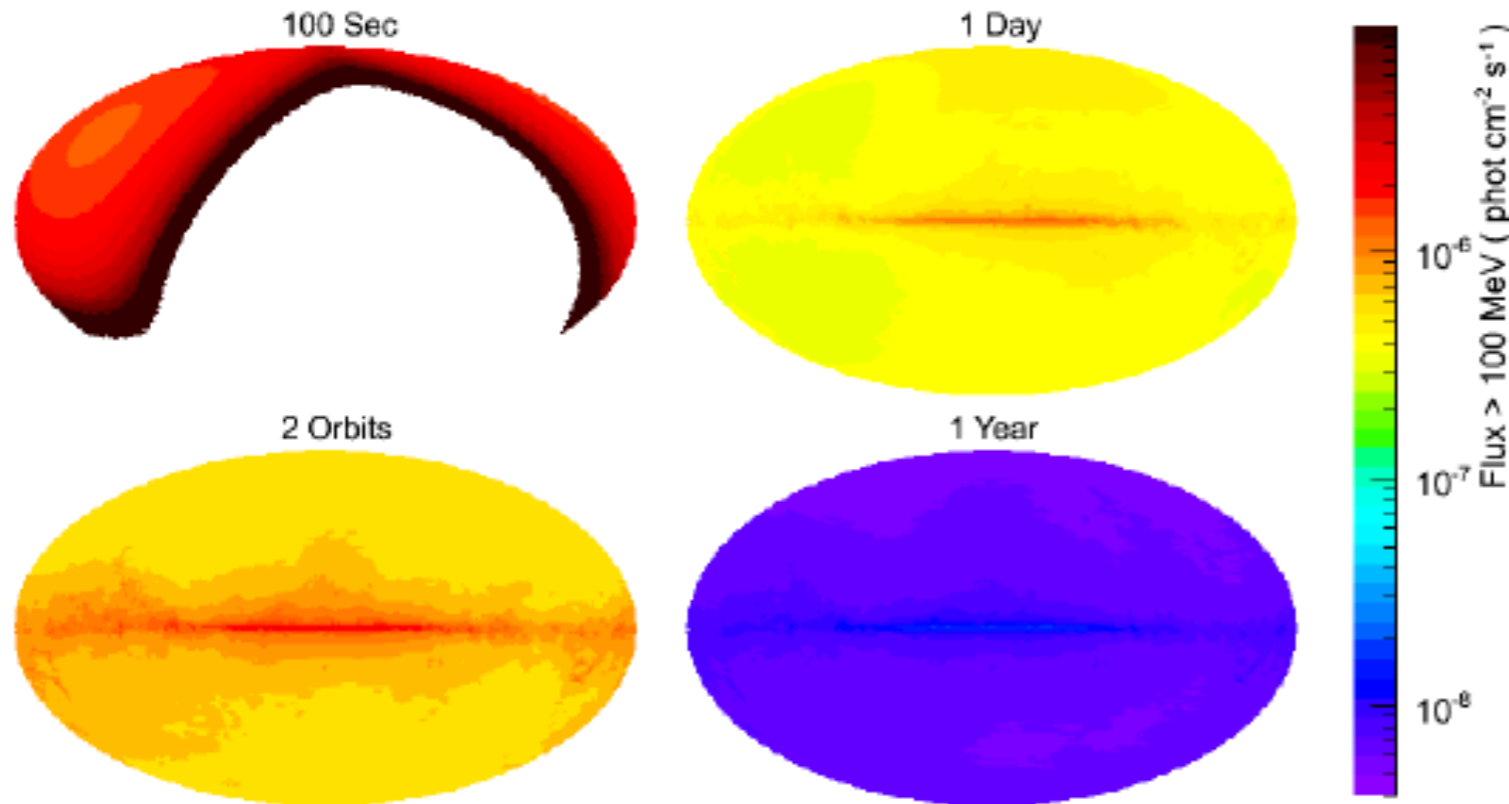


Gamma-ray Burst Monitor (GBM)

8 keV – 40 MeV (12+2 detectors)
Views entire unocculted sky



Operations and observing modes



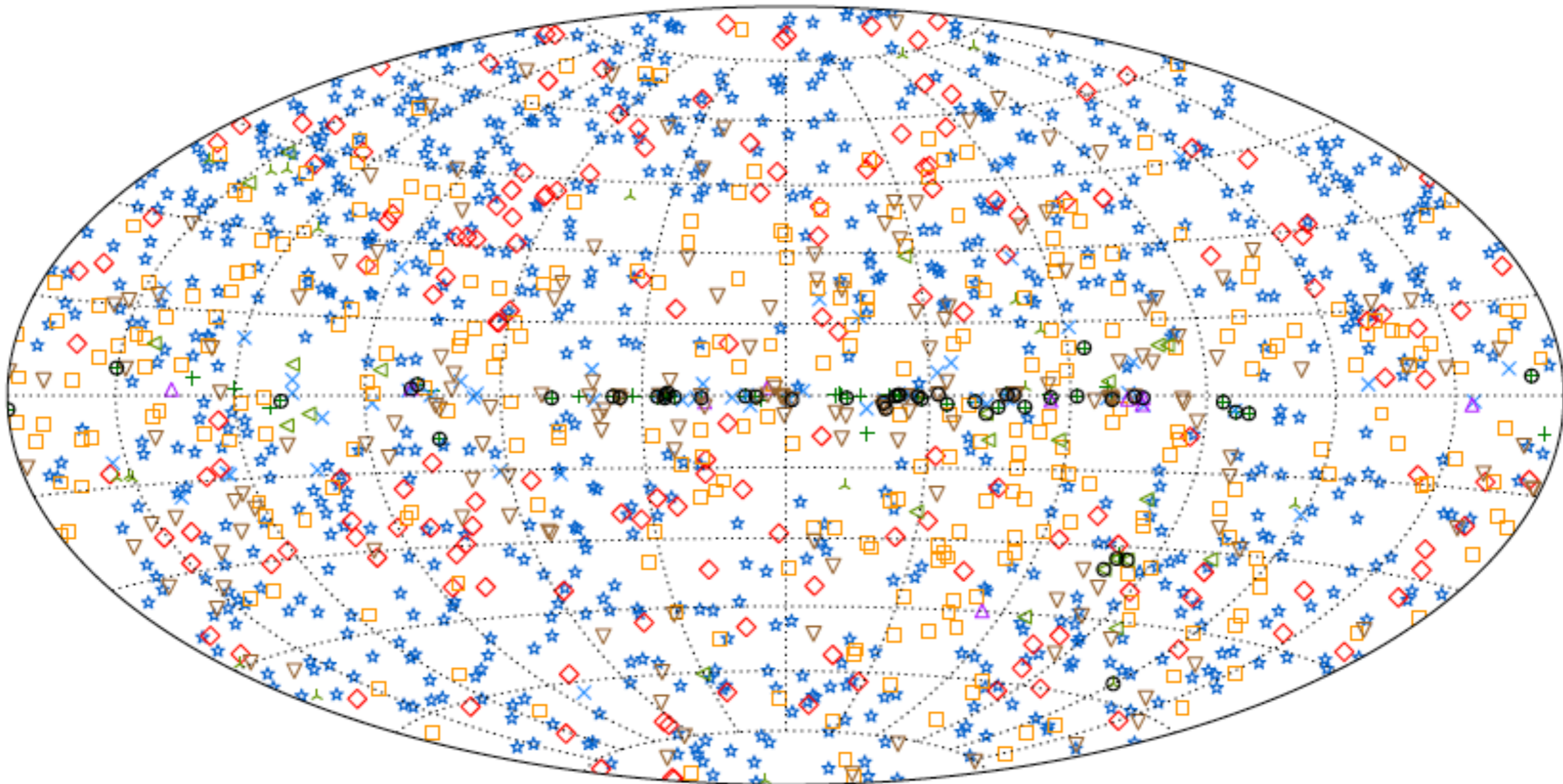
LAT sensitivity on 4 different timescales: 100 s, 1 orbit (96 mins), 1 day and 1 year

- ❑ Almost all observations in survey mode - the LAT observes the entire sky every two orbits (~3 hours), each point on the sky receives ~30 mins exposure during this time.
 - 39 deg rocking angle to Sept 2, 50 deg after September 3, 2009. Very high ontime! ,
- ❑ Autonomous Repointing
 - In response to bright GBM-detected GRBs, LAT-triggered GRBs
- ❑ Dedicated Pointings
 - Crab flares, bright blazars, γ -ray novae

Latest *Fermi*-LAT catalogs

Catalog	Range	Flux	Sources
3FGL (1501.02003)	100 MeV - 300 GeV	$F(1-100 \text{ GeV}) \approx 3 \times 10^{-10} \text{ cm}^{-2} \text{ s}^{-1}$	3033
4FGL (1902.10045)	50 MeV - 1 TeV	$F(1-100 \text{ GeV}) \approx 2 \times 10^{-10} \text{ cm}^{-2} \text{ s}^{-1}$	5098
2FHL (1508.04449)	50 GeV - 2 TeV	$F(50 \text{ GeV} - 2 \text{ TeV}) \approx 8 \times 10^{-12} \text{ cm}^{-2} \text{ s}^{-1}$	360
3FHL (1702.00664)	10 GeV - 2 TeV	$F(10 \text{ GeV} - 2 \text{ TeV}) \approx 3 \times 10^{-11} \text{ cm}^{-2} \text{ s}^{-1}$	1558

Plus FGES, 3LAC, 3-year PSRs, SNR, LAT-GRBs,
GBM-GRBs, 2FAV catalogs!



+	SNRs and PWNe	★	BL Lacs	□	Unc. Blazars	▲	Other GAL	▼	Unassociated
×	Pulsars	◆	FSRQs	▽	Other EGAL	△	Unknown	○	Extended

ky map, in Galactic coordinates and Hammer–Aitoff projection, showing the objects in the 3FHL catalog classified by their most likely sou

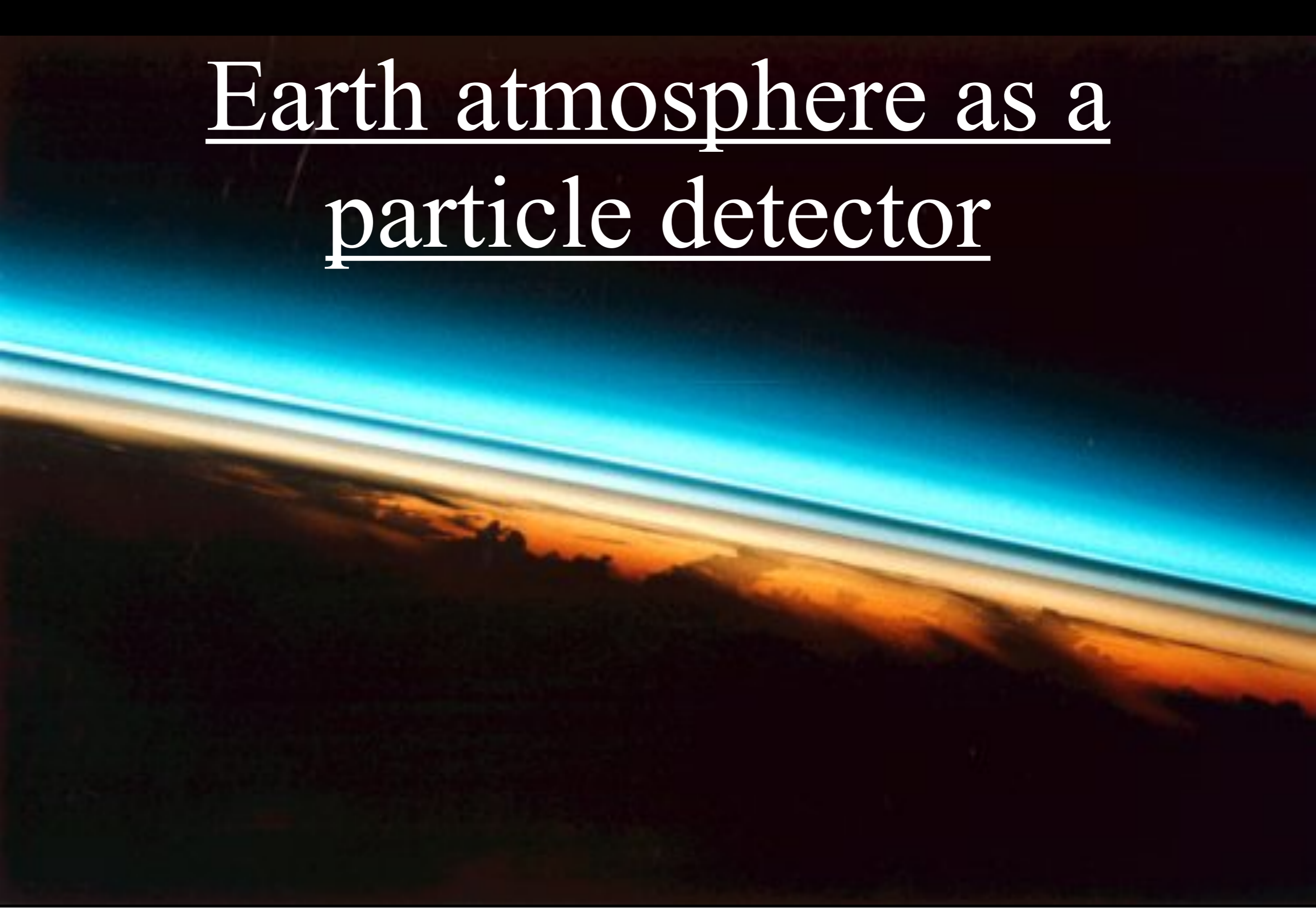
The 3FHL Fermi-LAT Catalog of celestial sources of photons with energies larger than 10 GeV. Out of 1556 sources, 1231 are AGN.

Table 7. LAT 4FGL Source Classes

Description	Identified		Associated	
	Designator	Number	Designator	Number
Pulsar, identified by pulsations	PSR	231
Pulsar, no pulsations seen in LAT yet	psr	10
Pulsar wind nebula	PWN	12	pwn	6
Supernova remnant	SNR	24	snr	15
Supernova remnant / Pulsar wind nebula	SPP	2	spp	90
Globular cluster	GLC	0	glc	30
Star-forming region	SFR	3	sfr	0
High-mass binary	HMB	5	hmb	3
Low-mass binary	LMB	1	lmb	1
Binary	BIN	1	bin	0
Nova	NOV	1	nov	0
BL Lac type of blazar	BLL	22	bll	1080
FSRQ type of blazar	FSRQ	42	fsrq	639
Radio galaxy	RDG	6	rdg	35
Non-blazar active galaxy	AGN	1	agn	16
Steep spectrum radio quasar	SSRQ	0	ssrq	2
Compact Steep Spectrum radio source	CSS	0	css	5
Blazar candidate of uncertain type	BCU	3	bcu	1152
Narrow line Seyfert 1	NLSY1	3	nlsy1	5
Seyfert galaxy	SEY	0	sey	1
Starburst galaxy	SBG	0	sbg	7
Normal galaxy (or part)	GAL	2	gal	2
Unknown	UNK	0	unk	118
Total	...	359	...	3215
Unassociated	1525

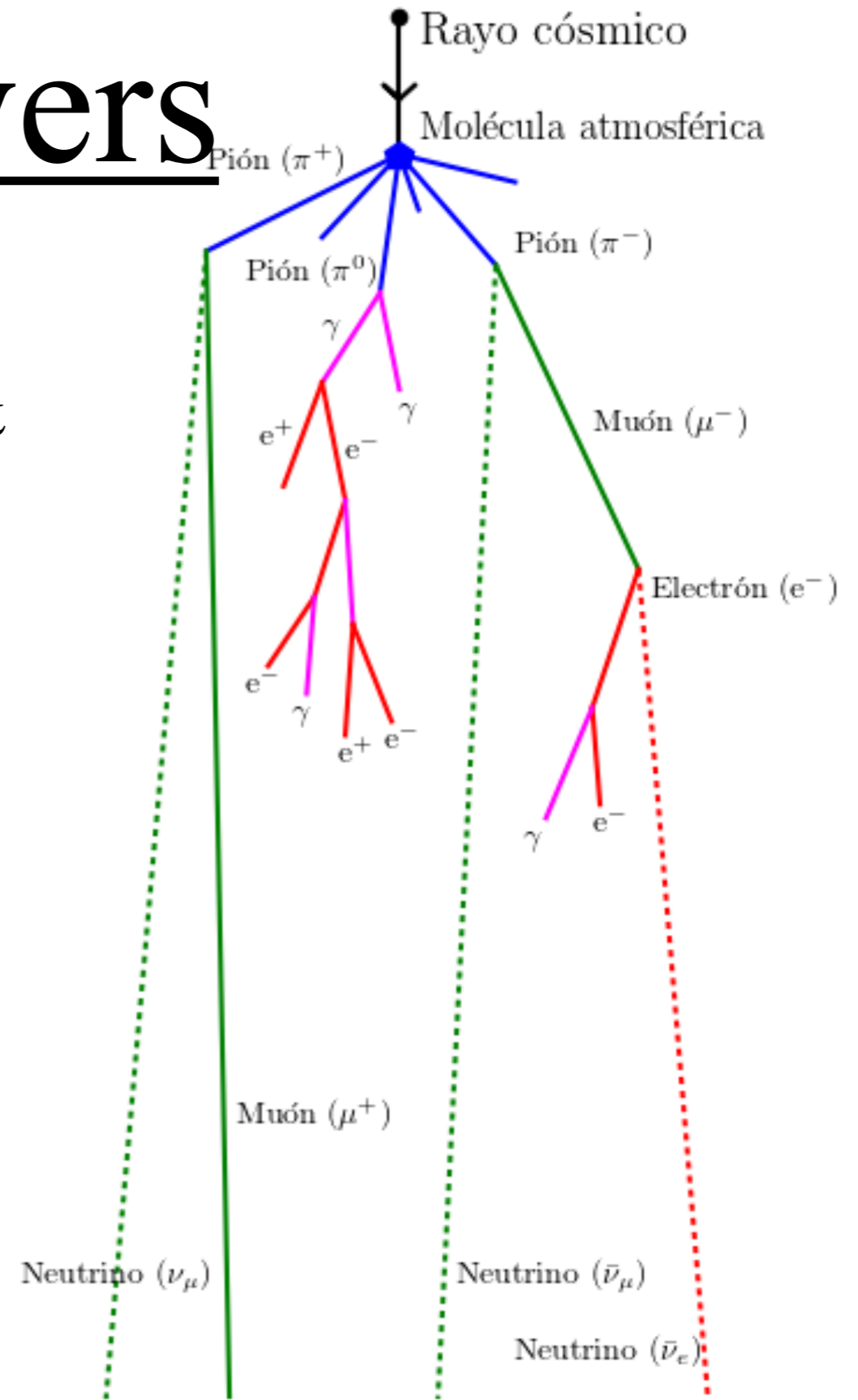
NOTE—The designation ‘spp’ indicates potential association with SNR or PWN. Designations shown in capital letters are firm identifications; lower case letters indicate associations.

Earth atmosphere as a particle detector



Air showers

- Atmospheric air shower cascades were discovered and first studied by Blackett & Occhialini (1933), Bruno Rossi (1934), Pierre Auger (1938).
- First cascade theories by Carlson & Oppenheimer (1936), Bhabha & Heitler (1936).
- Cascades develop down to respective thresholds.
- Detectable with ground based arrays; through atmospheric emission of light; or, more recently, radio emission.

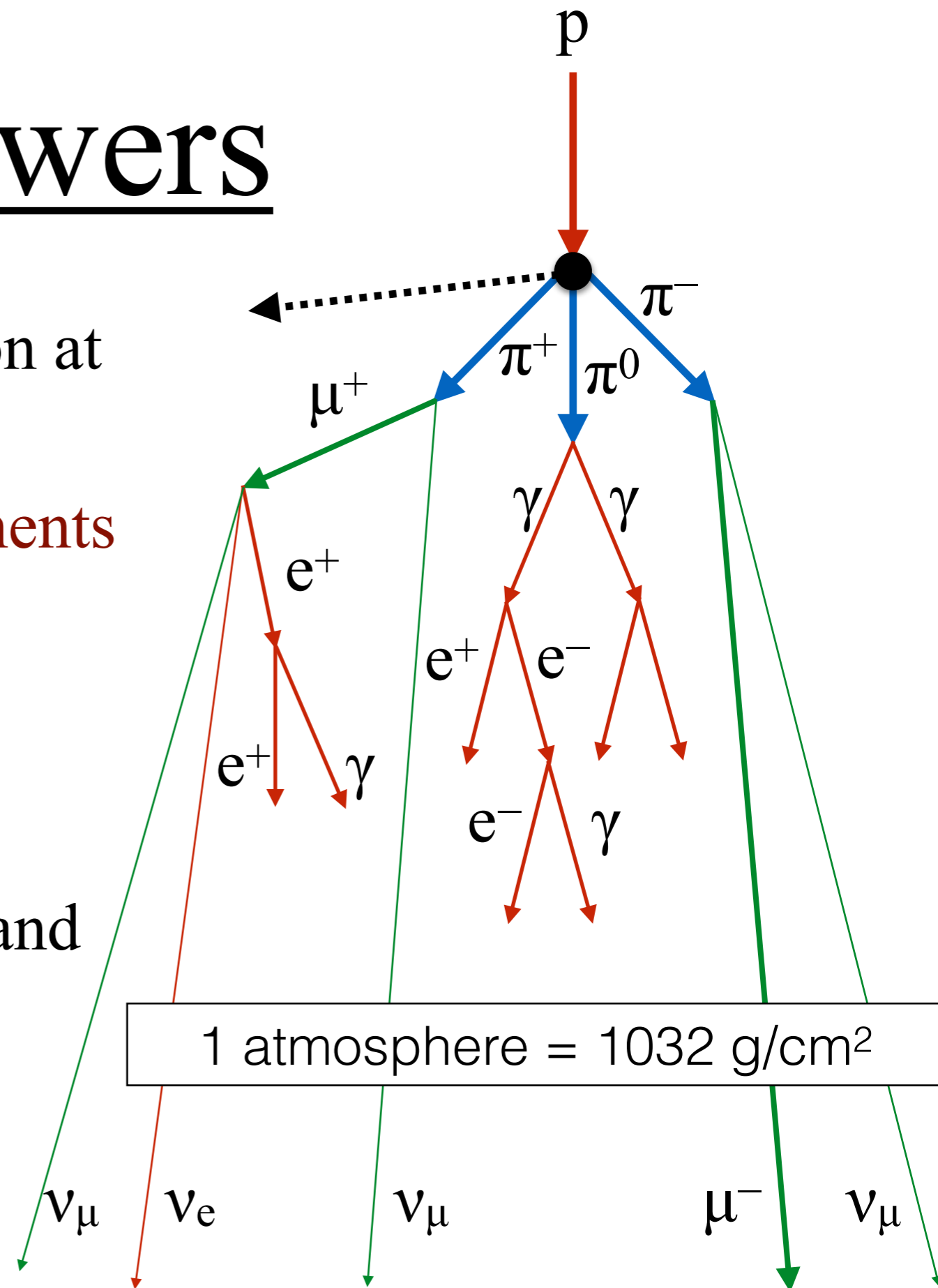


Hadronic showers

- Initiated by a nuclear interaction at about 80 g/cm²:



- The cascade has nuclear, muon and electromagnetic components.
- Muons and neutrinos continue traveling underground.



Electromagnetic showers

- Initiated by a photon or an electron.

- Pair production:

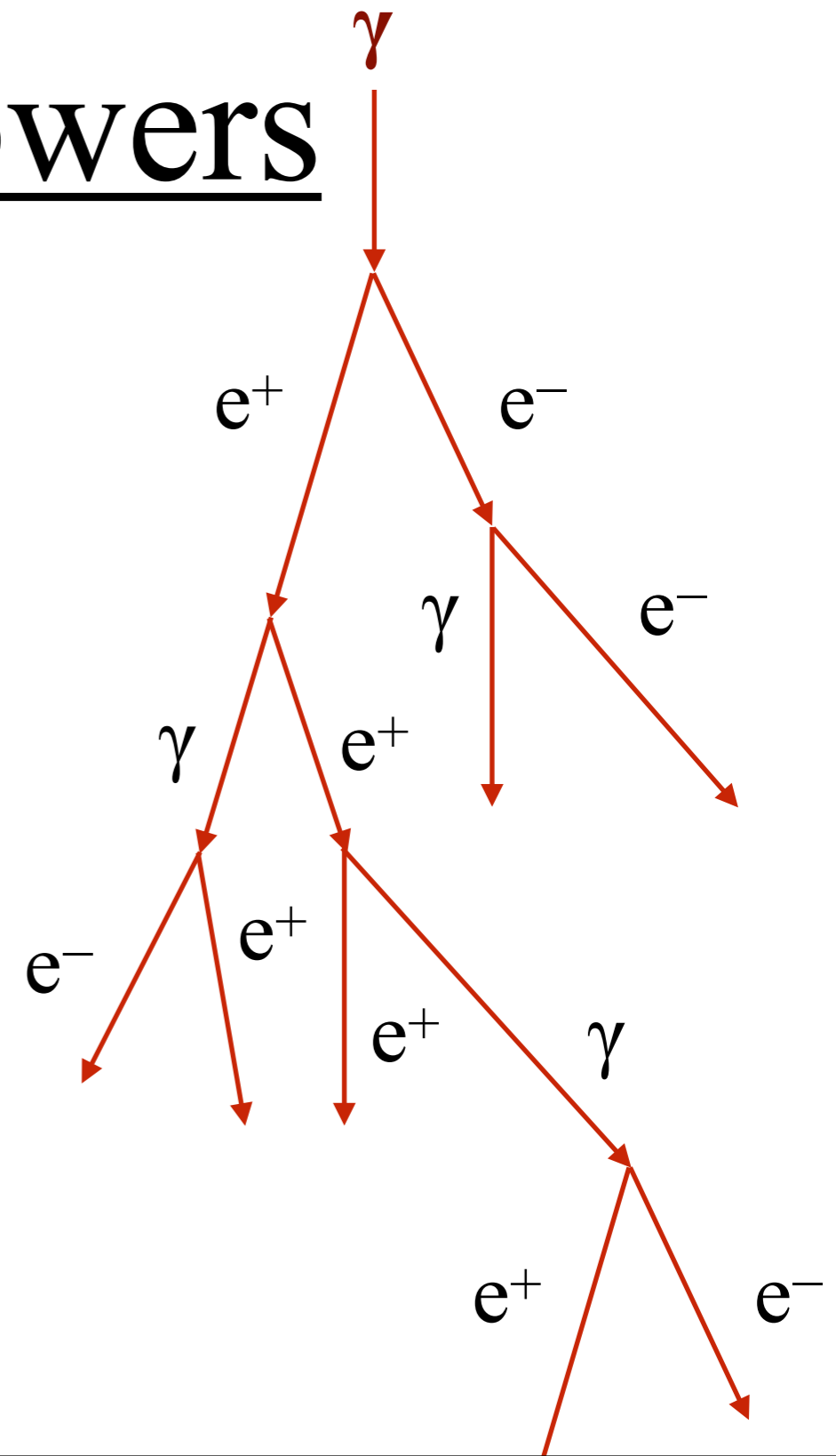


ceases when the energy is such that the Compton cross section becomes dominant ($\sim 80 \text{ MeV}$).

- Bremsstrahlung:



ceases when ionization becomes dominant ($\sim 35 \text{ MeV}$).

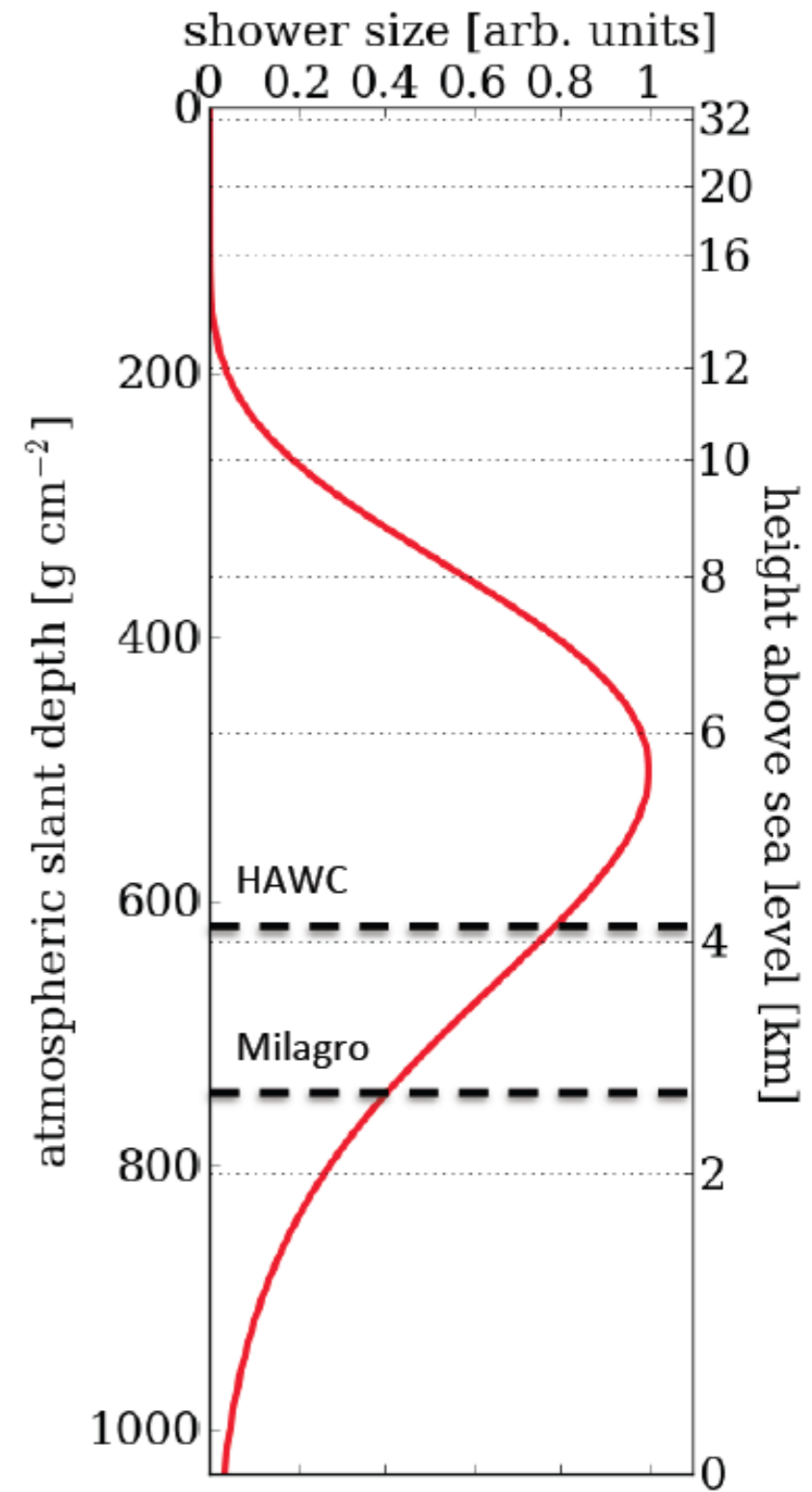
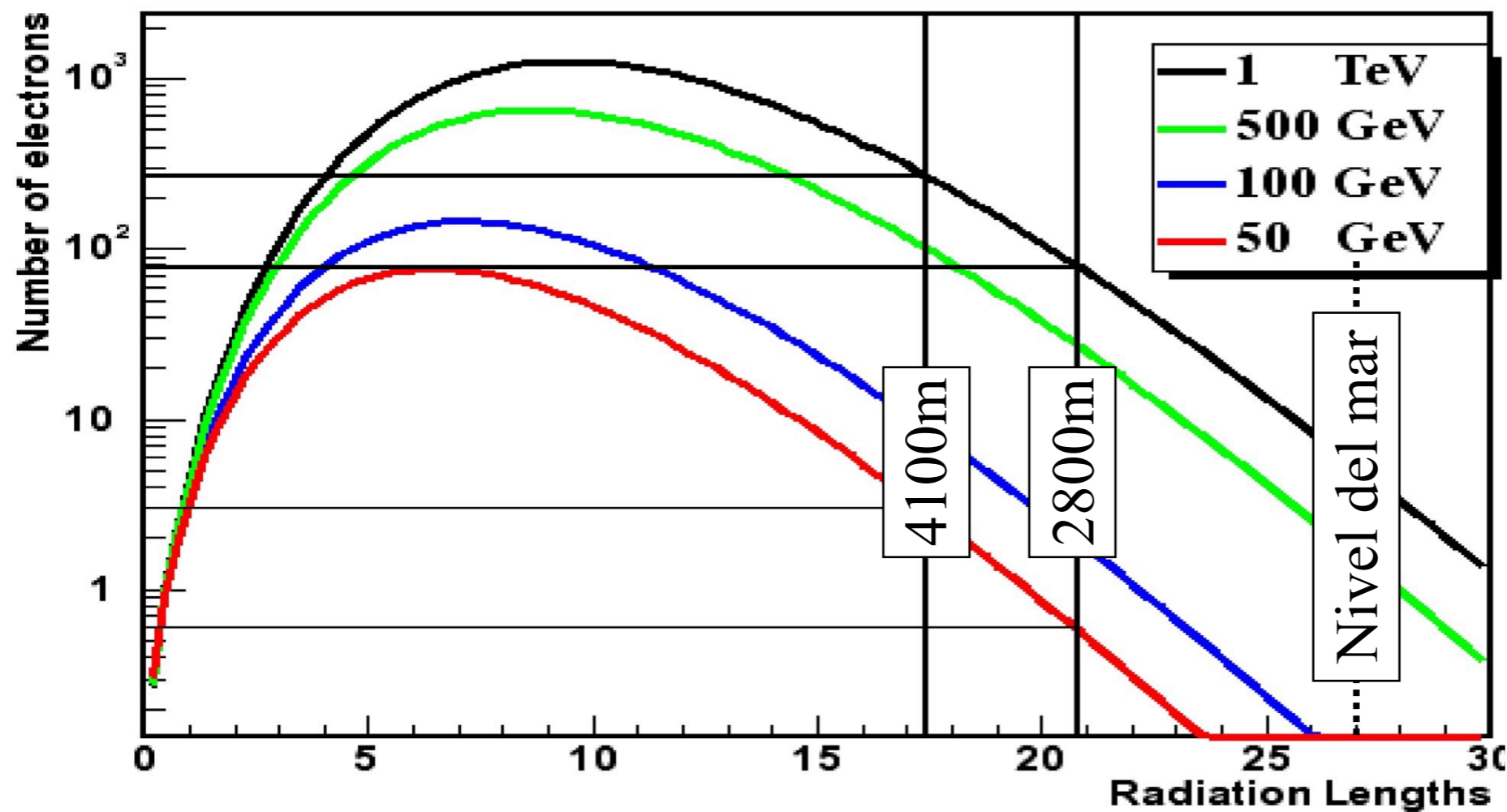


1 atmósfera = 1032 g/cm²

Techniques

- Detect Cherenkov light from secondary particles in the shower.
 - Detect fluorescent light induced by secondary particles in the shower.
 - Detect the secondary particles directly on the ground.
-
- Detect radio emission from secondary particles:
Askaryan effect.
 - Variations are used for UHE cosmic rays and neutrinos.

The atmosphere is part of the detector



Earth atmosphere

International Standard Atmosphere

Layer	Z_{g0} (km)	z_0 (km)	dT/dz (K/km)	$T(z_0)$ (°C)	$P(z_0)/g$ (g/cm ²)
Troposphere	0	0.0	-6.5	+15.0	1032
Tropopause	11	11.019	0.0	-56.5	231
Stratosphere (I)	20	20.063	+1.0	-56.5	56
Stratosphere (II)	32	32.162	+2.8	-44.5	8.9
Stratopause	47	47.350	0.0	-2.5	1.1
Mesosphere (I)	51	51.413	-2.8	-2.5	0.7
Mesosphere (II)	71	71.802	-2.0	-58.5	0.0
Mesopause	84.852	86	—	-86.2	0.0

AN EXPERIMENT ON AIR SHOWERS PRODUCED BY HIGH-ENERGY COSMIC RAYS

By Drs. G. CLARK, J. EARL, W. KRAUSHAAR, J. LINSLEY, B. ROSSI and F. SCHERB

Department of Physics and Laboratory for Nuclear Science, Massachusetts Institute of Technology, Cambridge, Massachusetts

PROBLEMS of interest to both the physicist and the astrophysicist single out the high-energy component of cosmic rays as a particularly promising subject of research. On one hand, the shape of the spectrum and the directional distribution of the incoming particles depend critically on the structure of the galaxy and on the mechanism responsible for the acceleration of cosmic rays. On the other hand, despite the remarkable progress of accelerators, we still have to turn to cosmic rays in order to obtain information on the fundamental problem of nuclear interactions at energies which, in the centre of mass of the colliding particles, are greatly in excess of the rest-energy of nucleons.

The cosmic-ray spectrum falls off rapidly with increasing energy. Thus particles of very high energies are exceedingly rare; for example, the rate of arrival of particles with more than 10^{16} eV. energy is of the order of one per year per square metre. Hence direct methods of detection are ruled out, and the only practical approach is the study of the giant showers that are produced in the atmosphere by high-energy cosmic-ray particles.

The essential features of this phenomenon are well known. After a comparatively short path through air, the primary particle collides against an atomic nucleus, producing a number of high-energy secondary particles. Among these are π^0 -mesons, which immediately decay into photons, and nuclear-active particles (charged π -mesons, nucleons, etc.), which go on to produce further interactions, so that a nuclear cascade develops. At each step a certain fraction of the energy goes into photons via the decay of π^0 -mesons; photons initiate electronic cascades and soon electrons and photons become the dominant component of the shower. Some of the charged π -mesons, however, decay before interacting and thus contribute an appreciable number of μ -mesons to the

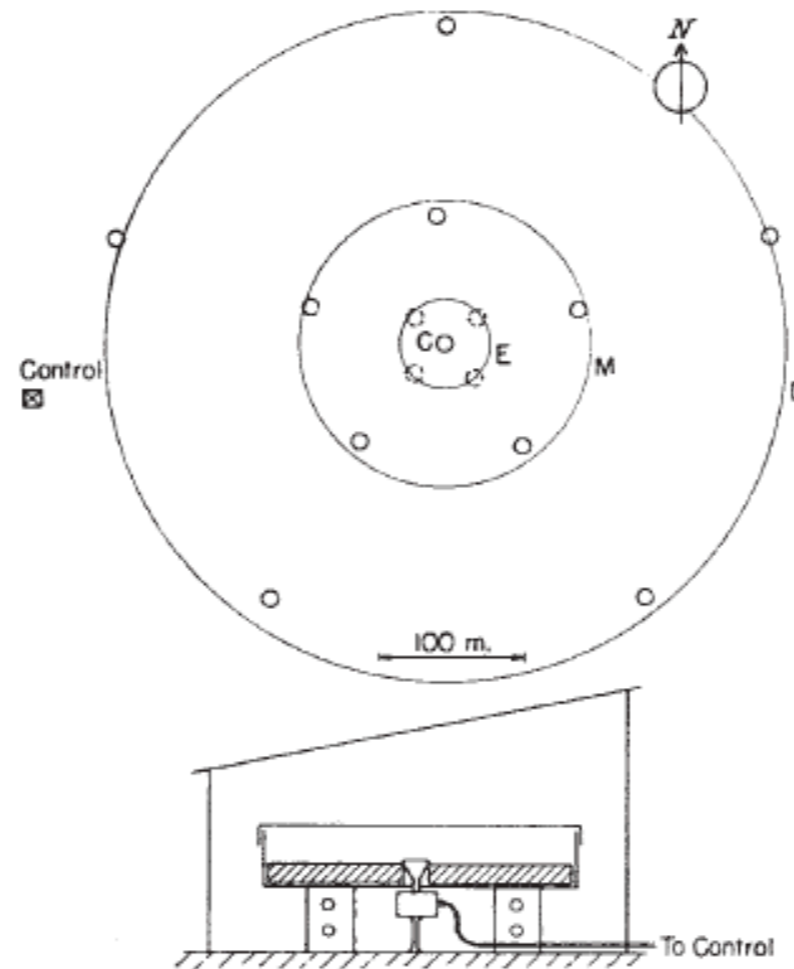


Fig. 1. Detector array and schematic diagram of a scintillation counter

detectors (*C*, *M* and *D* in Fig. 1), but during a short period we had four additional detectors placed near the centre of the array (*E* in Fig. 1) in order to extend our measurements to showers of smaller size than those which could be recorded in the main experiment. The detectors are connected by cables to separate oscilloscopes, which are situated in a control station and arranged one next to the other so that

Un estudio de cascadas por primarias con $E \geq 10^{16}$ eV

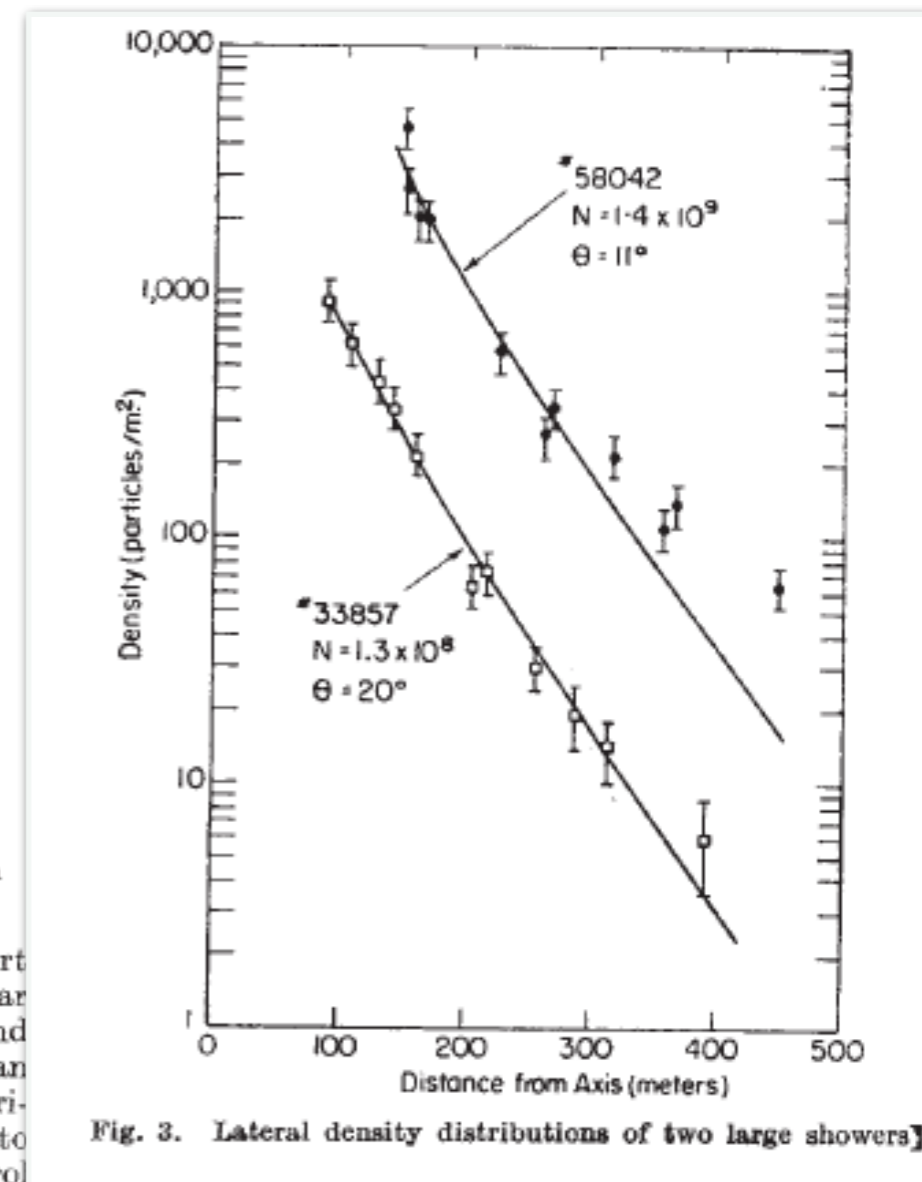


Fig. 3. Lateral density distributions of two large showers

Cherenkov radiation

- ▶ Cherenkov radiation occurs when a charged particle travels faster than light in a medium: $v > c/n$, with $n(\nu)$ the index of refraction of the medium.
- ▶ The emission is restricted to a cone of aperture $\cos \theta = 1/\beta n$.
- ▶ The emission per unit length is,

$$\frac{dE}{d\ell} = \frac{2\pi e^2 \nu}{c^2} \left(1 - \frac{1}{\beta^2 n(\nu)^2} \right).$$

Medium	n	Threshold (γ)	θ	$dE/d\ell$ (\circ) eV/cm
Air	1.00029	40.8	1.4	0.34
Water	1.335	1.5	41.2	327



By H. Seldon - vlastni dilo, own work, Public Domain, <https://commons.wikimedia.org/w/index.php?curid=2557072>



γ -ray detectors @ DRC-SMF - nov 2019



Gamma-ray astronomy

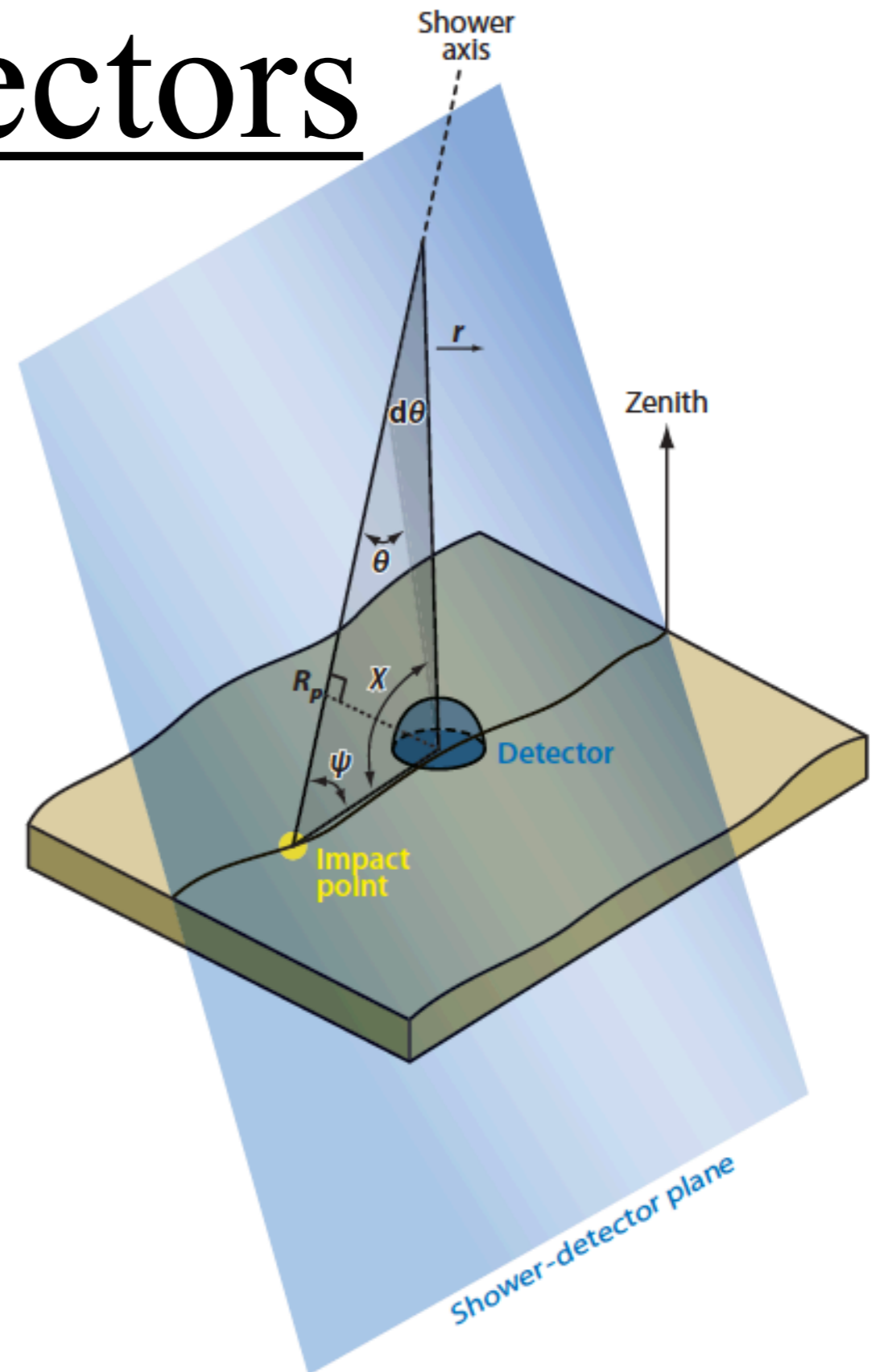
1947 Blackett estimates the contribution of cosmic-ray-induced **Cherenkov** light to be 0.01% of the total intensity of the night sky (general flux of cosmic rays)

1953 Bill Galbraith and John Jelley detect Cherenkov radiation from extended air showers with a dustbin, a 60 cm diameter mirror and a PMT at its focus in coincidence with a nearby Geiger-Müller array. They later confirm it is Cherenkov light in measurements at the Pic du Midi.



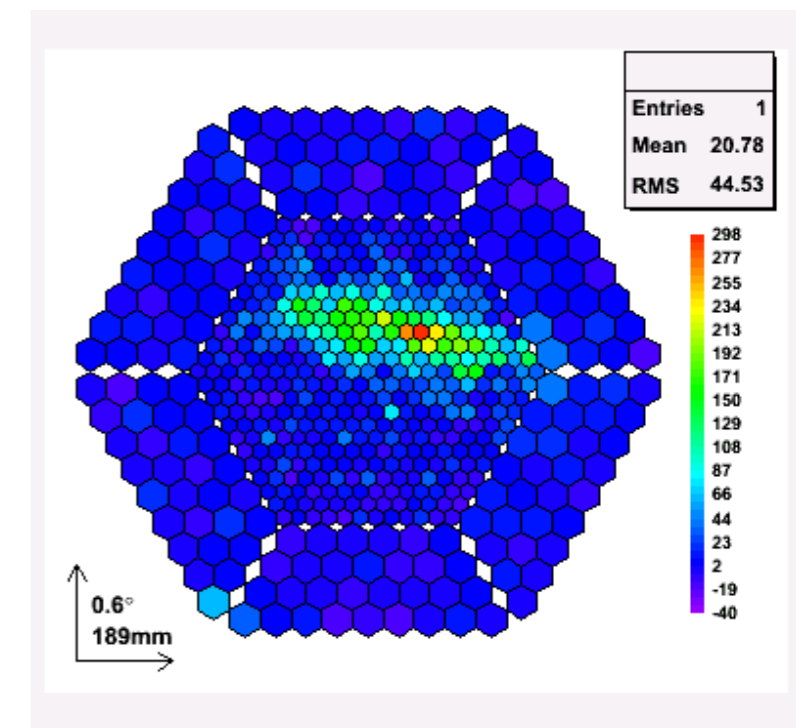
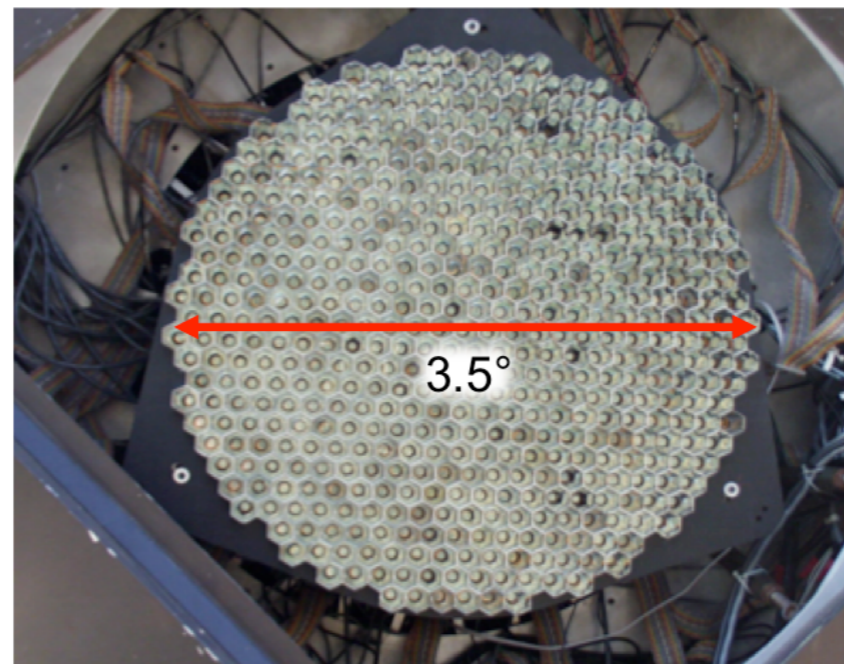
Fluorescence detectors

- High energy charged particles excite N_2 and N_2^+ molecules, which emit UV and visible light through fluorescence.
- The light emission is isotropic.
- At least two detectors are needed in stereo mode to trace the trajectory of the air shower.
- Successfully implemented at the Pierre Auger Observatory.



Atmospheric Cherenkov telescopes

- They operate through the detection of Cherenkov light produced by charged particles in the atmosphere.
- The light is a nano-second duration flash.
- The camera maps the image of the shower, in order to discriminate efficiently hadrons from photons.



Welcome to TeVCat!

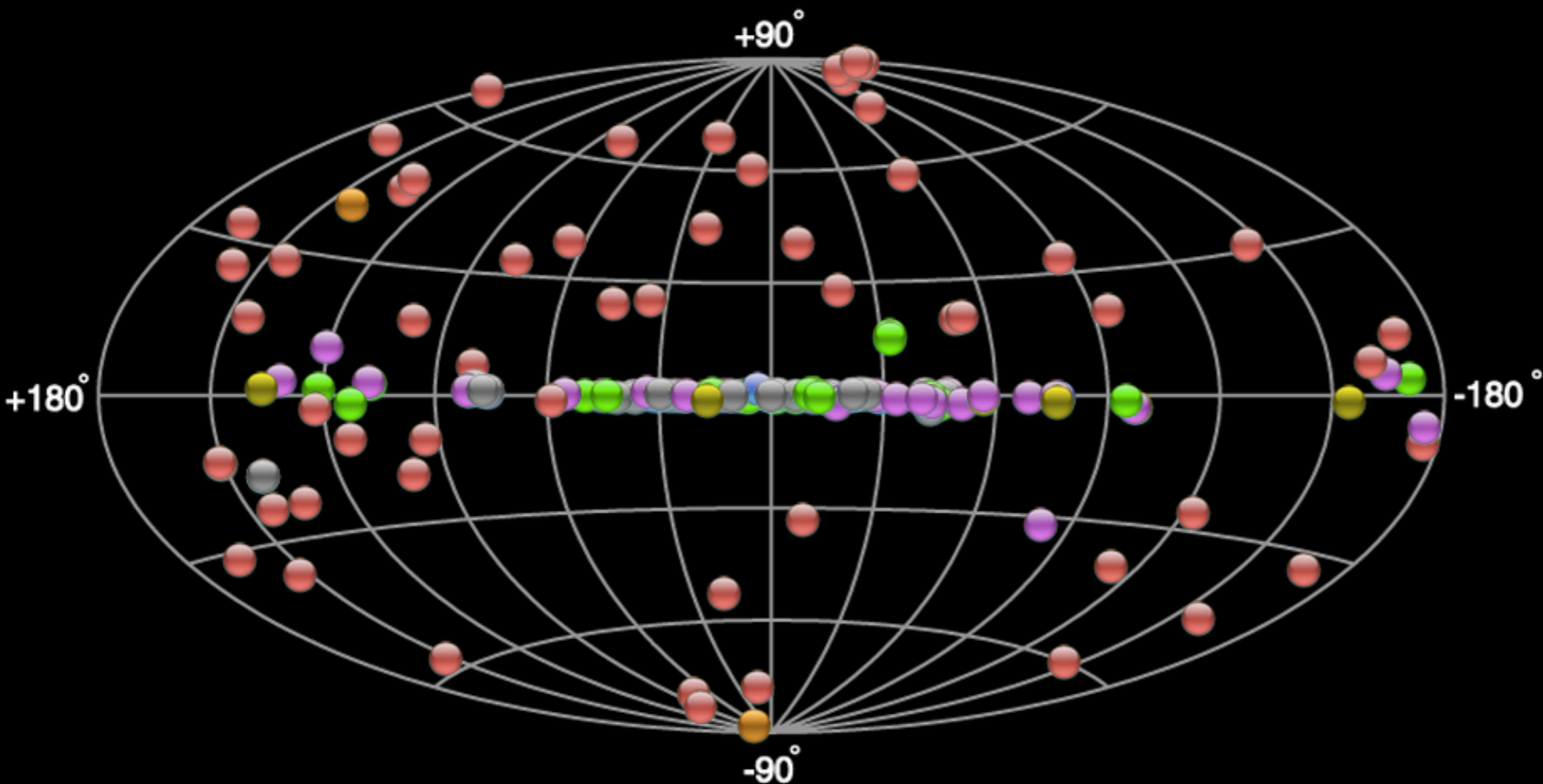


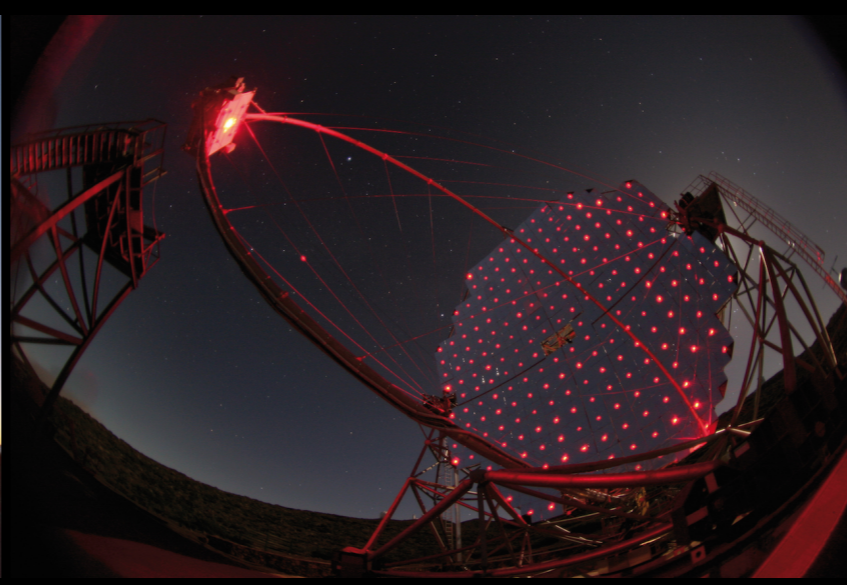
Table Cont... Map Cont... To... Lege...

- PWN
- Starburst
- HBL, IBL, FRI, Blazar, FSRQ, LBL, AGN (unknown type)
- Globular Cluster, Star Forming Region, uQuasar, Cat. Var., Massive Star Cluster, BIN, BL Lac (class unclear), WR
- Shell, SNR/Molec. Cloud, Composite SNR
- DARK, UNID, Other
- Binary, XRB, PSR, Gamma BIN

Export Black Export White

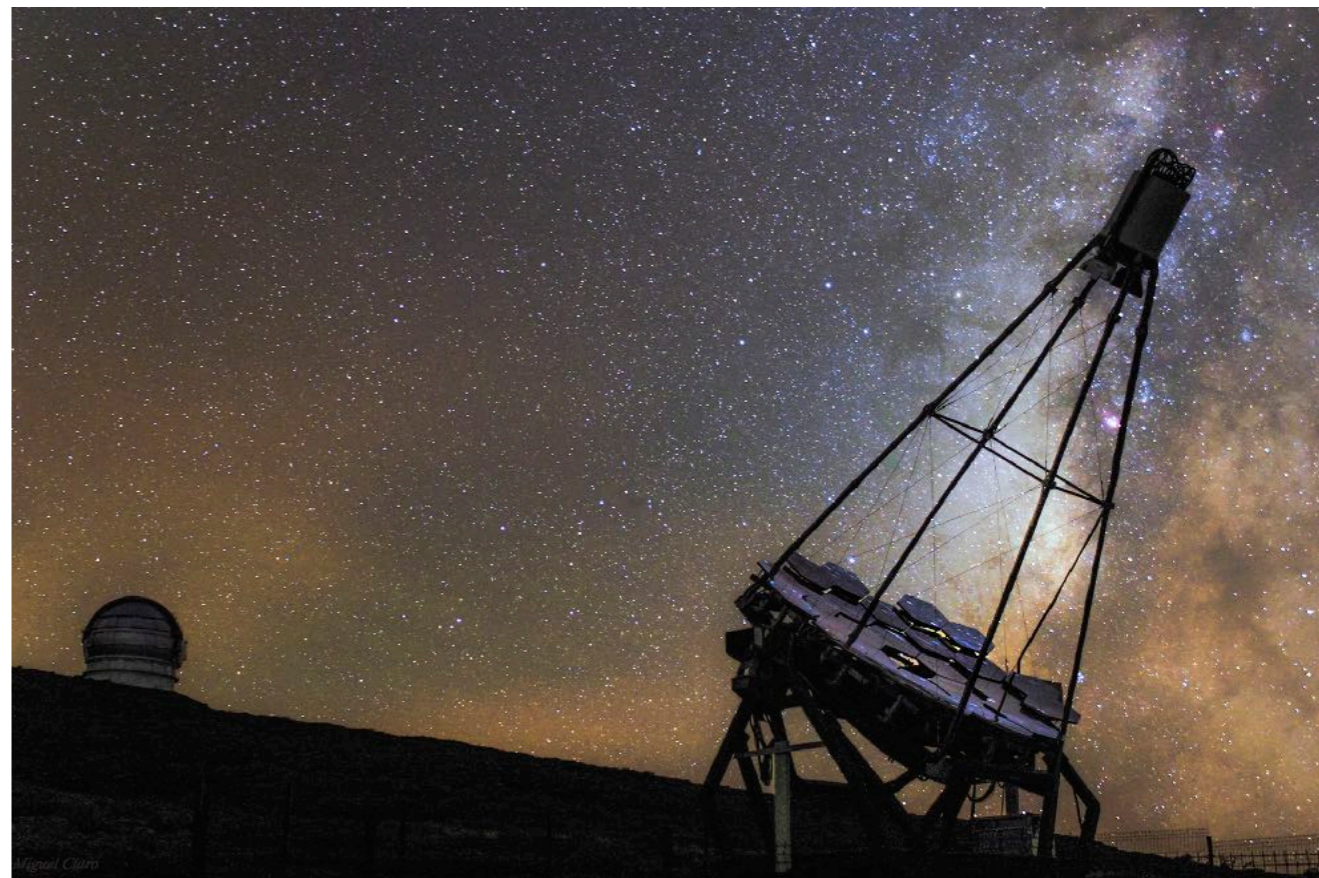
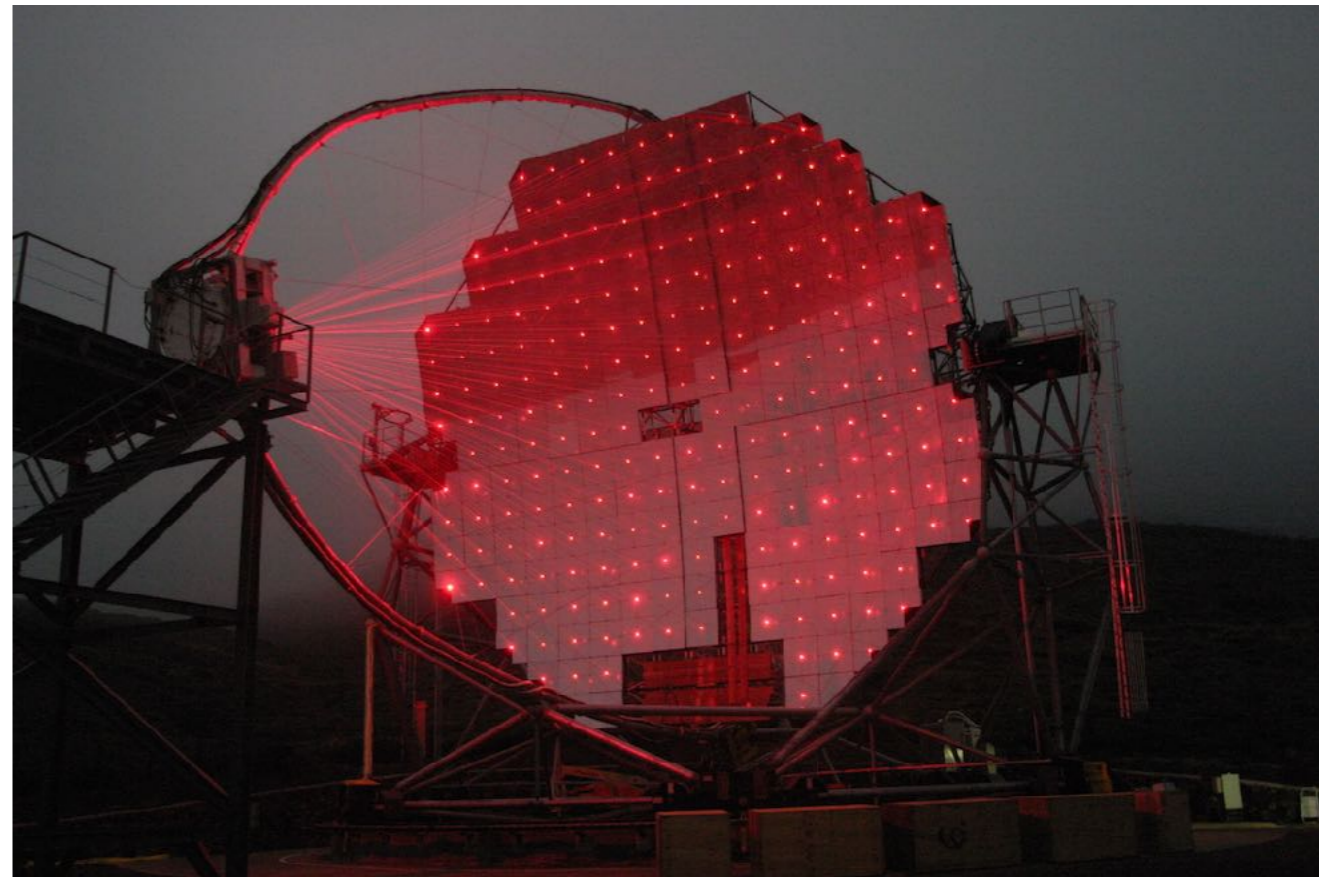


<http://tevcap.uchicago.edu/>



γ -ray detectors @ DRC-SMF - nov 2019





γ -ray detectors @ DRC-SMF - nov 2019





FIGURE 2. The VERITAS observatory, the newest of the third generation IACT observatories, saw first light in April, 2007. Note that VERITAS is in the exact same location as the telescopes shown in Figure 1. Each of the four telescopes has an aperture of 12m (collection area of 106m^2) and a camera with 499 pixels.

Weekes - astro-ph/0811.1197

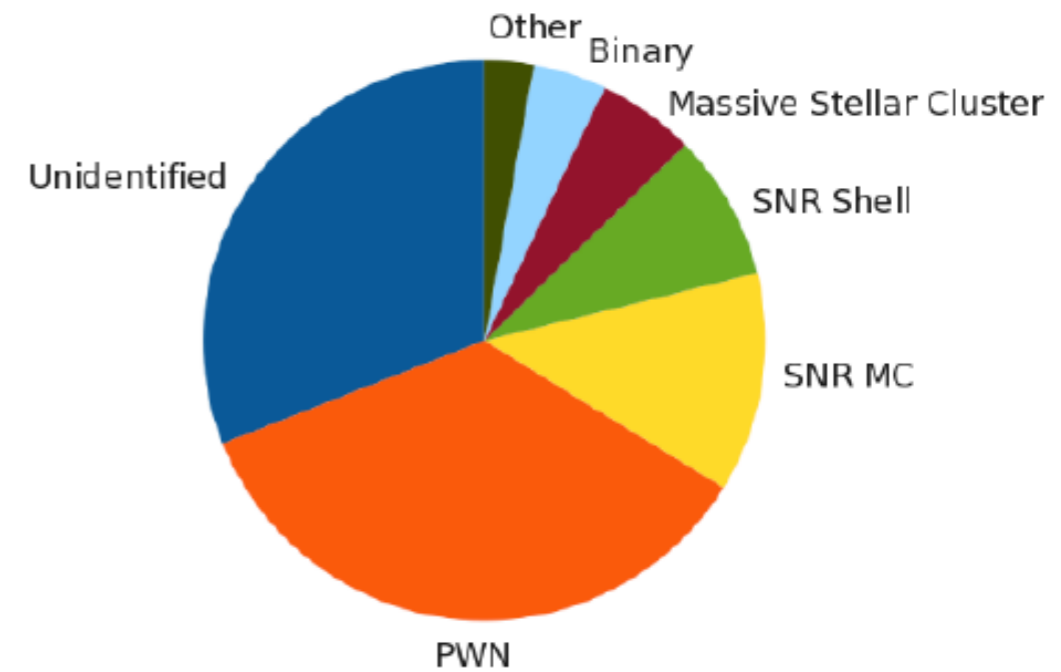
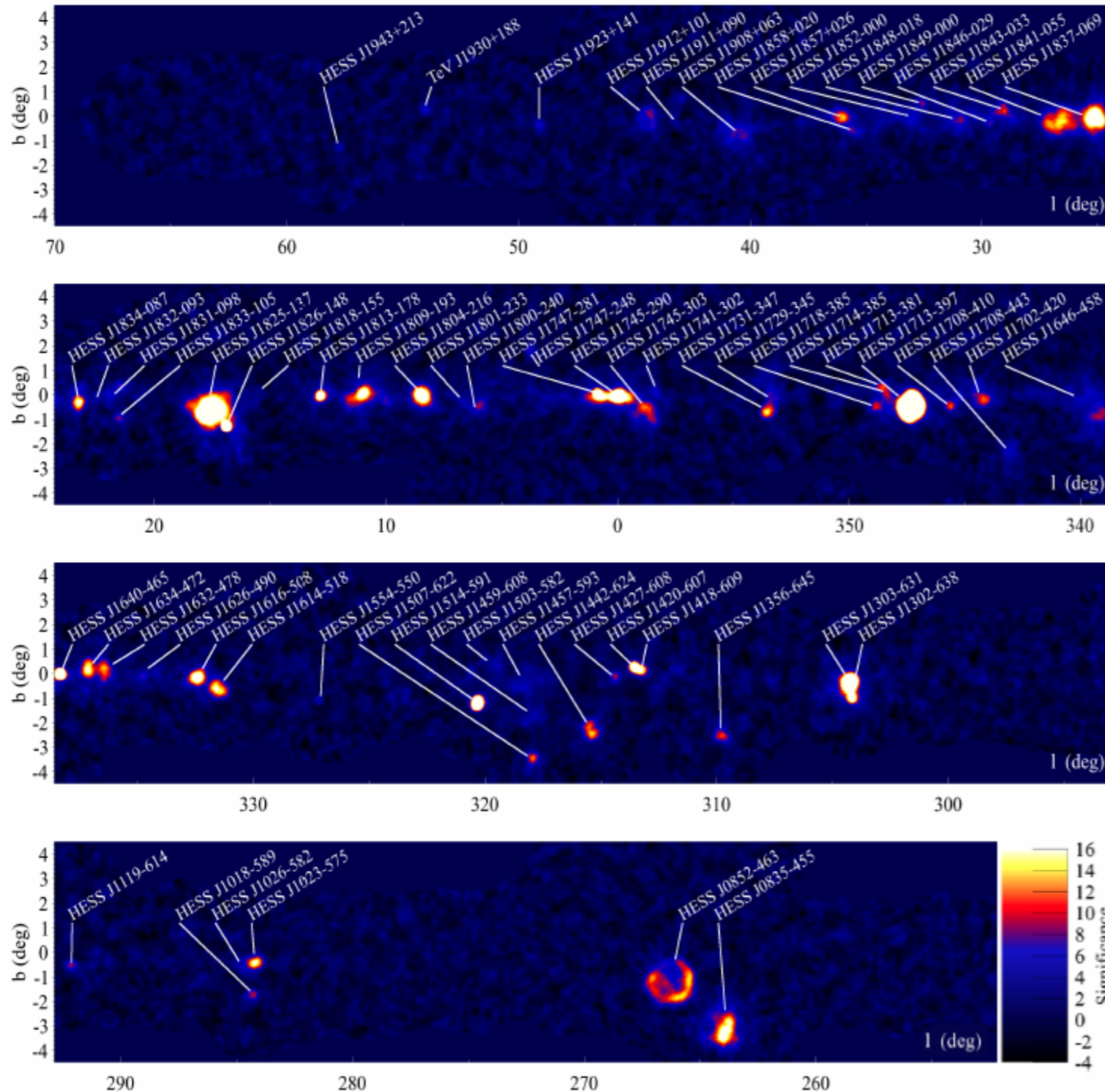
TABLE 1. Major Existing ACT Facilities

Observatory	Elevation (km)	Telescopes #	Mirror Area (m^2)	FoV (degrees)	First Light	Threshold (GeV)	Sensitivity (% Crab)
H.E.S.S.	1.8	4	428	5	2003	100	0.7
VERITAS	1.3	4	424	3.5	2007	100	1
MAGIC	2.2	1	236	3.5	2005	50	1.6
HAGAR	4.3	7	31	3	2008	60	9
Whipple	2.3	1	75	2.2	1985	400	10
CANGAROO III	0.1	3(4)	172 (230)	4	2006	400	10
PACT	1.1	24	107	3	2001	750	11
TACTIC	1.3	1	10	2.8	2001	1500	70
SHALON	3.3	1	11.2	8	1996	1000?	?

The HESS Galactic plane survey

Galactic latitudes $|b| < 4^\circ$
and longitudes from 250°
to 70° (i.e. $\Delta l = 180^\circ$)

$$\implies \Delta\Omega = 0.45 \text{ sr}$$

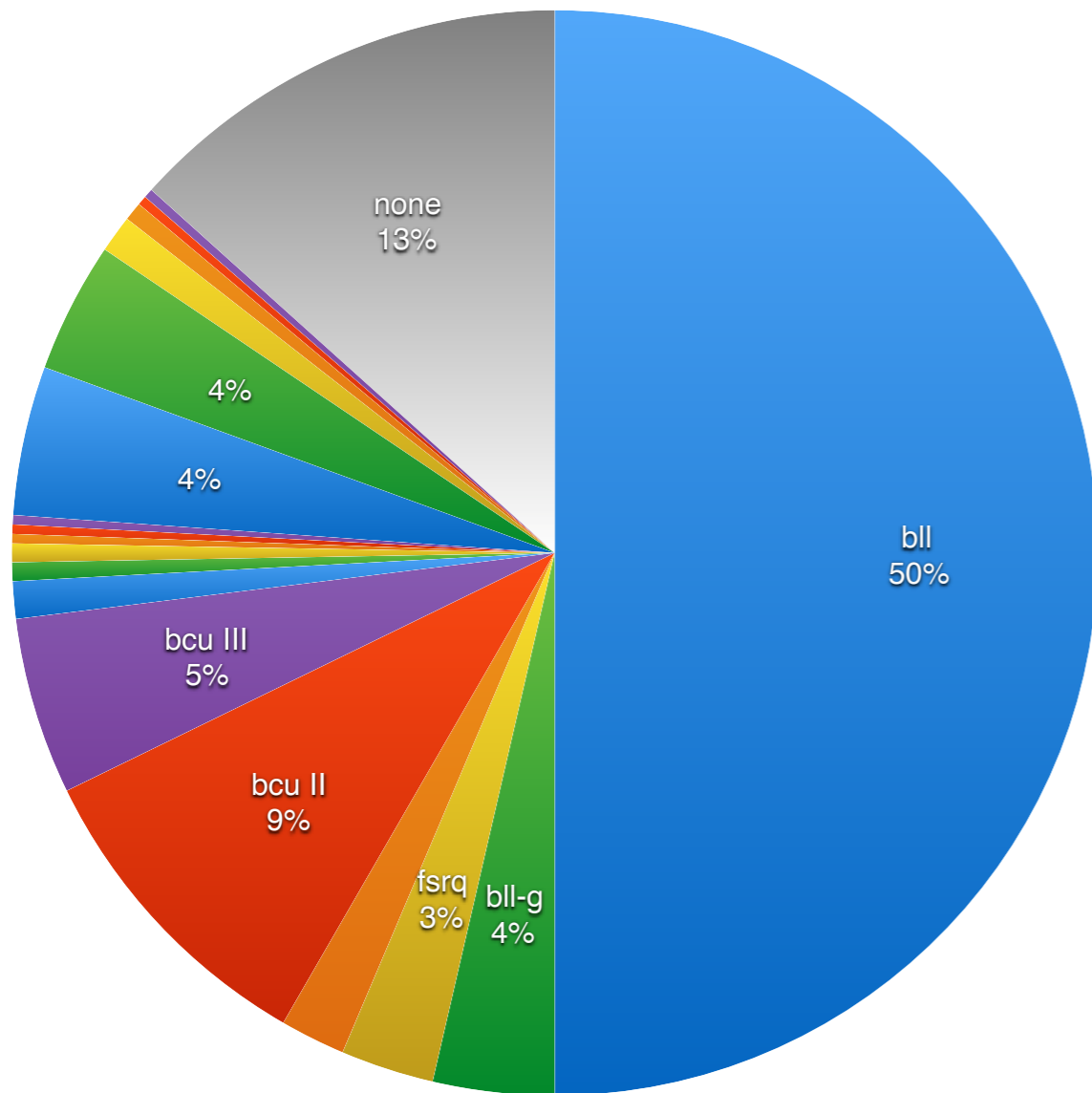


ICRC 2013 - 1307.4690

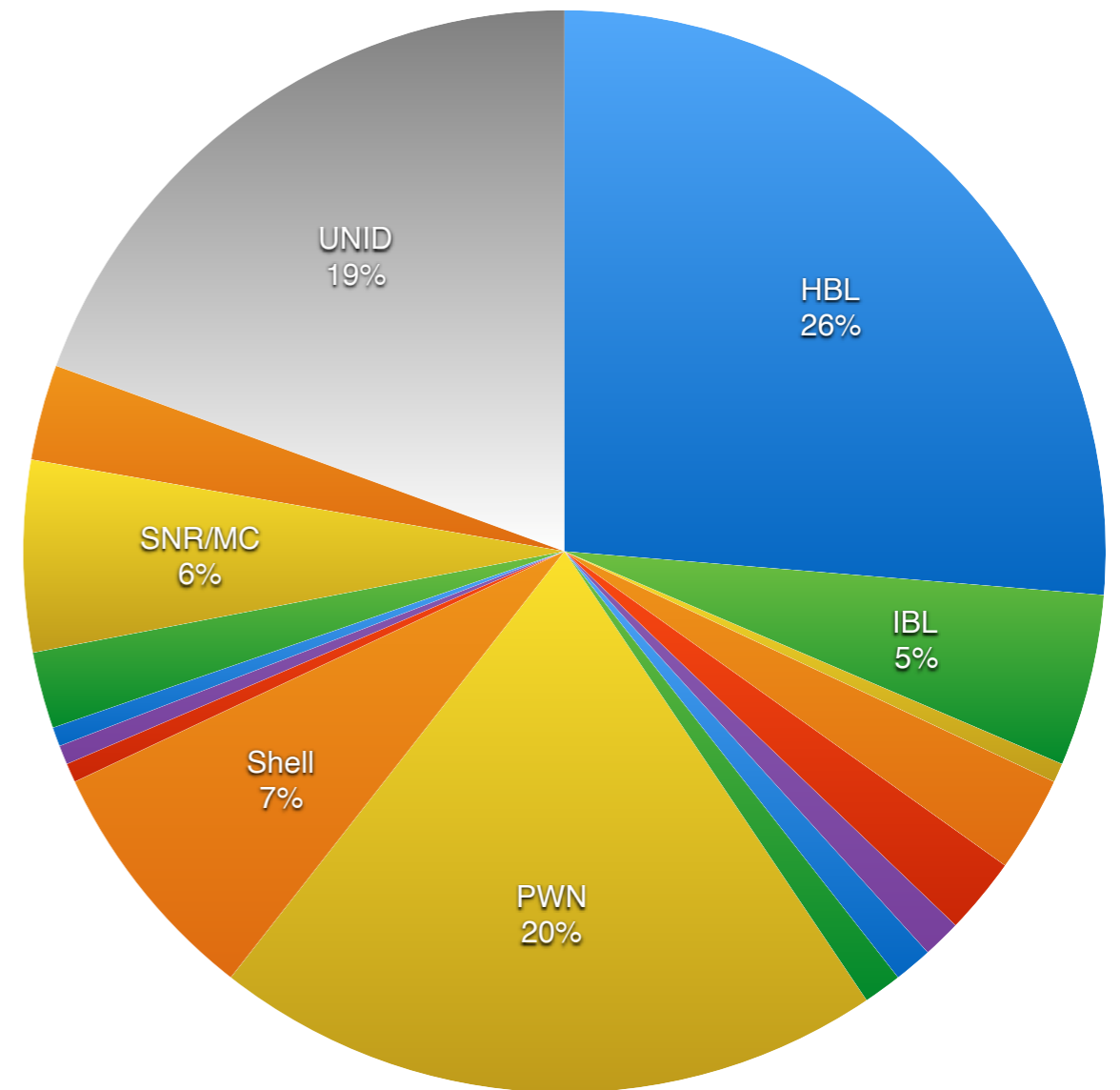
Paper de HGPS en 2018...

2FHL and TeVCat

2FHL (50 GeV) :: 360 sources



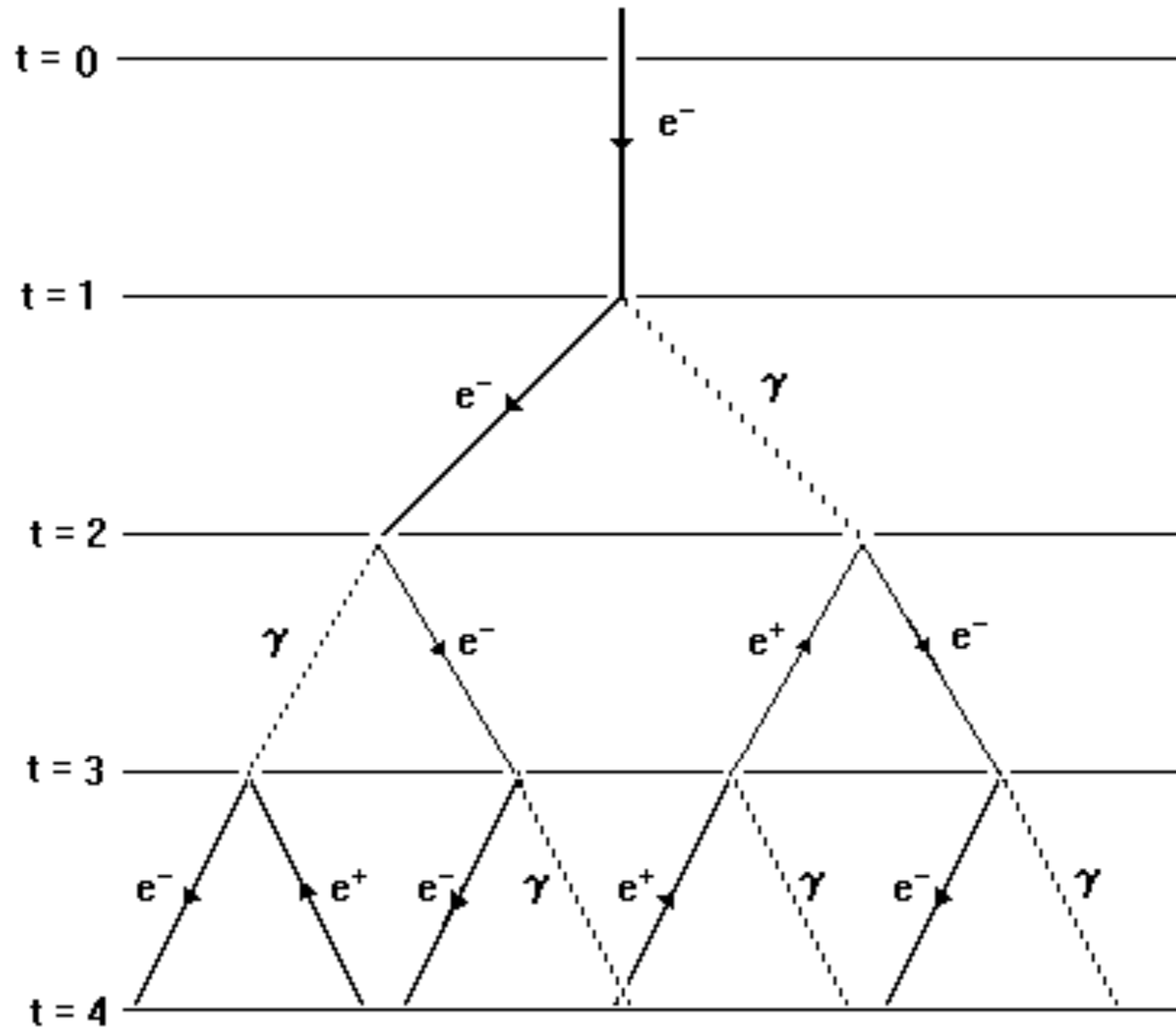
TeVcat (Nov 2015) - 175 sources



- | | | | | | |
|--------|-------------|--------|---------|----------|-----------|
| ● bll | ● bll-g | ● fsrq | ● bcu I | ● bcu II | ● bcu III |
| ● rdg | ● rdg / gll | ● agn | ● gal | ● galclu | ● psr |
| ● snr | ● pwn | ● spp | ● hmb | ● sfr | ● bin |
| ● none | | | | | |

- | | | | | | |
|-------|-------|----------|---------|--------|--------|
| ● HBL | ● IBL | ● blz | ● fsrq | ● RDG | ● SBG |
| ● SBu | ● PSR | ● PWN | ● Shell | ● csnr | ● dark |
| ● GC | ● MSC | ● SNR/MC | ● Bin | ● UNID | |

EM cascade toy model

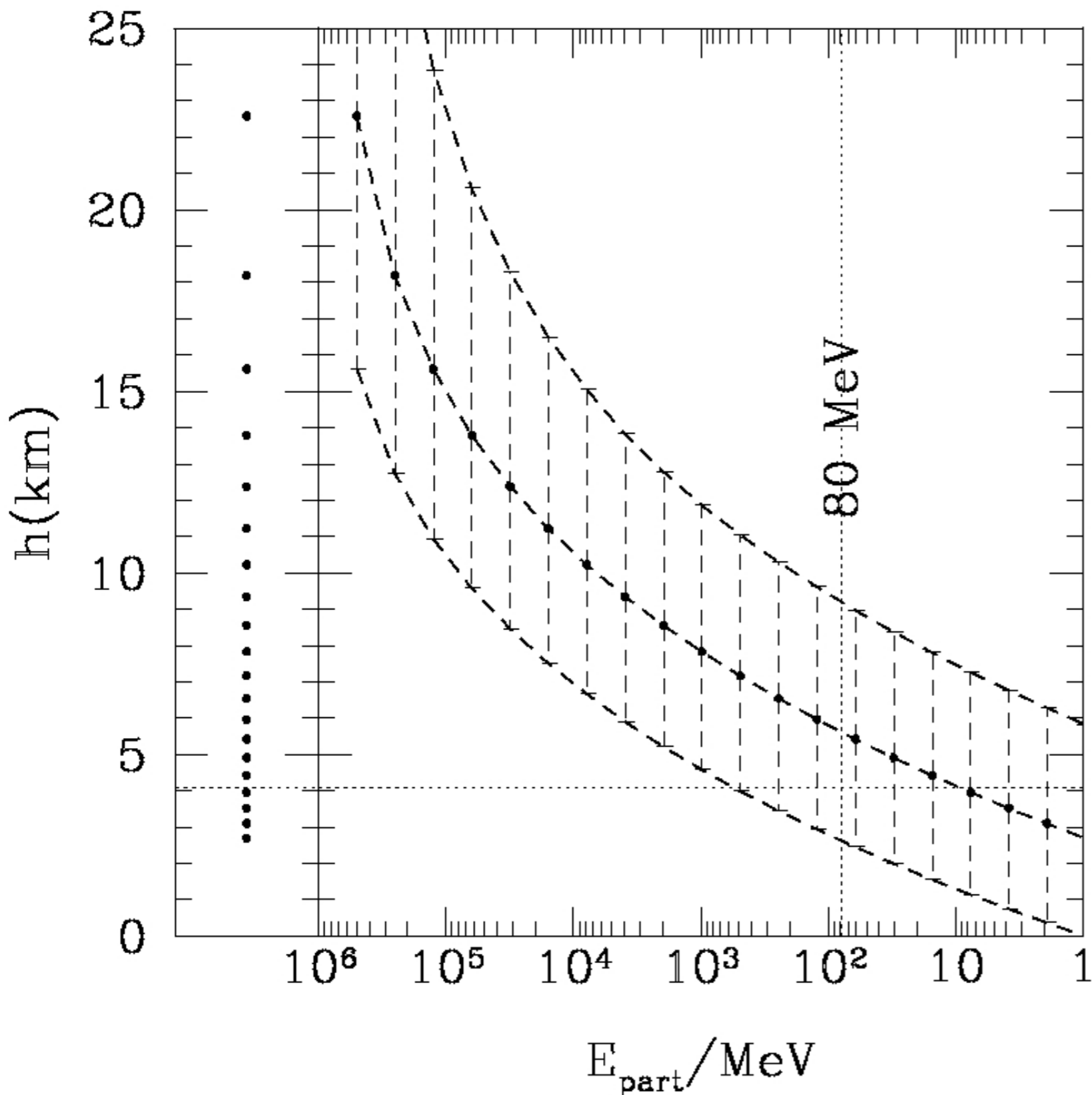


Heitler model

EM cascade toy model

t	X (g/cm ²)	N	P	E
0 - 1	0 - 37	1	γ	1 TeV
1 - 2	74	2	ee	500 GeV
2 - 3	111	4	$e\gamma e\gamma$	250 GeV
3 - 4	148	8	$e\gamma e e e\gamma e e$	125 GeV
4 - 5	185	16	$e\gamma e e e\gamma e\gamma$ $e\gamma e e e\gamma e\gamma$	62.5 GeV
5 - 6	222	32	$e\gamma e e e\gamma e\gamma$ $e\gamma e e e\gamma e e$ $e\gamma e e e\gamma e\gamma$ $e\gamma e e e\gamma e e$	31.25 GeV
...
17 - 18	592 - 629	131,072	$\{43,680 \times \gamma\}$ $\{87,382 \times e^{\pm}\}$	7.63 MeV

bars indicate 90% probability of interaction



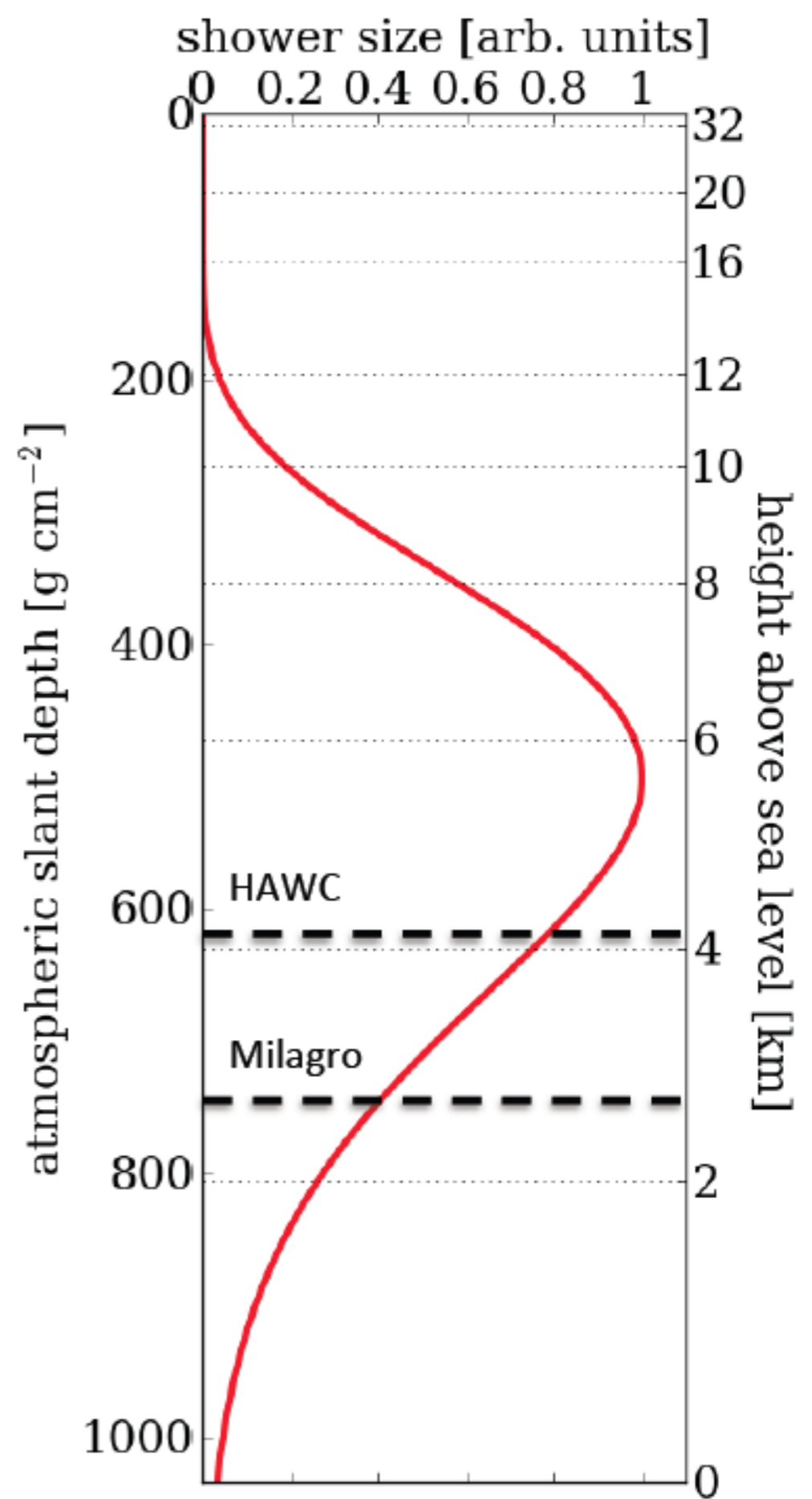
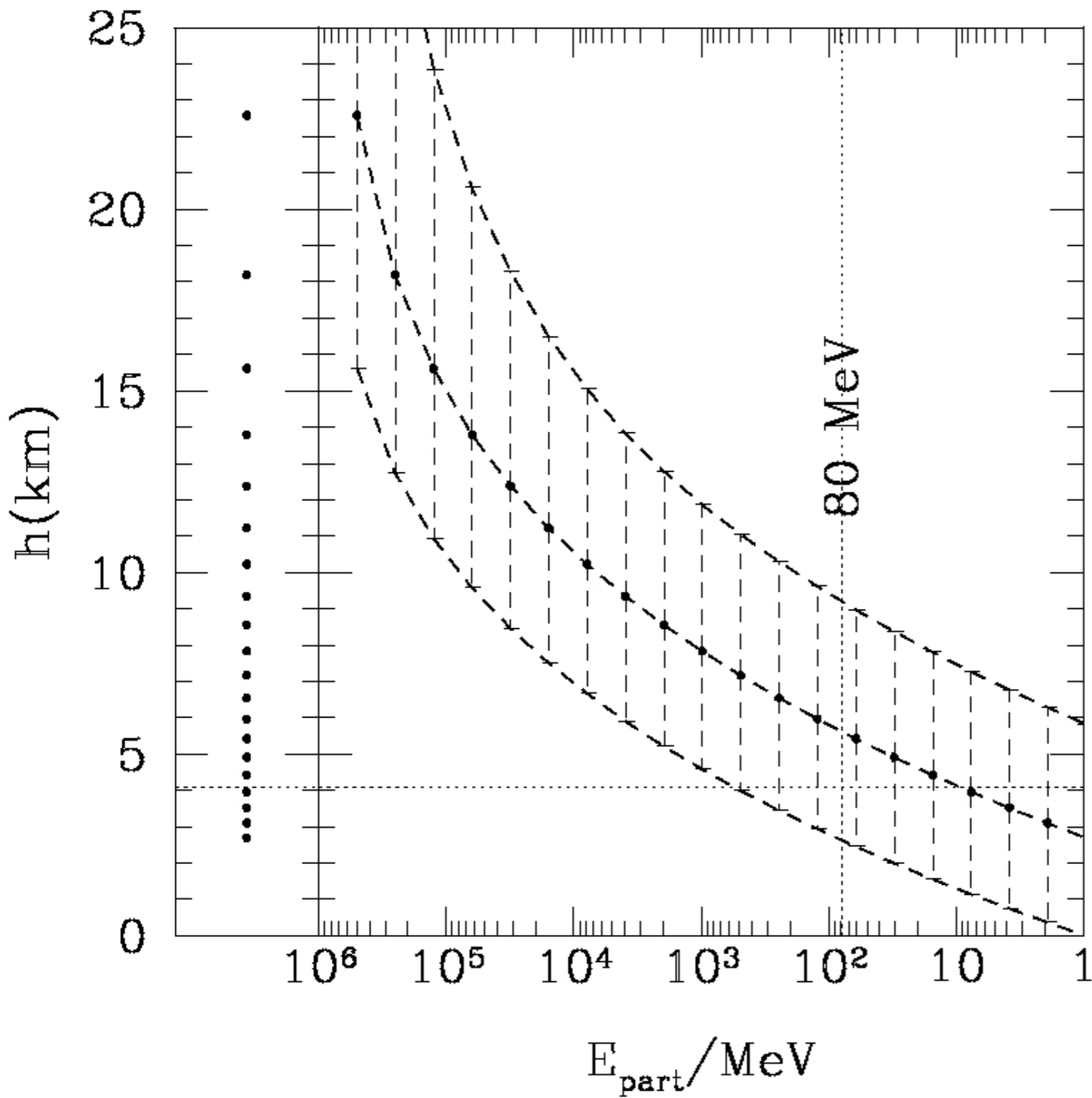
The cascade ceases developing when photon energies get below 80 MeV.

For 17 radiation lengths:
 $80 \text{ MeV} * 2^{17} \approx 10 \text{ TeV}$

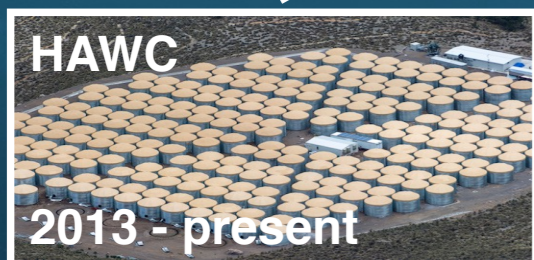
Every interaction is a random process.
Fluctuations are important in the development of the cascade.

Translation to height requires a model for the atmosphere.

bars indicate 90% probability of interaction



High altitude EAS for γ -ray astronomy



LHAASO!

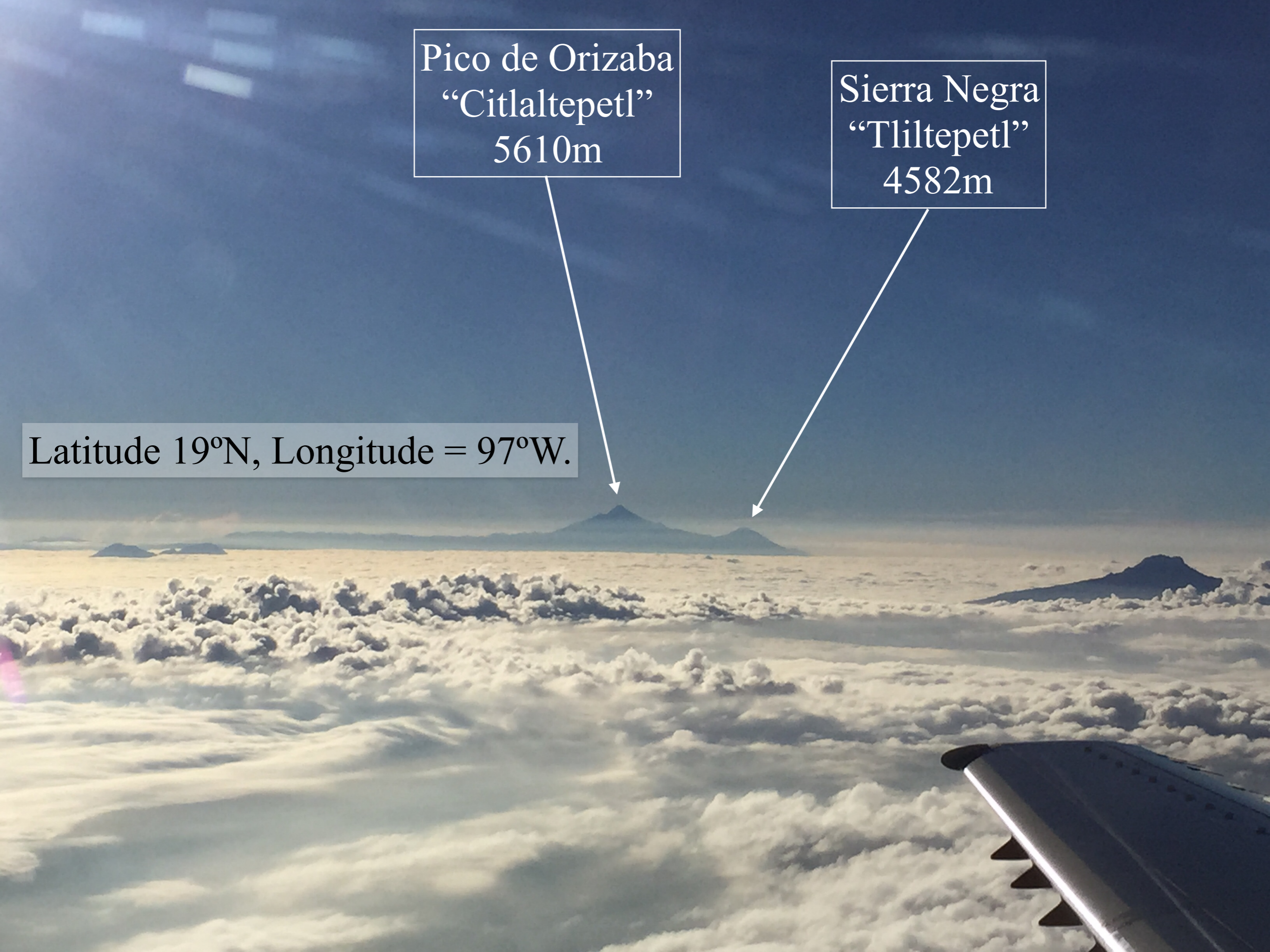
Should we break?



Pico de Orizaba
“Citlaltepetl”
5610m

Sierra Negra
“Tliltepetl”
4582m

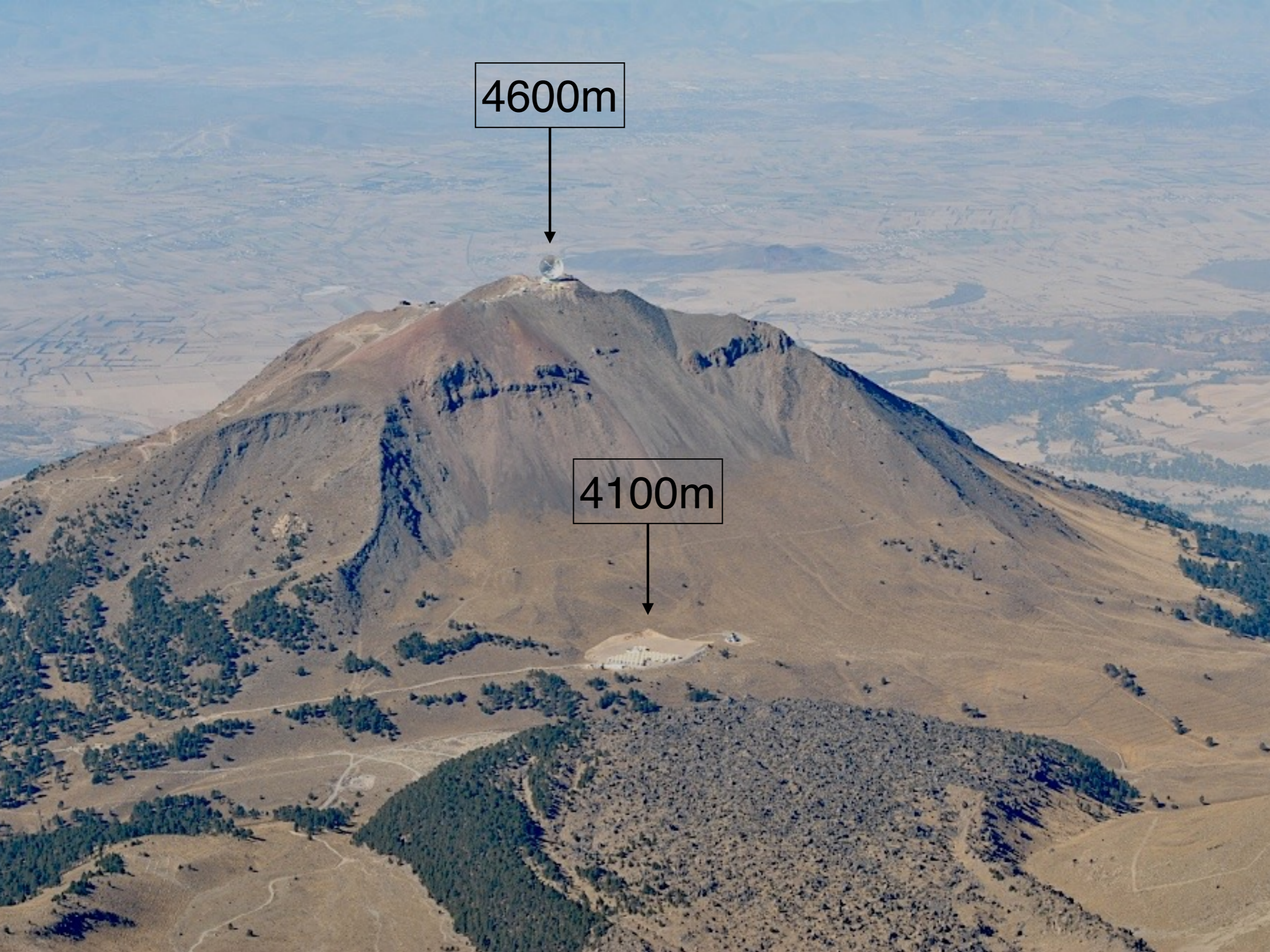
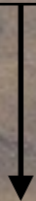
Latitude 19°N, Longitude = 97°W.

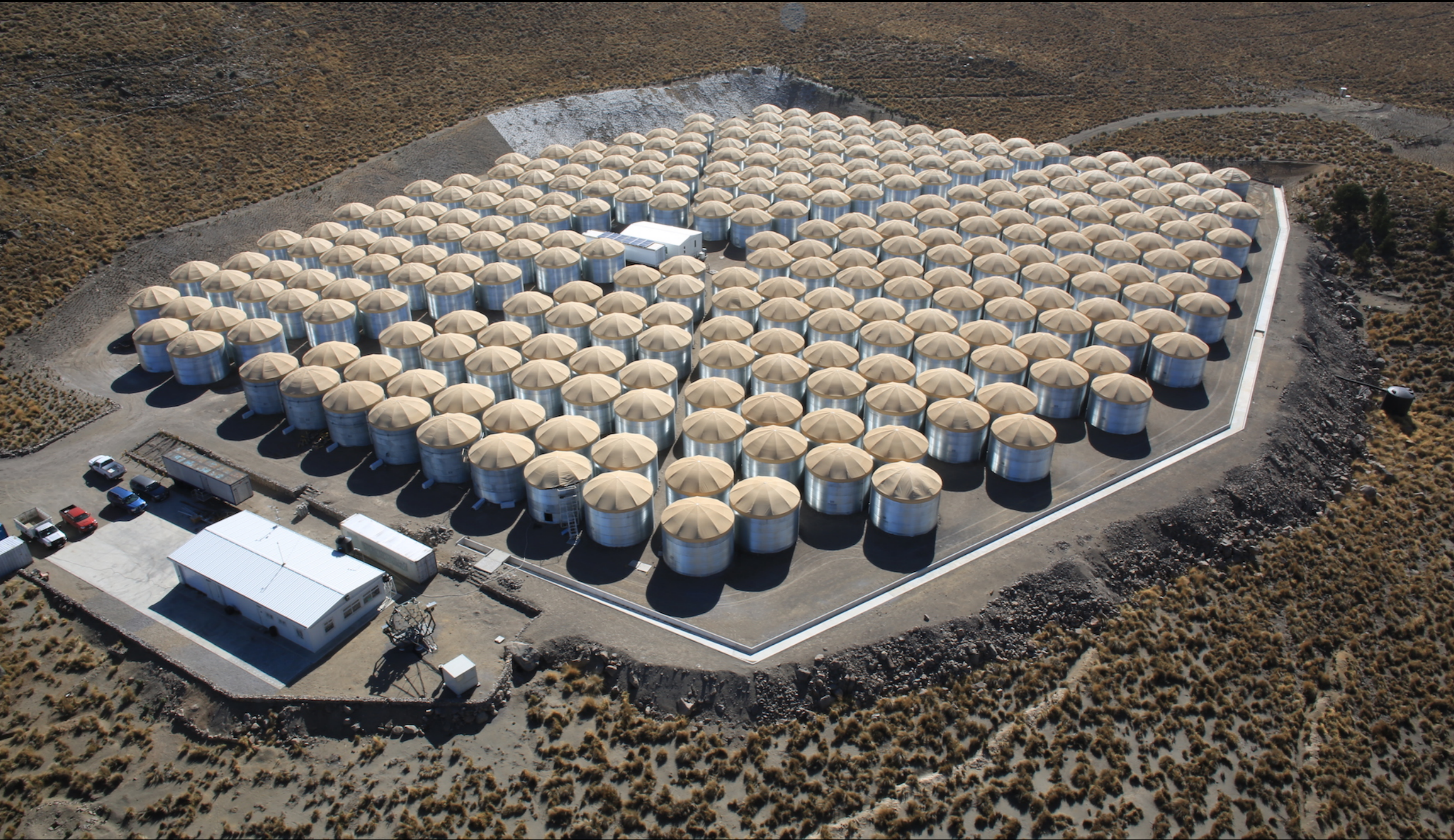


4600m



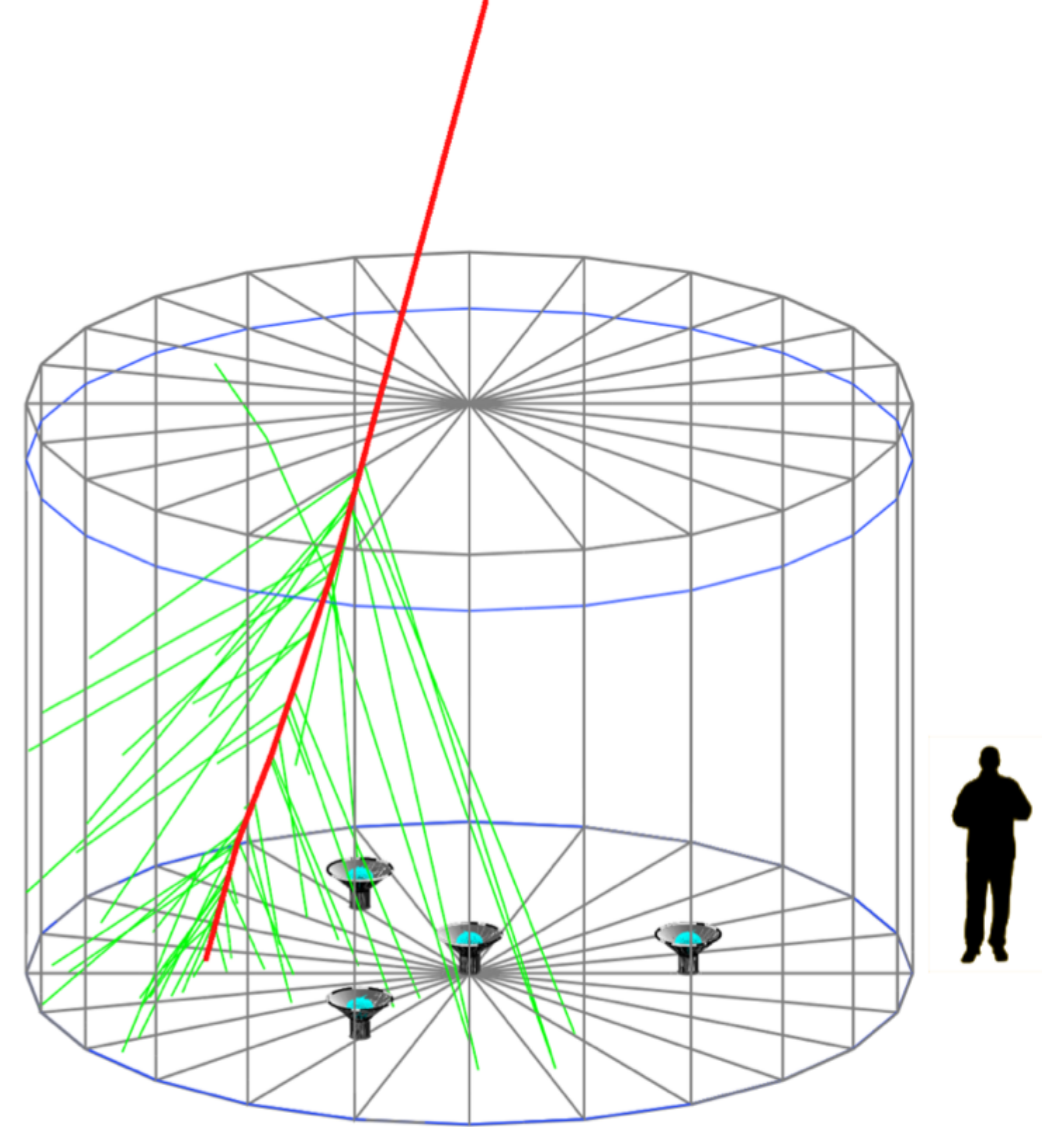
4100m





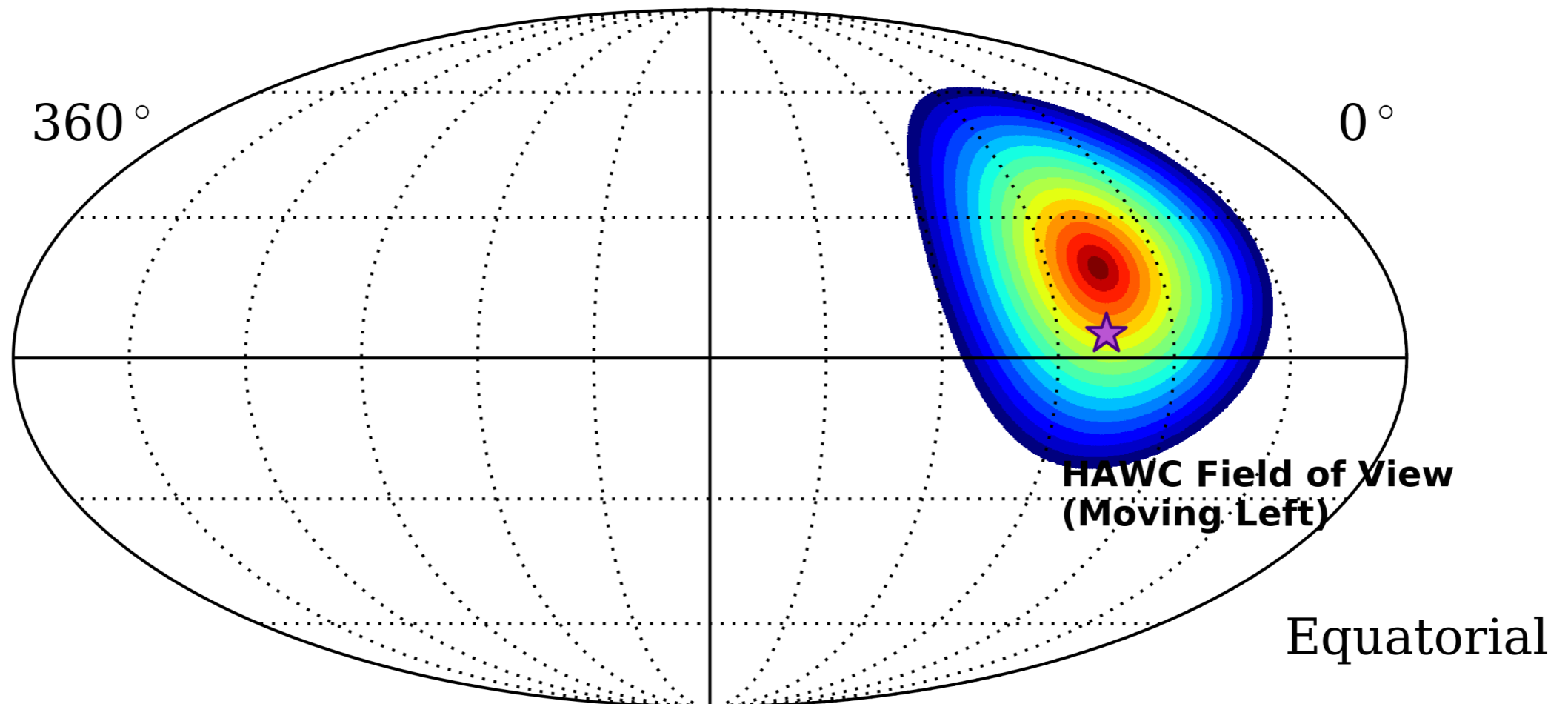
The HAWC array

- 300 individual water Cherenkov detectors (WCDs).
- Each WCD is a water tank 7.2m diameter and 4.5m height: 180,000 liters of water in darkness.
- Water filtered for maximal transparency.
- Each WCD has four PMTs: 3 of 8” and one 10”.

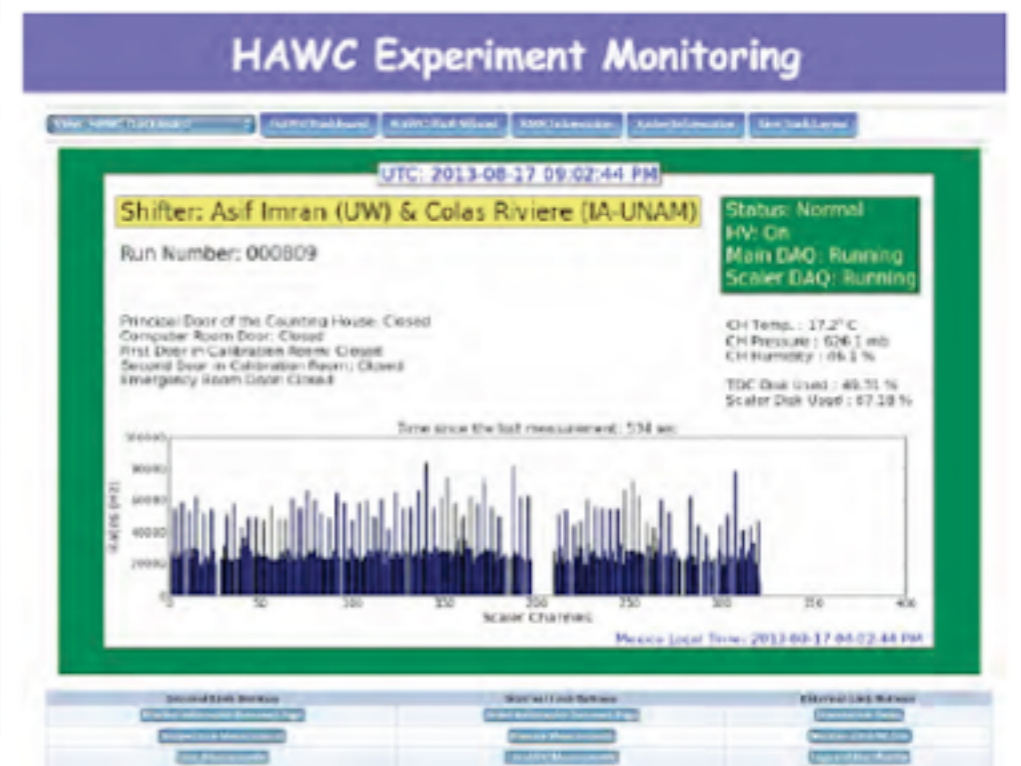
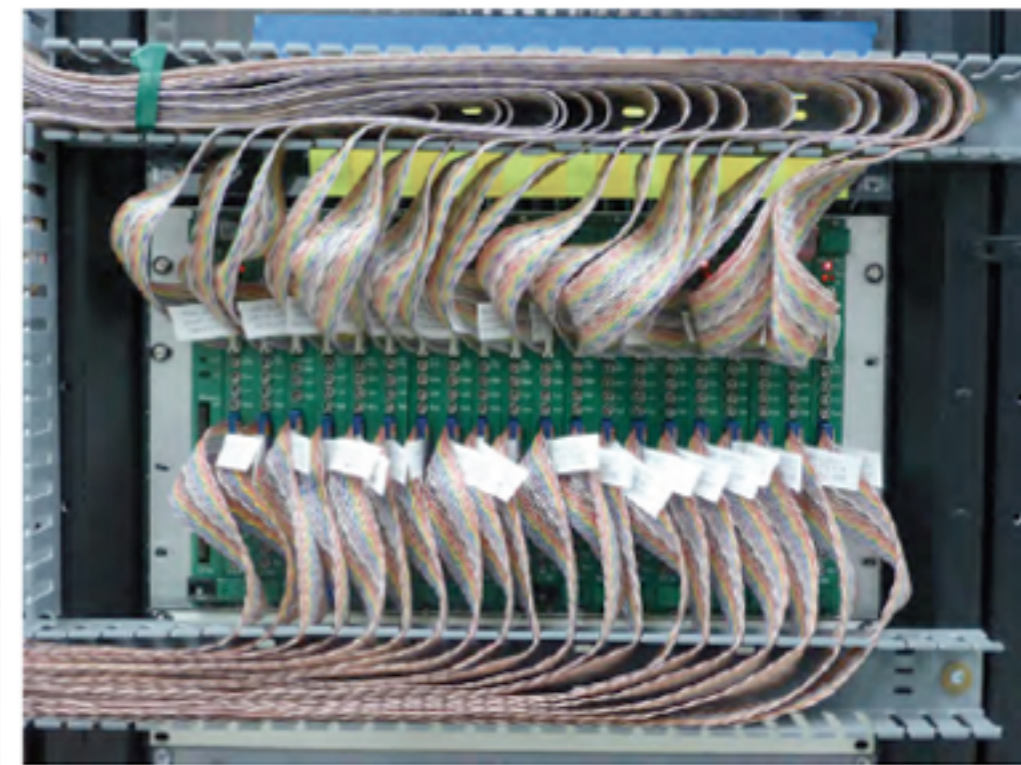


Operation mode

2018-03-01 01:00:00 [UTC]



HAWC observes constantly the sky around its zenith, with an aperture of 45° . It scans $2/3$ of the celestial sphere every sidereal day. Data accumulates daily, resulting in a deeper and deeper exposure of the sky.

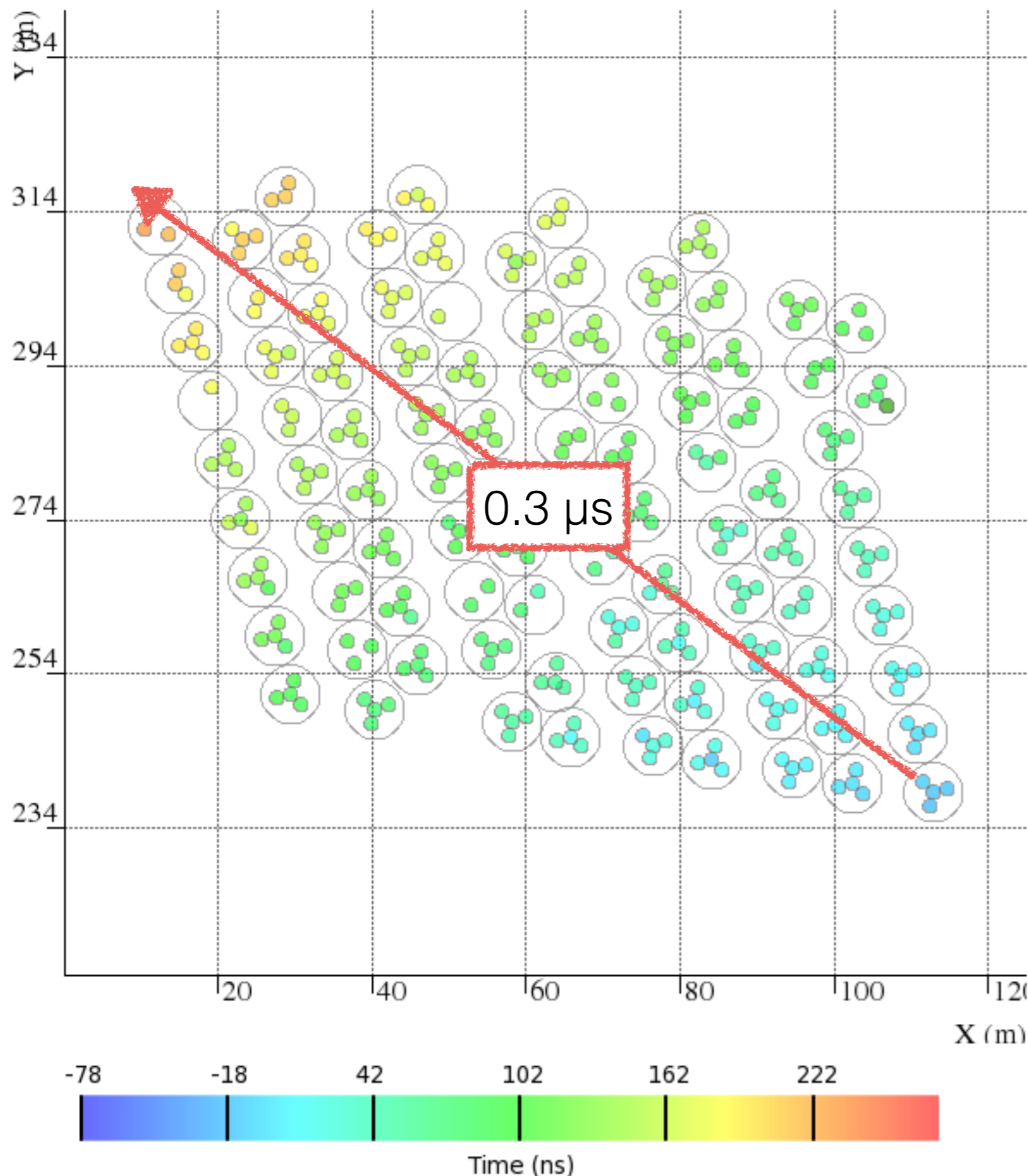


HAWC registers over 20,000 cosmic rays per second, generating 2 Terabytes of data per day - every day.

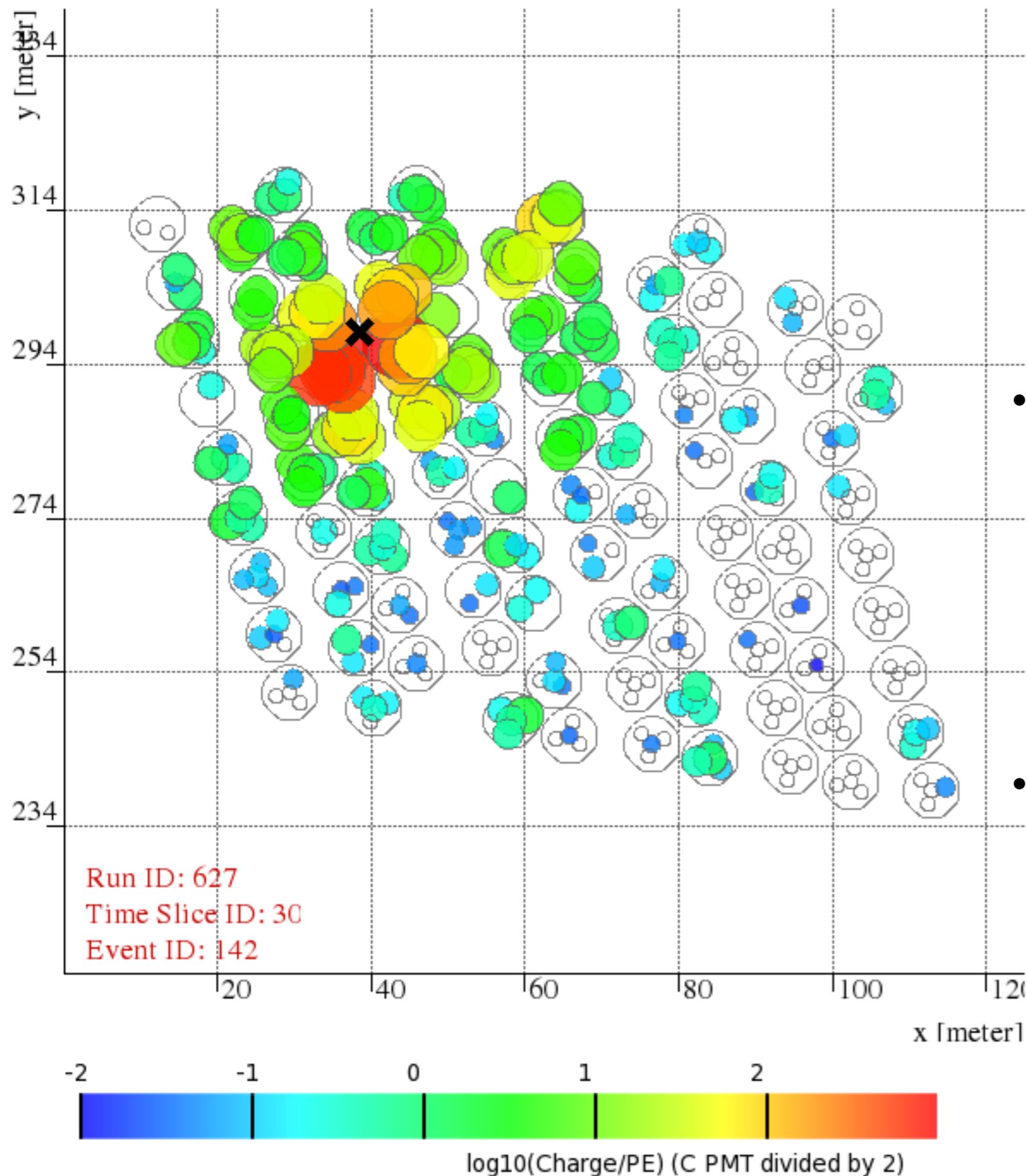
Event location

The front of particles takes 20 ns to travel from one detector to the next.

Measuring with precision the relative arrival times at each detector allows to locate the event on the sky.



Charge deposits



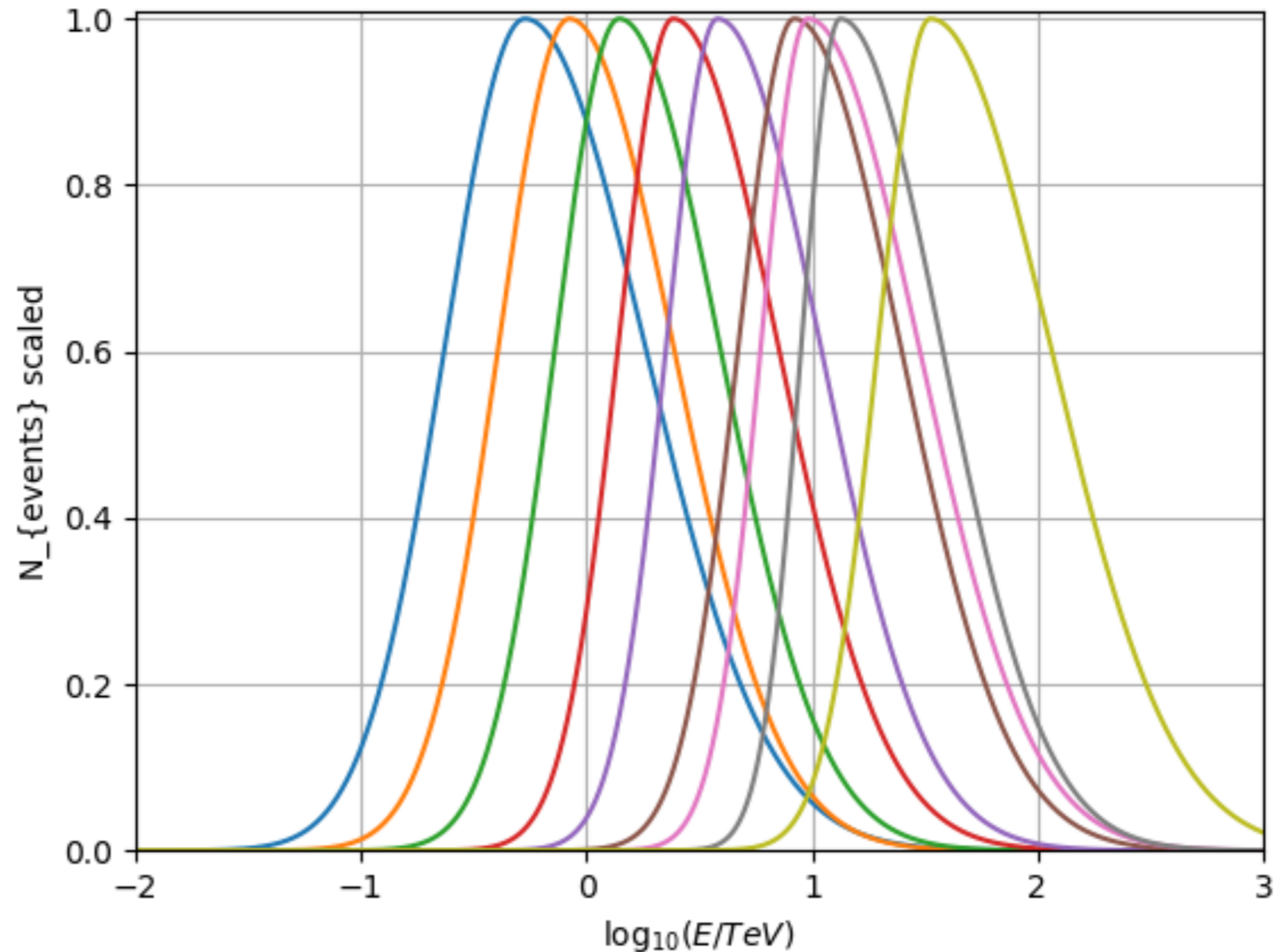
- Light pulses at each PMT allow:
 - (1) energy estimation.
 - (2) γ/h discrimination.
- Locating the core of the cascade is needed to adjust standard shower models (NKG).

Energy estimators

- A parametrization is needed; it is to be compared to Montecarlo simulations and validated with data.
- Crab 2017: fhit bins
- Crab 2019: NKG fit

Energy estimation: f-hit bins

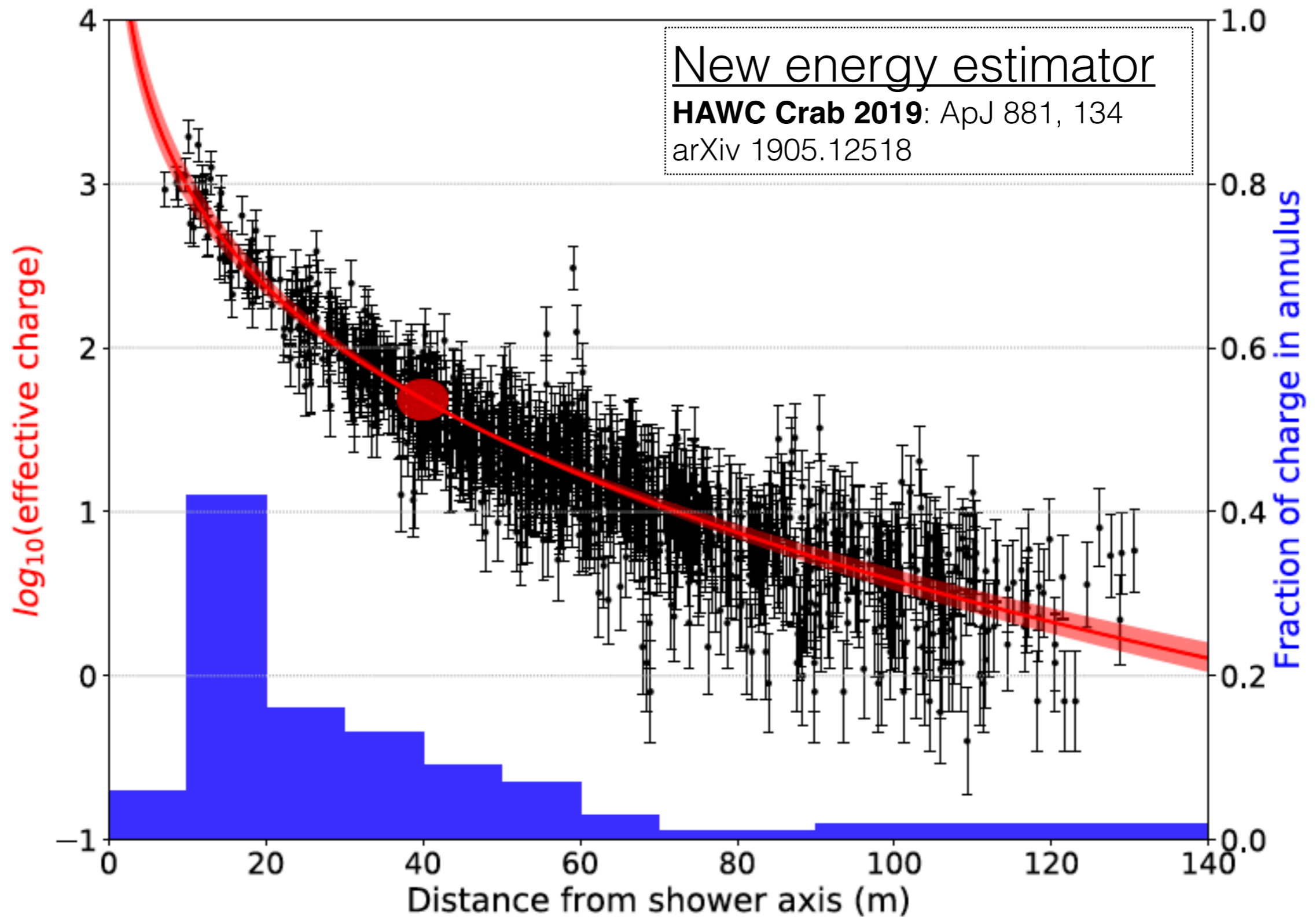
B	f_{hit}
1	6.7% - 10.5%
2	10.5% - 16.2%
3	16.2% - 24.7%
4	24.7% - 35.6%
5	35.6% - 48.5%
6	48.5% - 61.8%
7	61.8% - 74.0%
8	74.0% - 84.0%
9	84.0% - 100%



HAWC Crab 2017: Abeysekara et al. 2017, ApJ 843, 39

Energy estimation: f-hit bins

B	f_{hit}	ψ_{68} (°)	P max	C min	Crab excess per transit
1	6.7% - 10.5%	1.03	< 2.2	> 7.0	68.4 ± 5.0
2	10.5% - 16.2%	0.69	3.0	9.0	51.7 ± 1.9
3	16.2% - 24.7%	0.50	2.3	11.0	27.9 ± 0.8
4	24.7% - 35.6%	0.39	1.9	15.0	10.58 ± 0.26
5	35.6% - 48.5%	0.30	1.9	18.0	4.62 ± 0.13
6	48.5% - 61.8%	0.28	1.7	17.0	1.78 ± 0.07
7	61.8% - 74.0%	0.22	1.8	15.0	1.02 ± 0.05
8	74.0% - 84.0%	0.20	1.8	15.0	0.433 ± 0.033
9	84.0% - 100%	0.17	1.6	3.0	0.407 ± 0.032



Energy estimator

Lateral distribution function is adjusted to a NKG/ r fit,

$$\log_{10}(sig_r) = A + s \left[\log_{10} \left(\frac{r}{r_m} \right) + \log_{10} \left(1 + \frac{r}{r_m} \right) \right] - 3 \log_{10} \left(\frac{r}{r_m} \right) - 4.5 \log_{10} \left(1 + \frac{r}{r_m} \right),$$

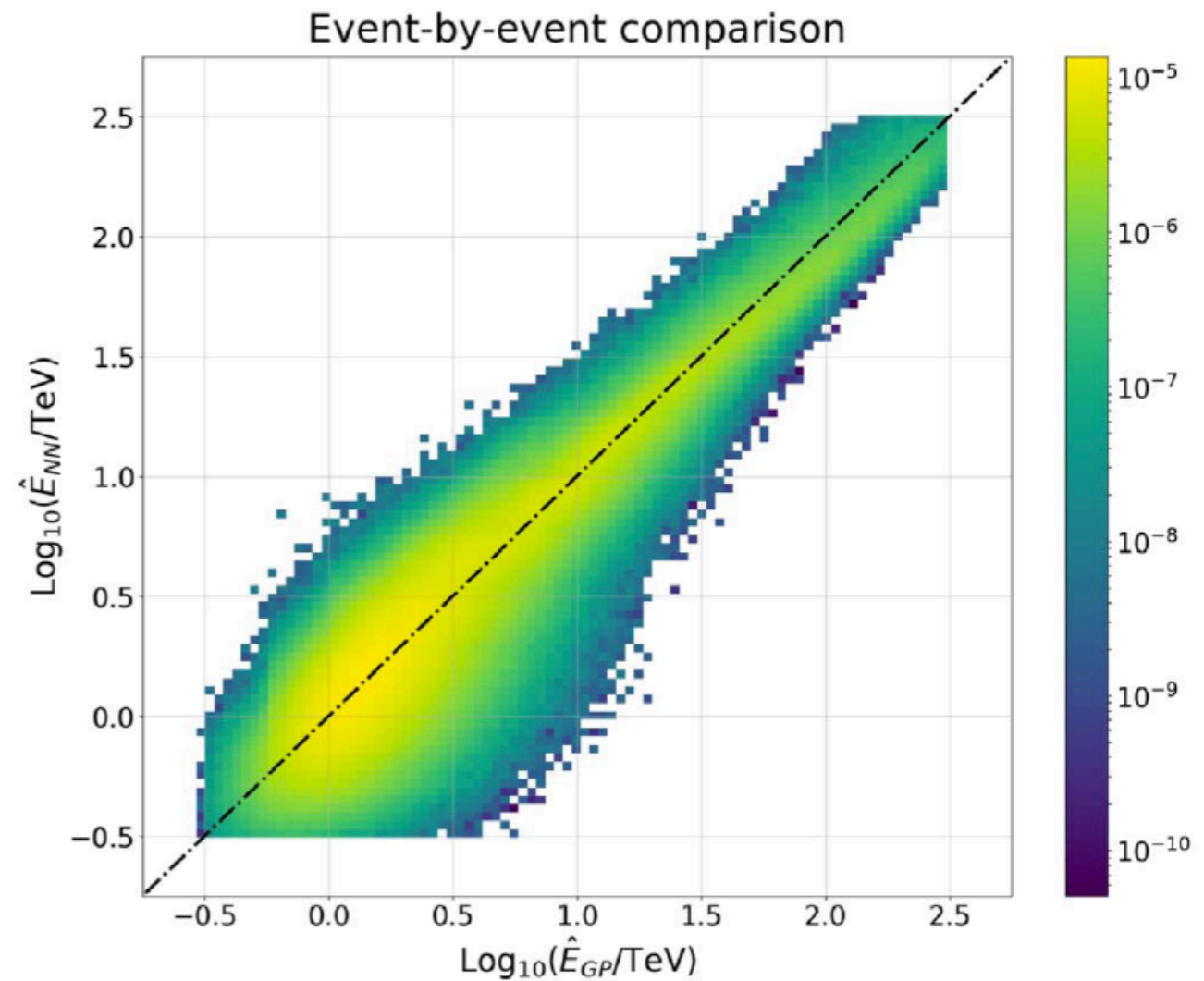
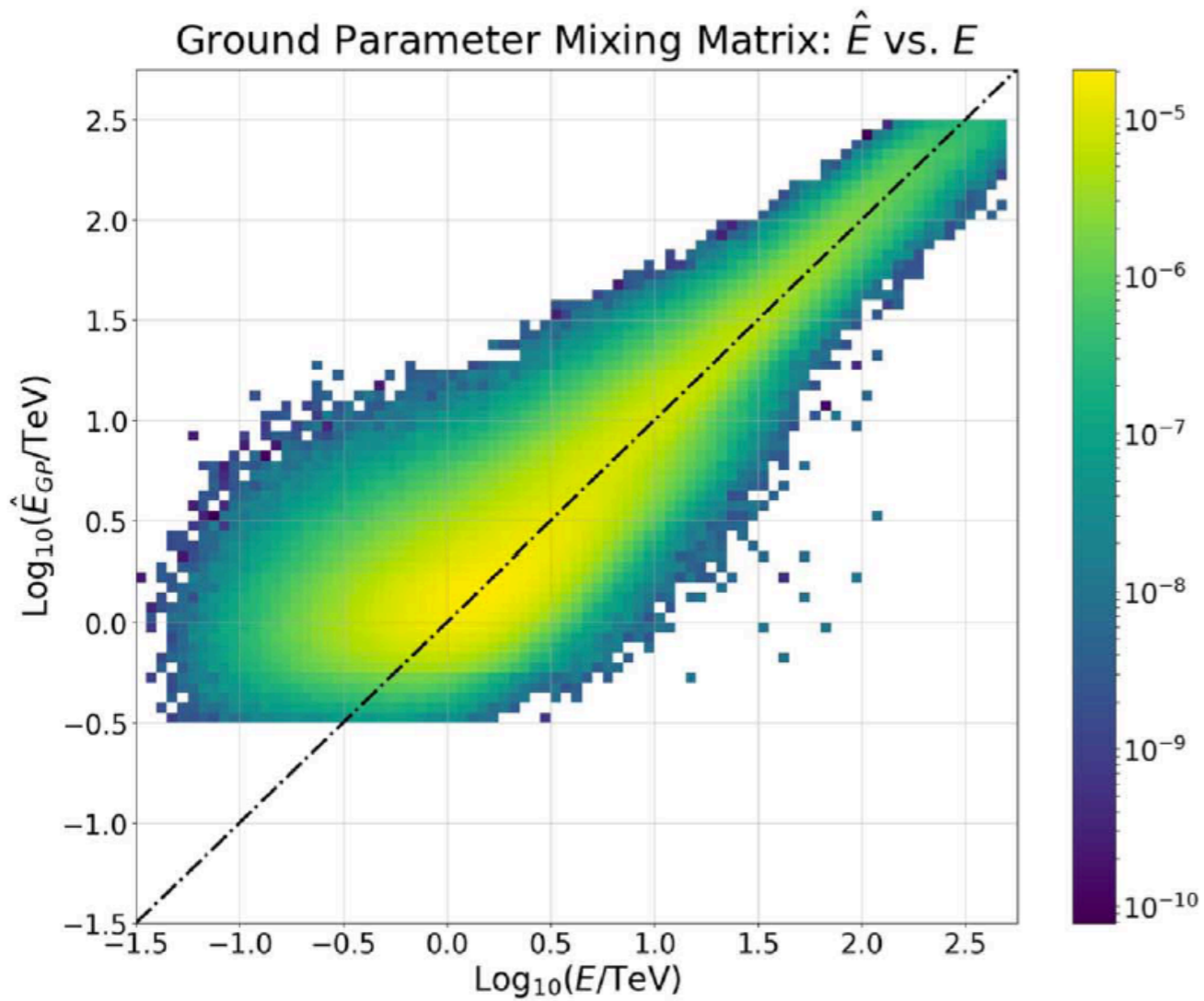
where A =log amplitude of fit; s shower age parameter; $r_m \sim 124$ m Molière radius.

$$\log_{10} \hat{E} = m(\theta) \log_{10} sig_{40} + c(\theta),$$

with m and c determined functions of zenith angle θ .

HAWC Crab 2019: ApJ 881, 134
arXiv 1905.12518

Energy estimators



Gamma - hadron discrimination

- An energy dependent parametrization is needed.
- Crab 2017: PINCness and Compactness
- Newer ones in development (for example Neural Networks)

Compactness and PINCness

Parameters for γ /hadron separation:

- ▶ Compactness:

$$c = \frac{N_{hit}}{C_x PE_{40}}, \quad (1)$$

where $C_x PE_{40}$ is the effective charge measured in the PMT with largest effective charge outside a radius of 40 m from the shower core.

- ▶ PINCness:

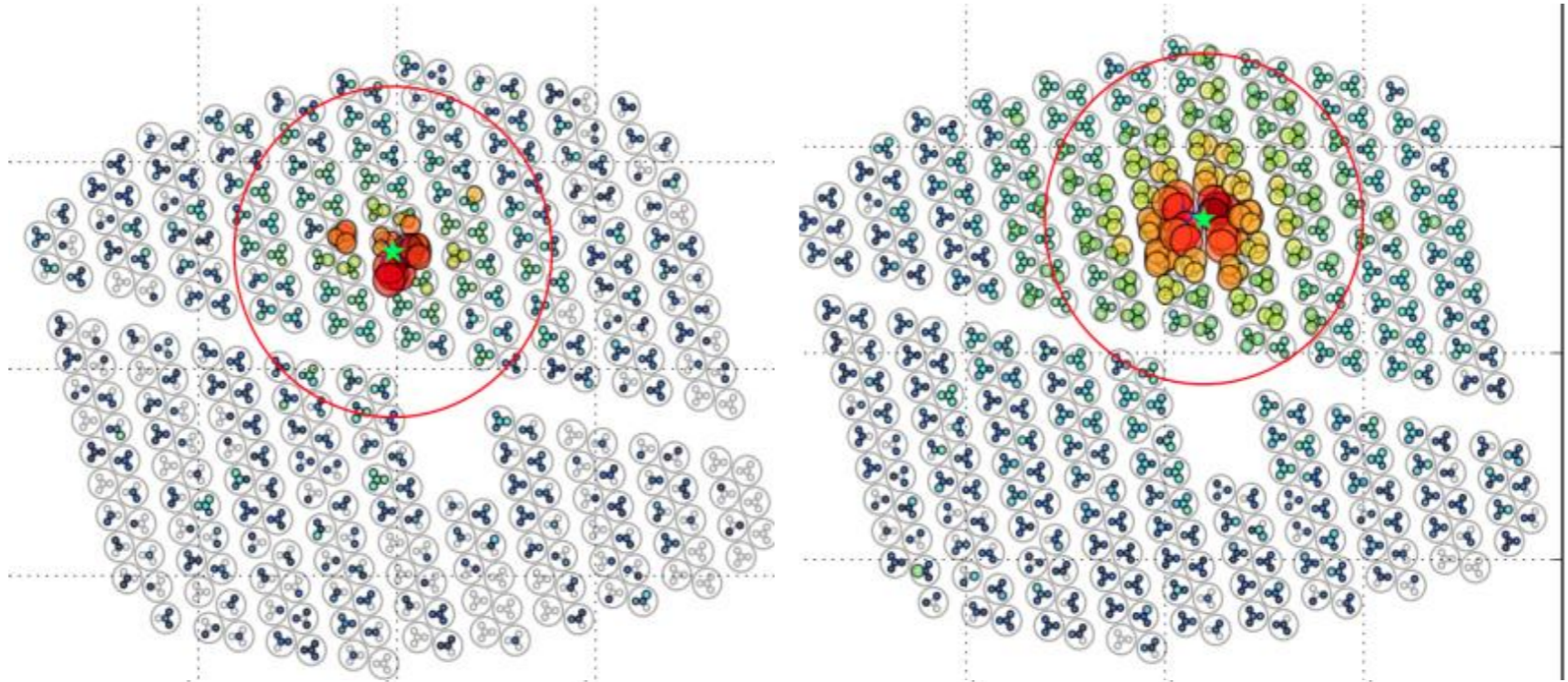
$$\mathcal{P} = \frac{1}{N} \sum_{i=0}^N \frac{(\zeta_i - \langle \zeta \rangle)^2}{\sigma(\zeta)^2}, \quad (2)$$

defined using the lateral distribution for N PMTs hit with $\zeta_i = \log_{10}(Q_{eff}, i)$.

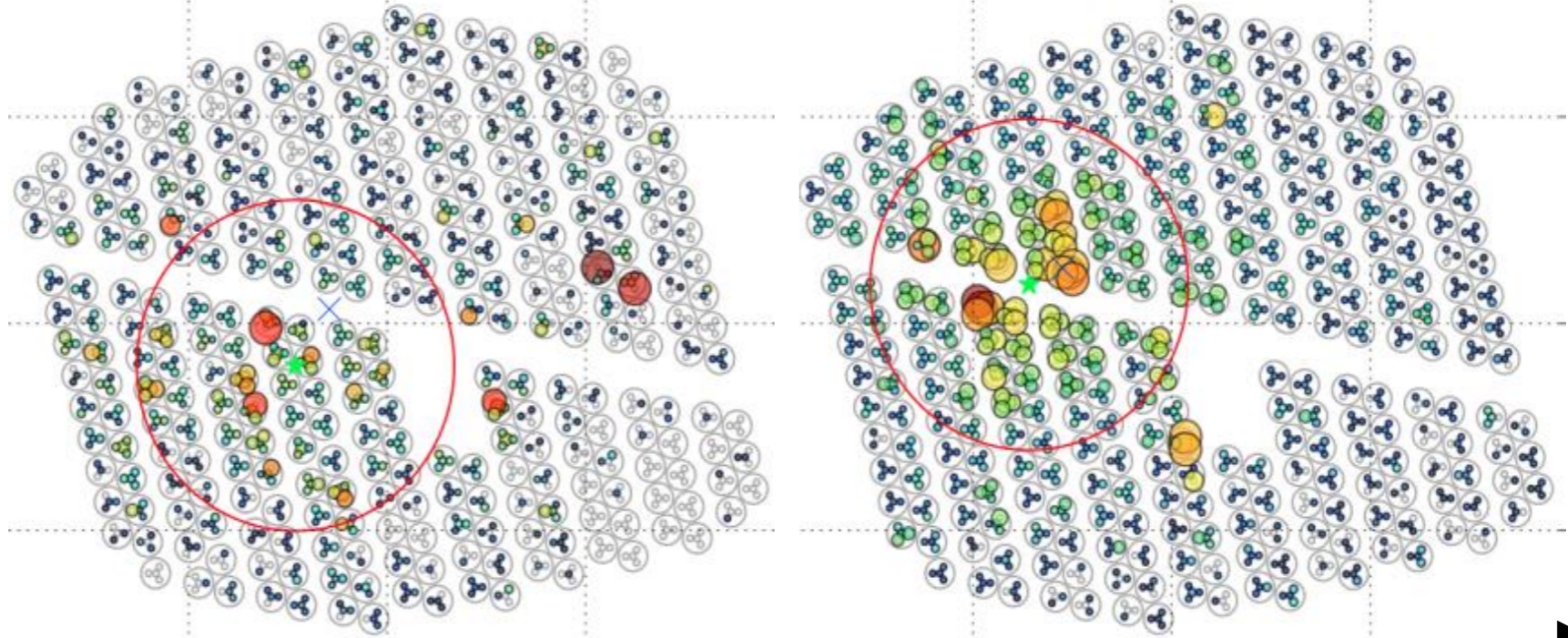
HAWC Crab 2017: Abeysekara et al. 2017, ApJ 843, 39

Gamma - hadron discrimination

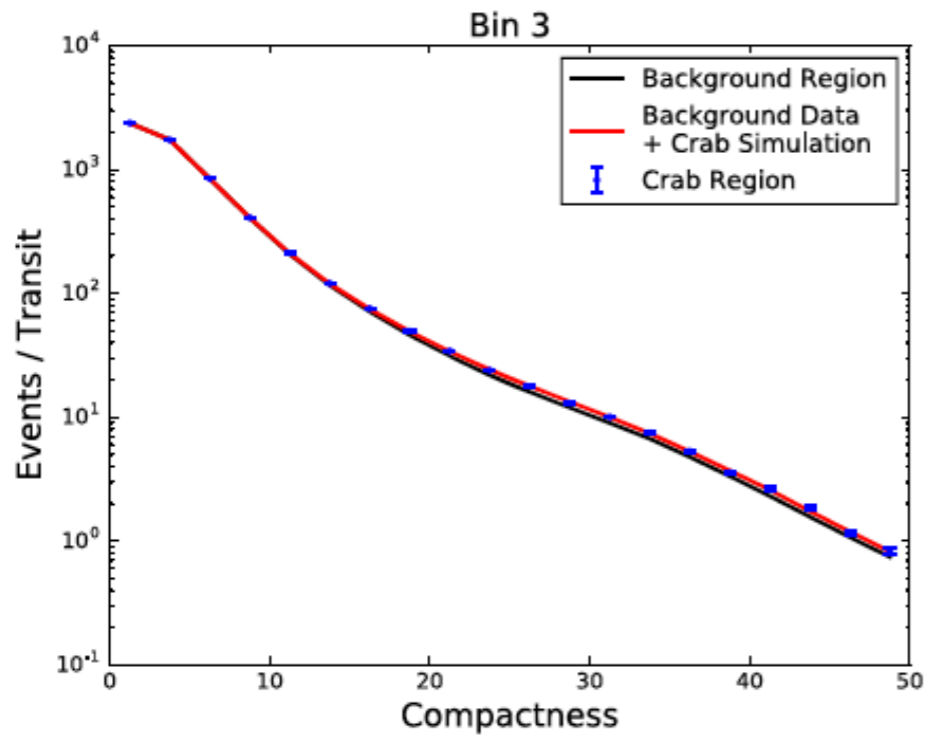
γ rays



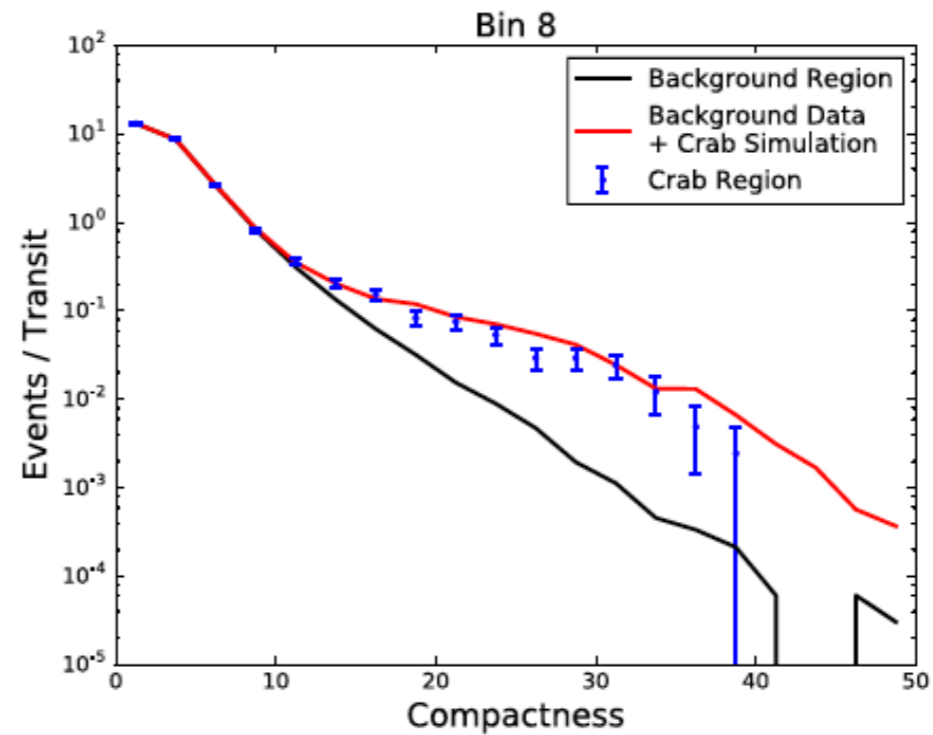
Hadrons



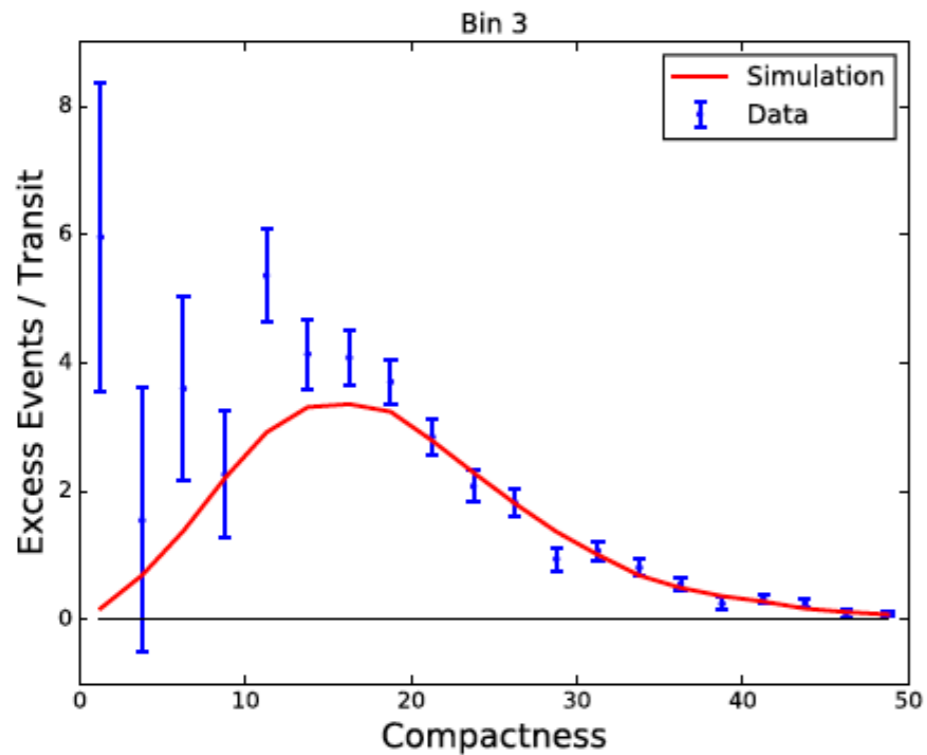
—————▶ E



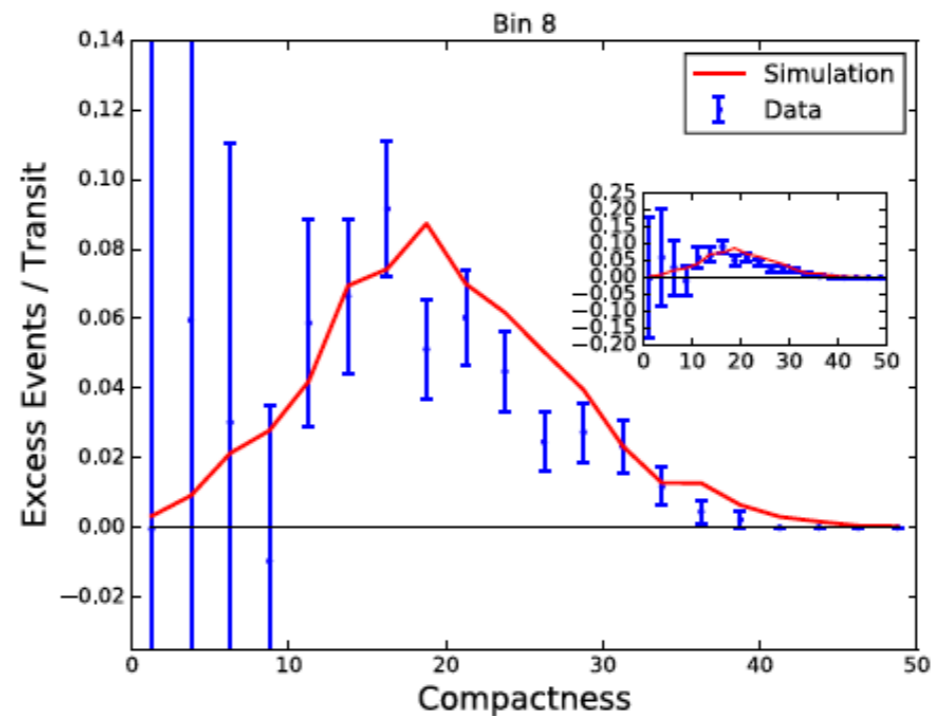
(a) $\mathcal{B} = 3$ Signal and Background



(b) $\mathcal{B} = 8$ Signal and Background

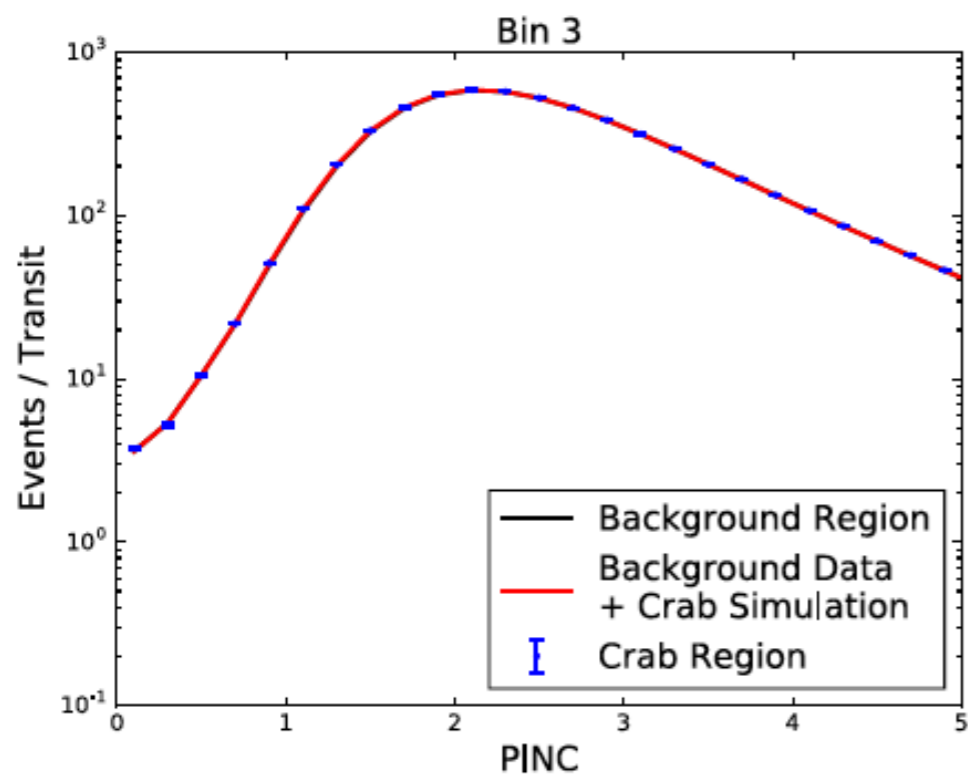


(c) $\mathcal{B} = 3$ Background Subtracted

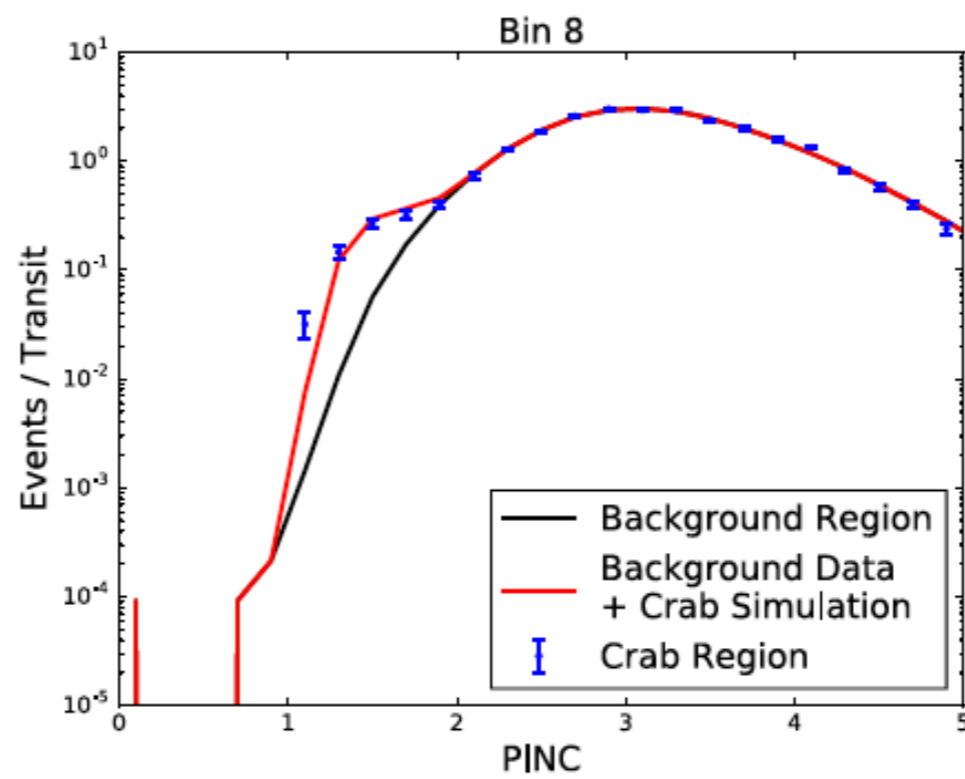


(d) $\mathcal{B} = 8$ Background Subtracted

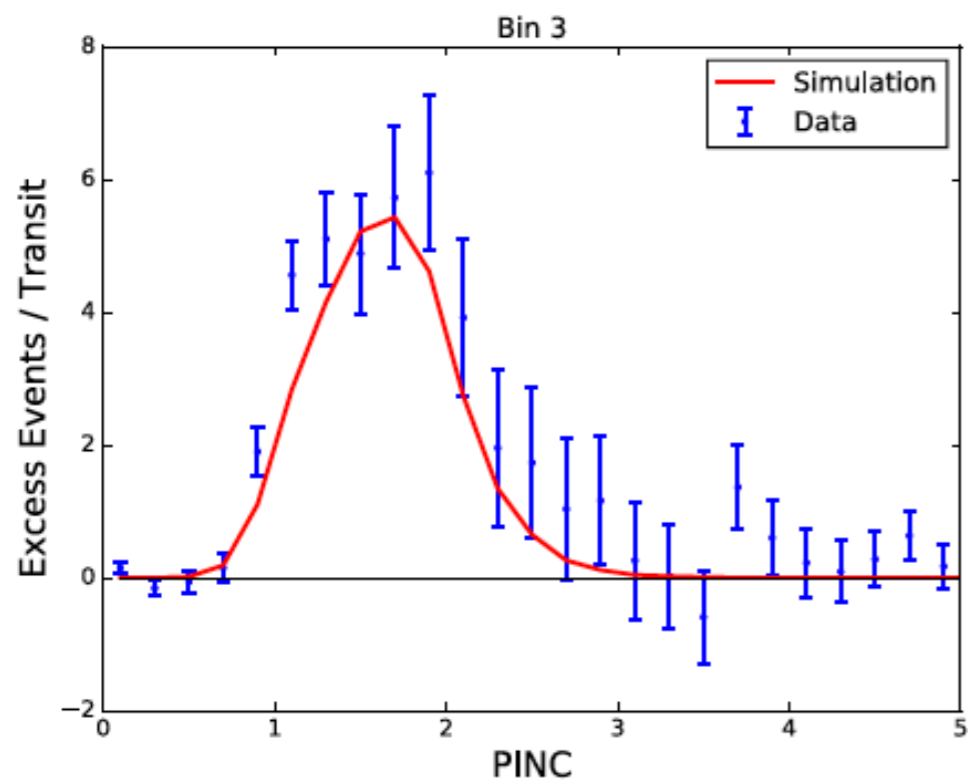
Crab region = events within $1.5\psi_{68}$



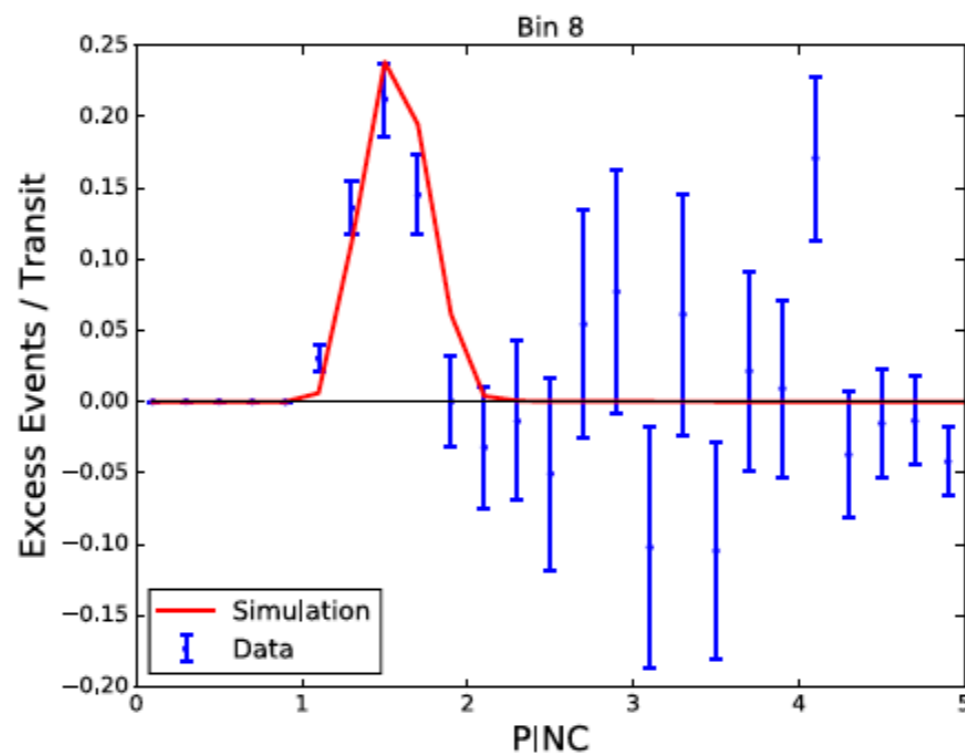
(a) $\mathcal{B} = 3$ Signal and Background



(b) $\mathcal{B} = 8$ Signal and Background



(c) $\mathcal{B} = 3$ Background Subtracted



(d) $\mathcal{B} = 8$ Background Subtracted

Crab region = events within $1.5\psi_{68}$

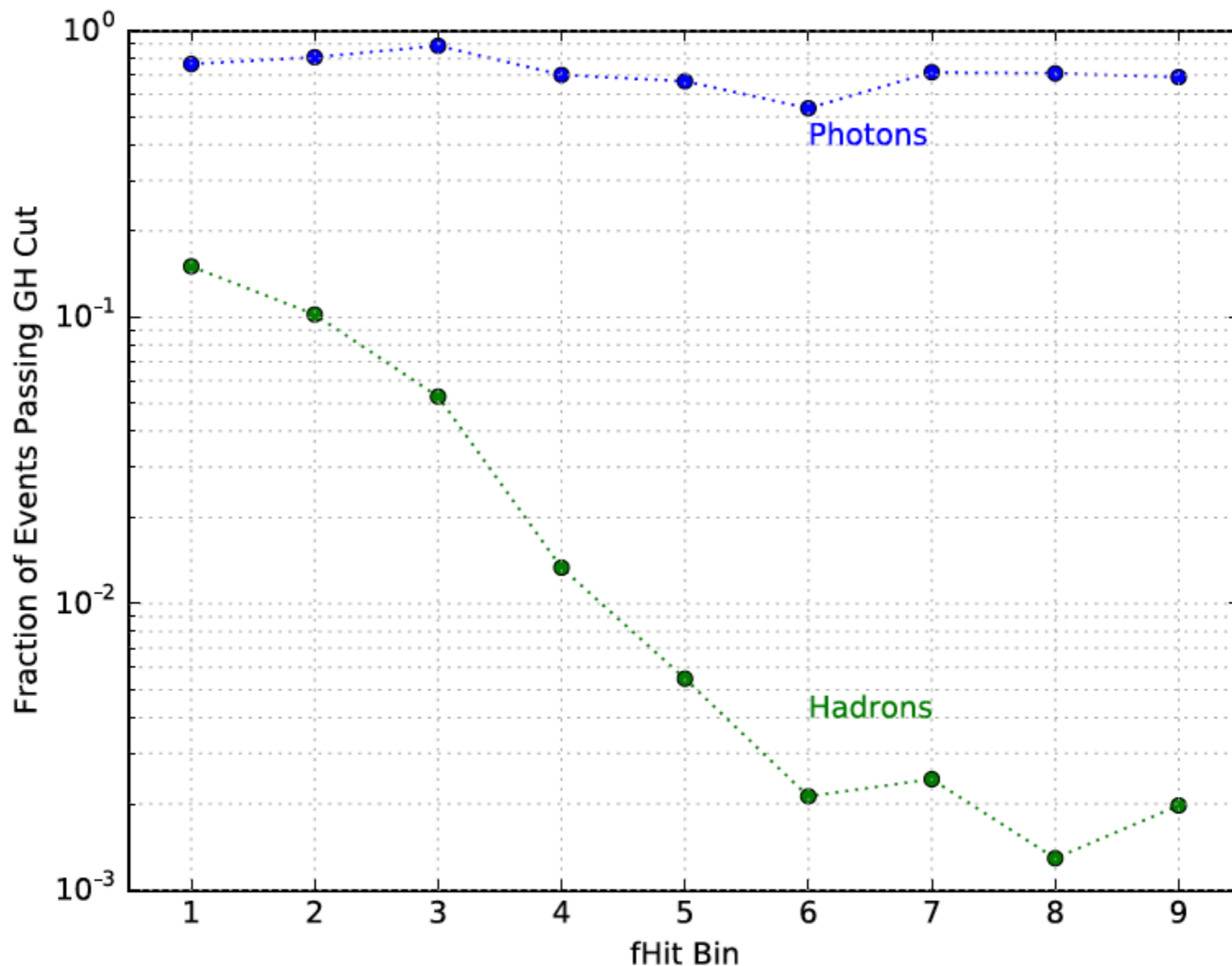
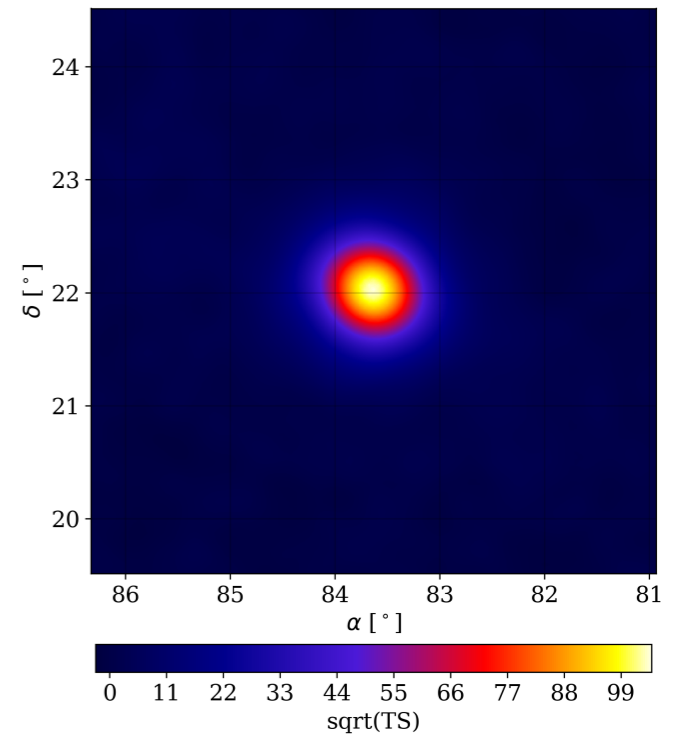
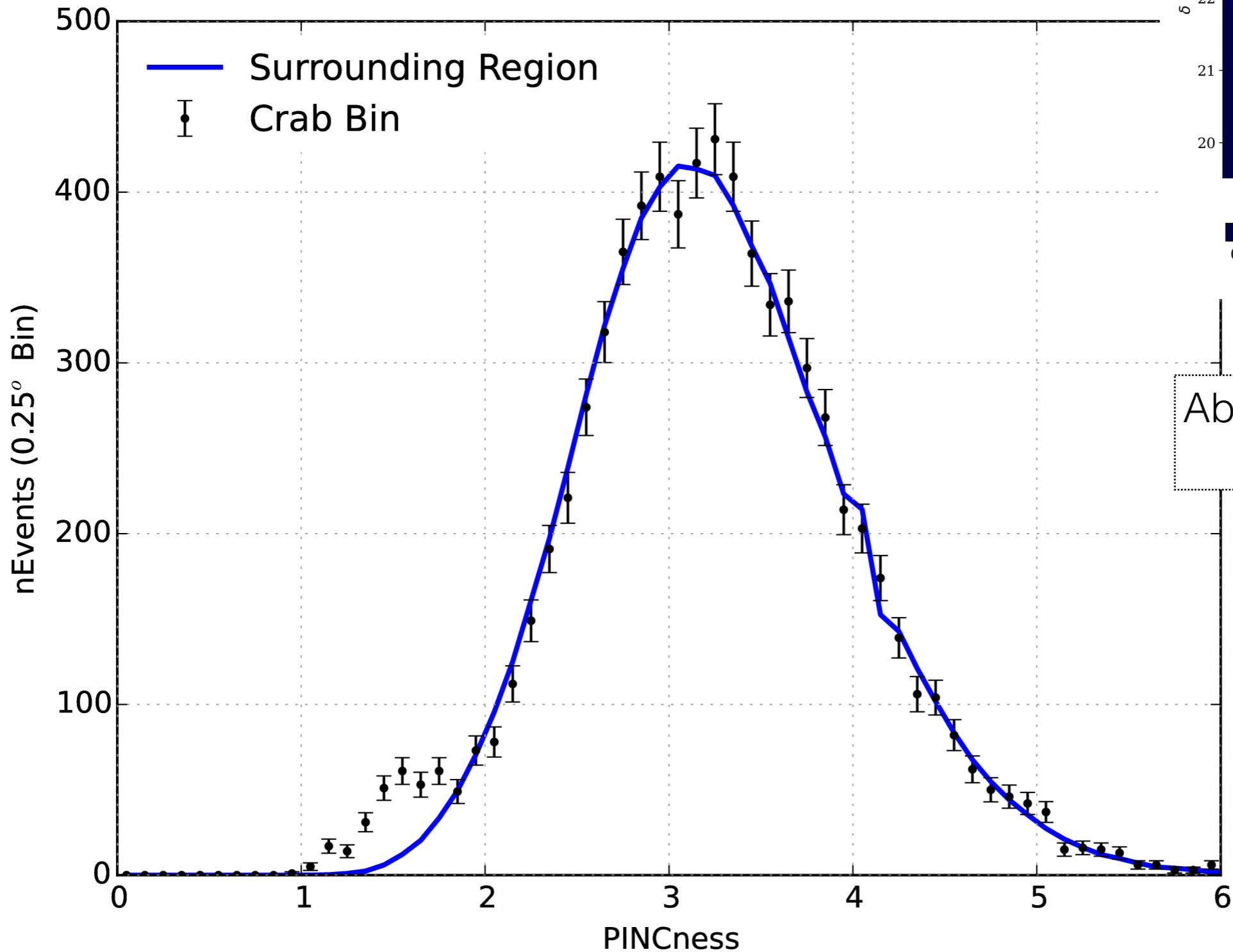


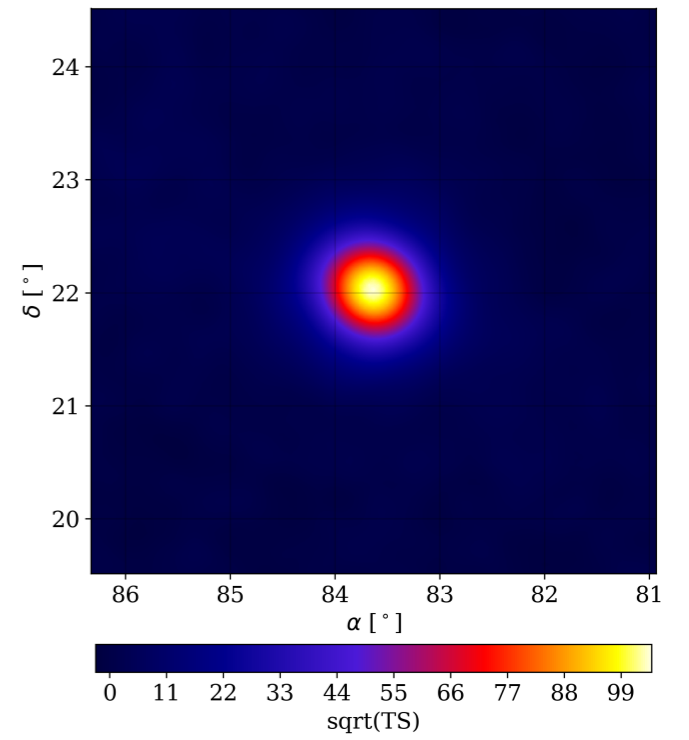
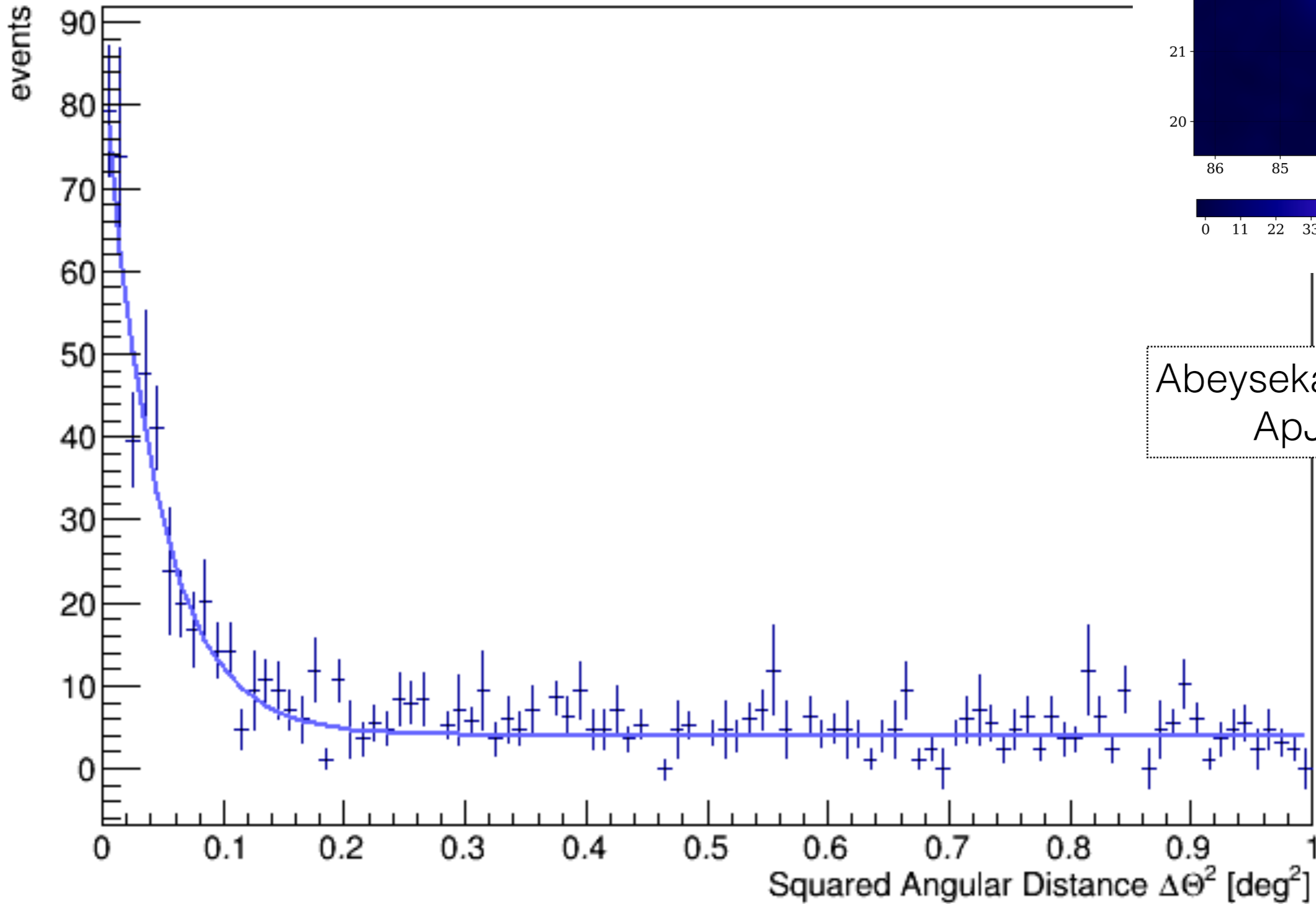
Figure 11. Fraction of gamma rays and background hadron events passing photon/hadron discrimination cuts as a function of the event size, \mathcal{B} . Good efficiency for photons is maintained across all event sizes, with hadron efficiency approaching 1×10^{-3} for high-energy events.

HAWC Crab



Abeysekara et al. 2017
ApJ 843, 39

HAWC Crab



Abeysekara et al. 2017
ApJ 843, 39

The 2HWC catalog

- Skymap for declinations -20° to $+60^\circ$, using HealPix grid.
- Maximum likelihood analysis of 507 effective days of data using parameters the Crab validation.

Table 1

Properties of the Nine Analysis Bins: Bin Number \mathcal{B} , Event Size f_{hit} , 68% PSF Containment ψ_{68} , Cut Selection Efficiency for Gammas $\epsilon_{\gamma}^{\text{MC}}$ and Cosmic Rays $\epsilon_{\text{CR}}^{\text{data}}$, and Median Energy for a Reference Source of Spectral Index -2.63 , at a Declination of 20° $\tilde{E}_{\gamma}^{\text{MC}}$

\mathcal{B}	f_{hit} (%)	ψ_{68} ($^{\circ}$)	$\epsilon_{\gamma}^{\text{MC}}$ (%)	$\epsilon_{\text{CR}}^{\text{data}}$ (%)	$\tilde{E}_{\gamma}^{\text{MC}}$ (TeV)
1	6.7–10.5	1.03	70	15	0.7
2	10.5–16.2	0.69	75	10	1.1
3	16.2–24.7	0.50	74	5.3	1.8
4	24.7–35.6	0.39	51	1.3	3.5
5	35.6–48.5	0.30	50	0.55	5.6
6	48.5–61.8	0.28	35	0.21	12
7	61.8–74.0	0.22	63	0.24	15
8	74.0–84.0	0.20	63	0.13	21
9	84.0–100.0	0.17	70	0.20	51

2HWC skymap

THE ASTROPHYSICAL JOURNAL, 843:40 (21pp), 2017 July 1

Abeyssekara et al.

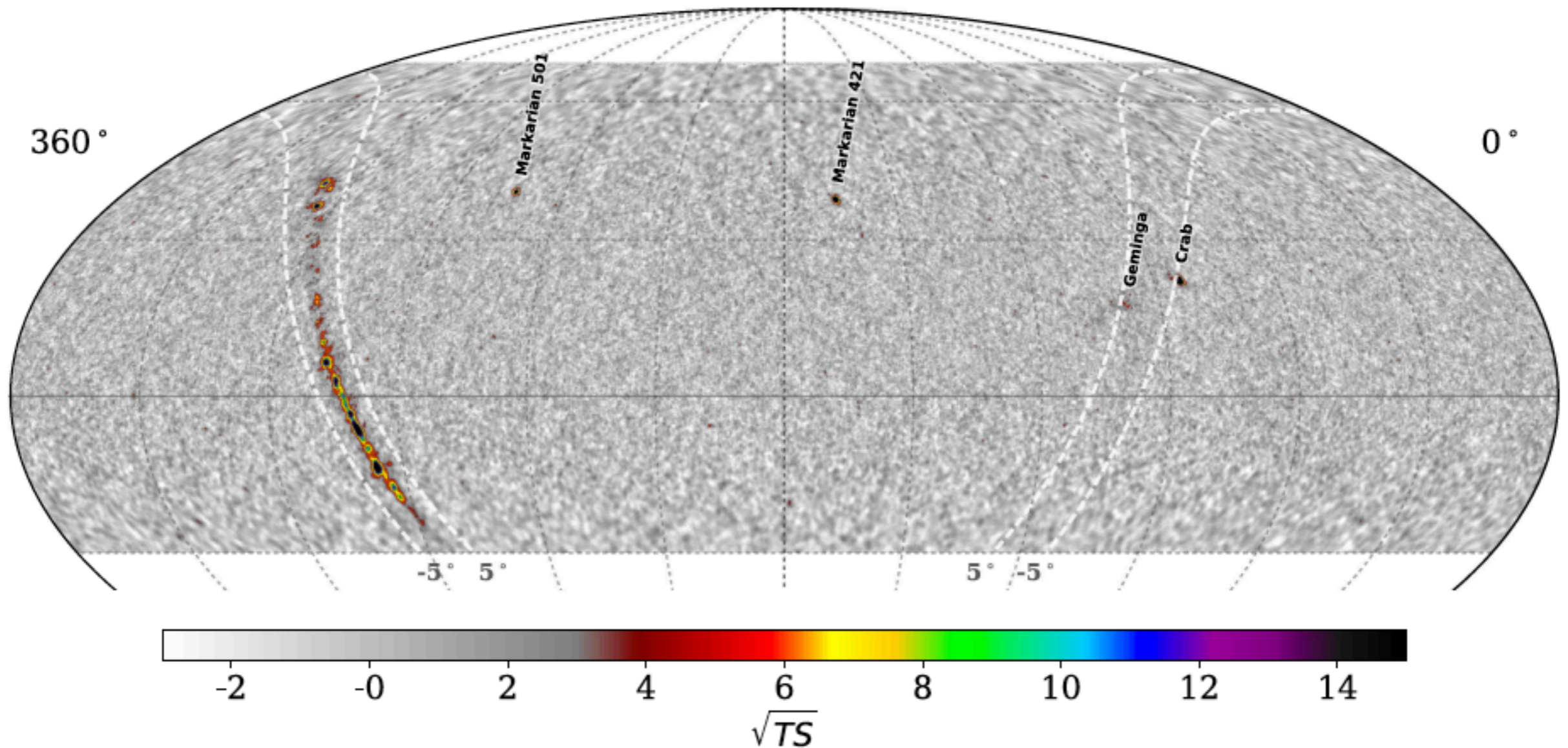


Figure 3. Equatorial full-sky TS map, for a point source hypothesis with a spectral index of -2.7 . Black graticule corresponds to the equatorial coordinate system, and white lines indicate Galactic latitudes $\pm 5^\circ$.

2HWC point sources

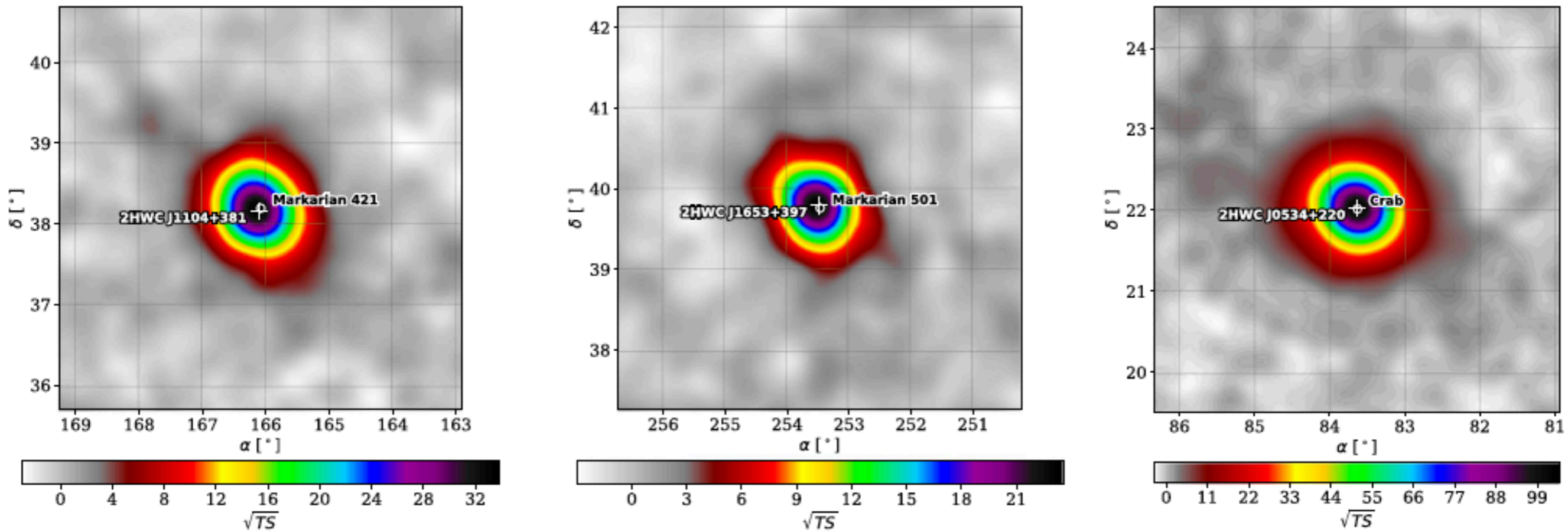
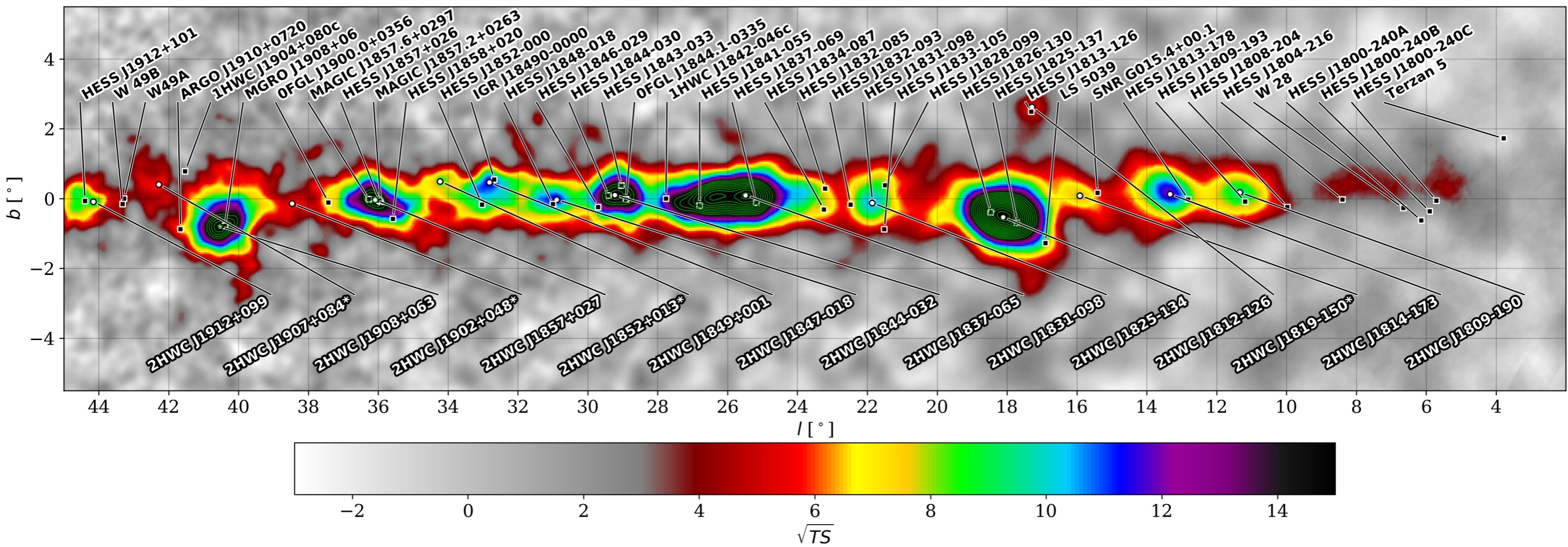
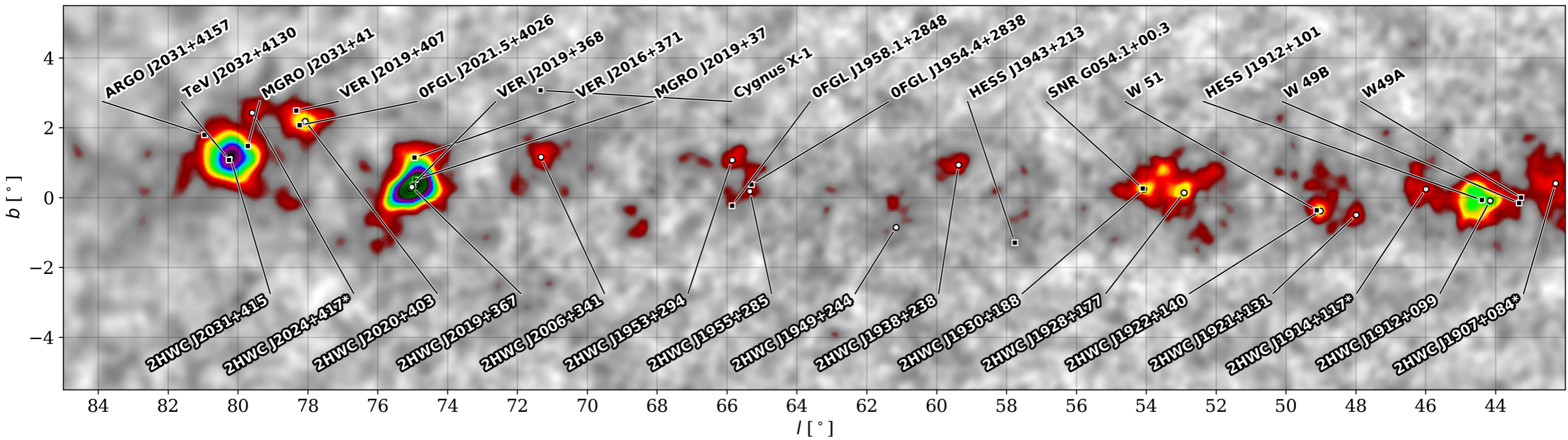
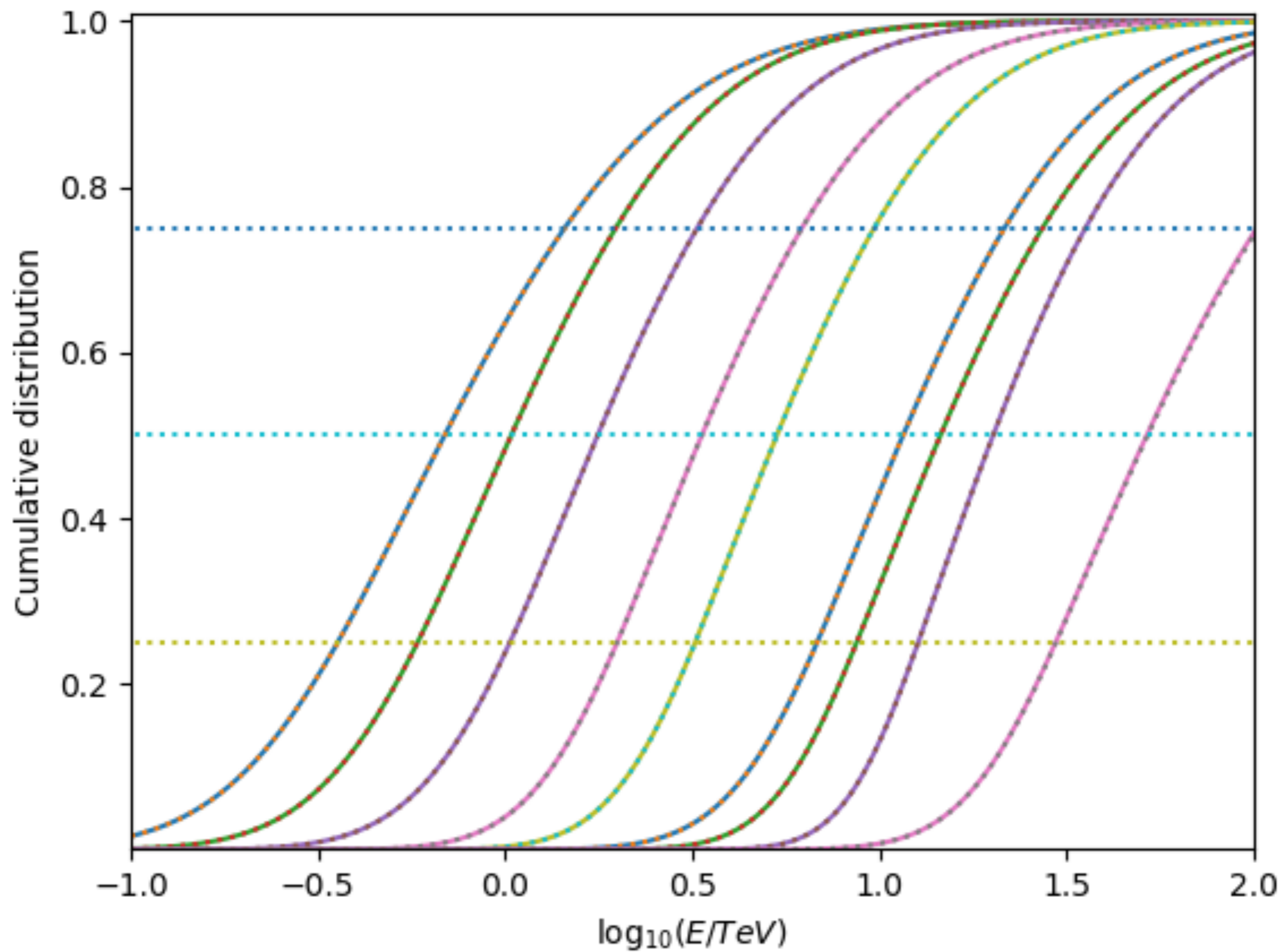


Figure 4. Regions around Markarian 421, Markarian 501, and the Crab Nebula: equatorial TS maps, for a point source hypothesis with a spectral index of -2.7 . In this figure and the following, 2HWC sources are represented by white crosses and labels below them, whereas the sources listed in TeVCat are represented with black circles and labels above them.



RESPALDOS



Energy estimator

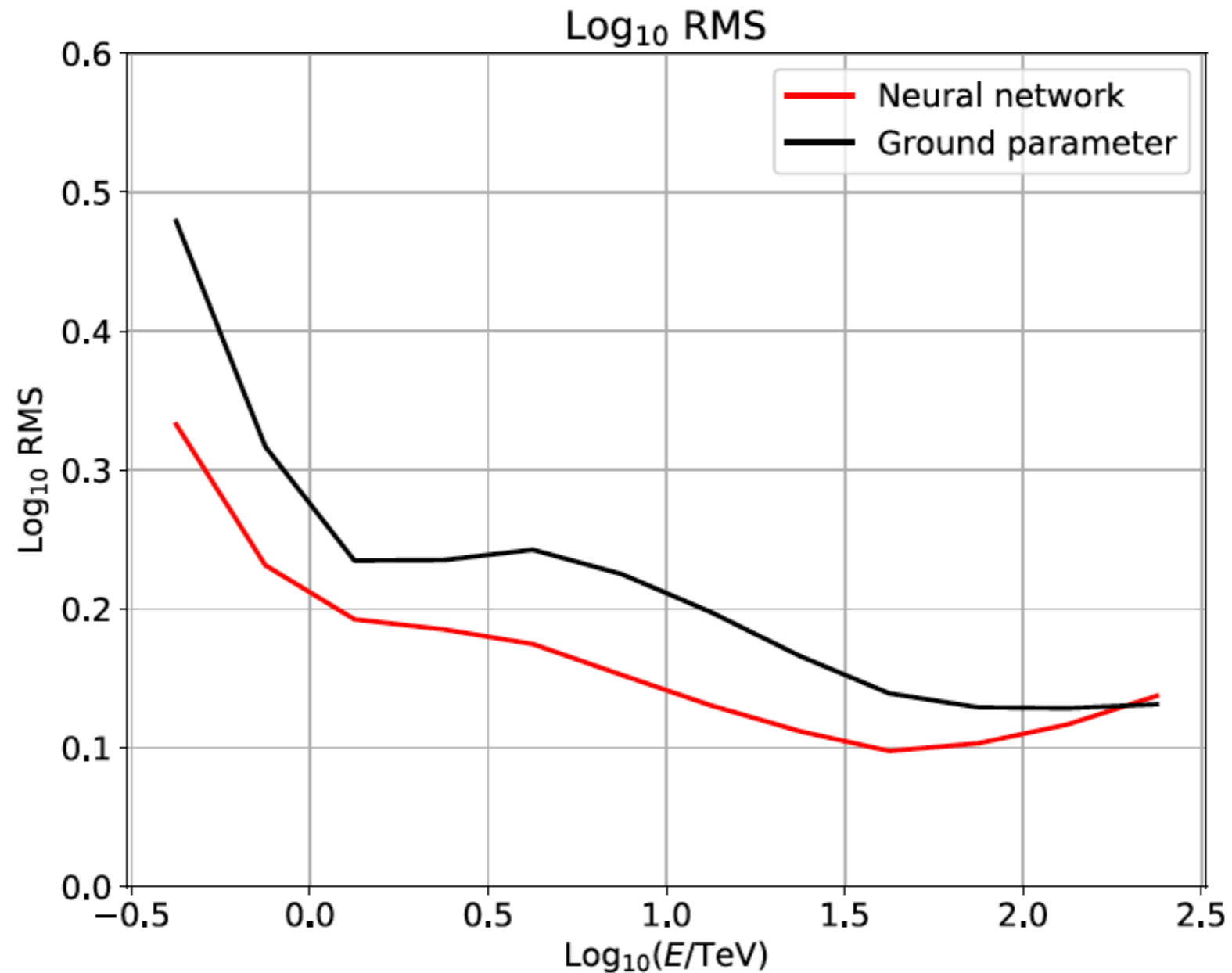


Figure 7. The log rms error for the GP and NN estimators. Gamma/hadron separation cuts have been applied. This is defined as $\rho \equiv \sqrt{\langle (\log_{10} \hat{E} - \log_{10} E)^2 \rangle}$.

Ground parameter angular resolution

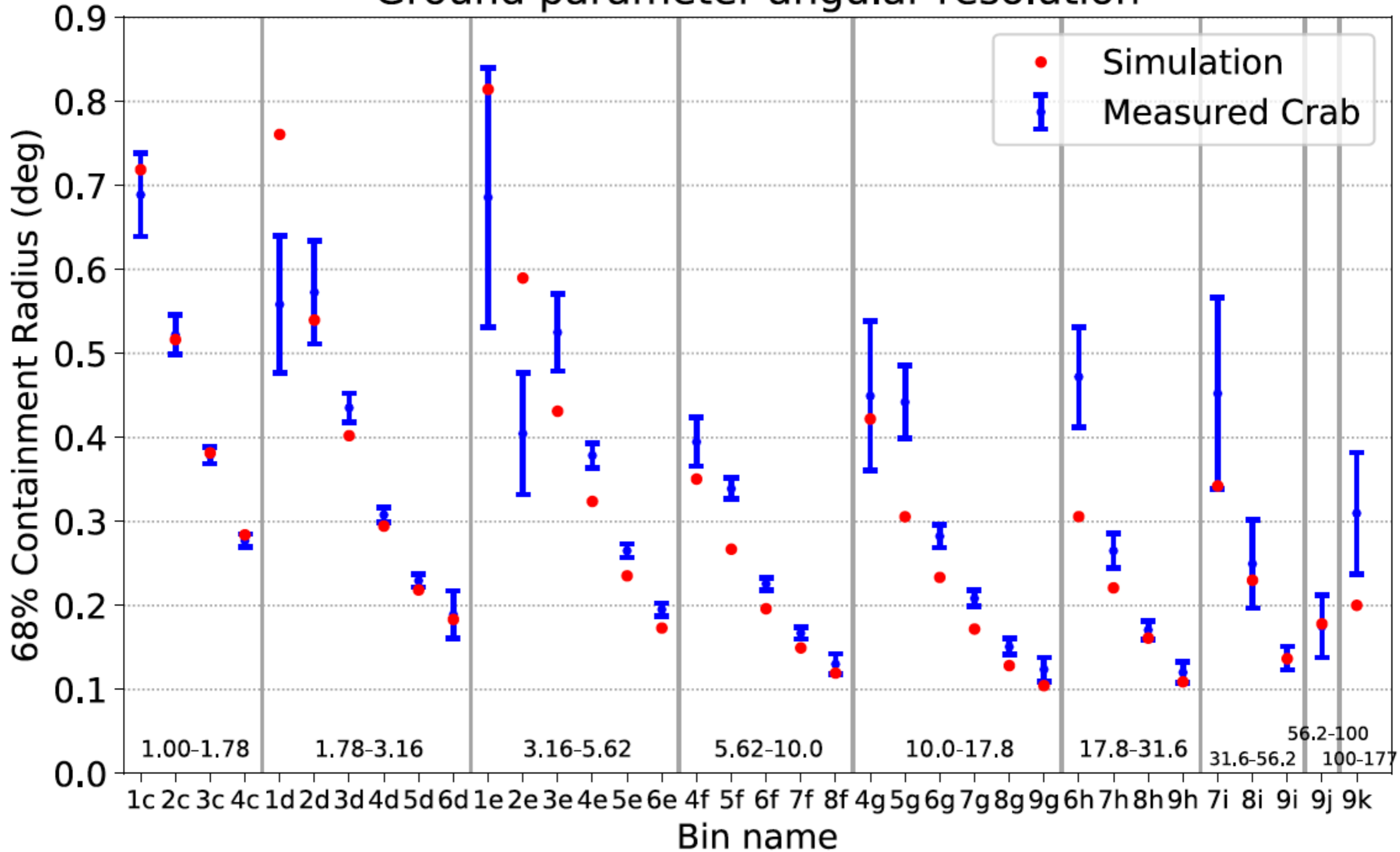


Table 1
Energy Bins

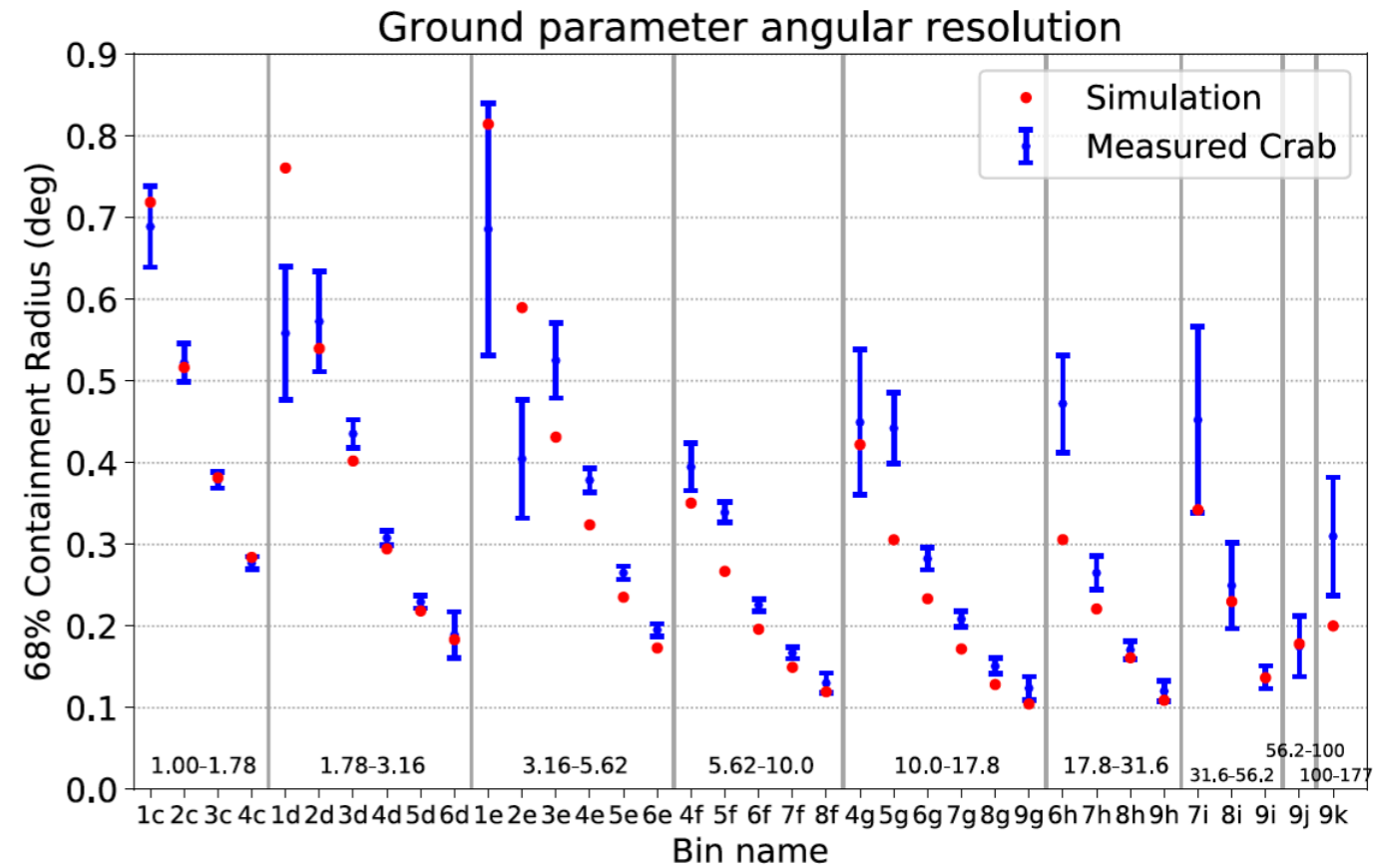
Bin	Low Energy (TeV)	High Energy (TeV)
a	0.316	0.562
b	0.562	1.00
c	1.00	1.78
d	1.78	3.16
e	3.16	5.62
f	5.62	10.0
g	10.0	17.8
h	17.8	31.6
i	31.6	56.2
j	56.2	100
k	100	177
l	177	316

Note. The energy bins. Each bin spans one-quarter of a decade. Note that the first two bins are not used in this analysis, as the estimate is highly biased, as explained in Section 3.3.

Table 2
 β Bins

Bin Number	Low Fraction Hit	High Fraction Hit
1	0.067	0.105
2	0.105	0.162
3	0.162	0.247
4	0.247	0.356
5	0.356	0.485
6	0.485	0.618
7	0.618	0.740
8	0.740	0.840
9	0.840	1.00

Note. The β (fraction of PMTs hit) analysis bins used in this paper.



2HWC sensitivity

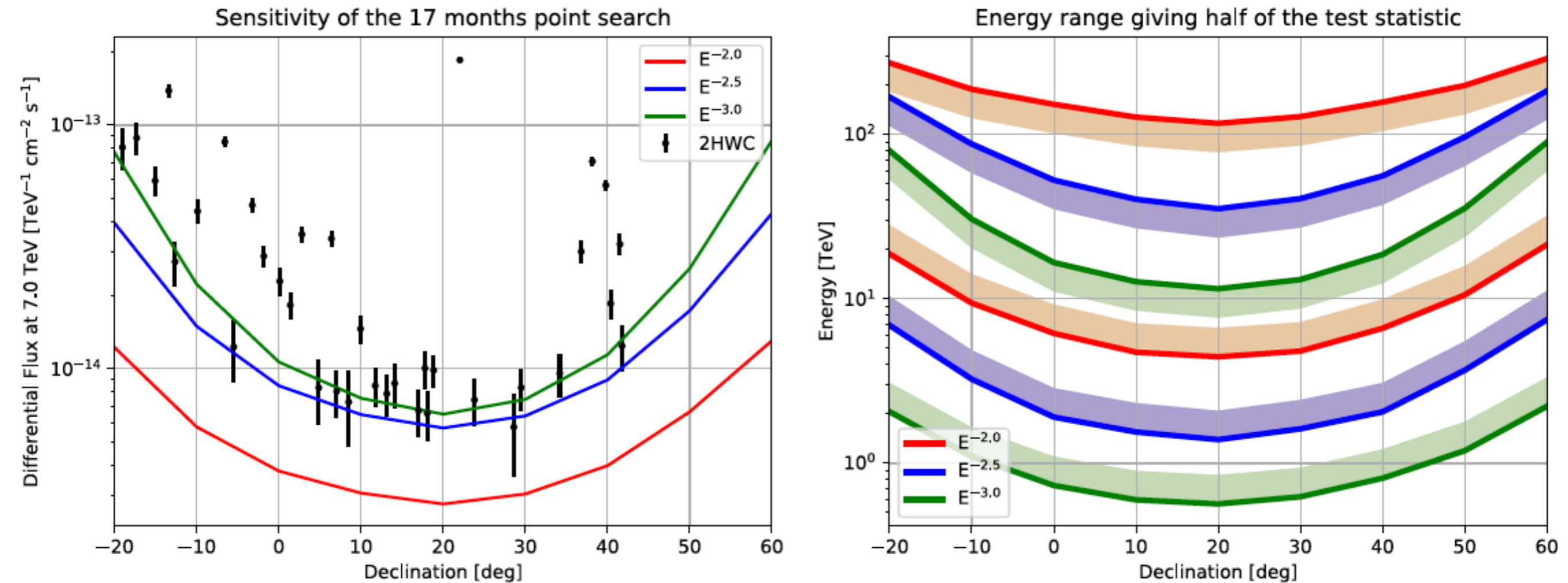


Figure 10. Left: sensitivity of the point source search for three spectral hypotheses, as a function of declination. We show the flux required to give a certain detection of 5σ , for the present analysis. The differential fluxes of the sources detected in the point source search are also shown with their statistical uncertainties. Right: Upper and lower ends of the energy range contributing to the central half of the test statistic of the point source search (see text).

